NTNU – Trondheim
Norwegian University of
Science and Technology

Design and Analysis of Mooring System for Semi-submersible Floating Wind Turbines in Shallow Water

Kun Xu

Marine Technology
Submission date: June 2015
Supervisor: Torgeir Moan, IMT
Co-supervisor: Zhen Gao, IMT
Constantine Michailides, IMT

Norwegian University of Science and Technology
Department of Marine Technology

NTNU Trondheim
Norwegian University of Science and Technology
Department of Marine Technology – Group of Marine Structures

MSC THESIS IN MARINE TECHNOLOGY

SPRING 2015

FOR

STUD.TECHN. Kun Xu

Design and Analysis of Mooring System for Semi-submersible Floating Wind Turbines in Shallow Water

Background:
Semi-submersible floaters have been proposed to support large-scale offshore wind turbines. One of the advantages of a semi-submersible floating wind turbine is the relatively small draft, in the order of 20-40m, which allows them to be deployed in shallow waters (50-100m). While, floating wind turbines with spar and TLP floaters may have to be considered for water depths of more than 100-200m.

However, mooring system design is particularly challenging for floating structures in shallow water. On one hand, the mooring system should be properly designed so that the natural periods for horizontal motion modes are sufficiently larger than the periods of most relevant waves (in the order of 5-25s). On the other hand, it should have enough stiffness to limit the offset of the floater under mean wind force. Cateneray mooring lines might be used in combination with clump weights and buoys. In order to avoid excessive mooring line tension induced by the dynamic motions of the floater, the linear part of the mooring line characteristic should be utilized. A very long mooring line in shallow waters is normally needed with a large part laying on the seabed. The mooring lines should have sufficient ultimate and fatigue strengths under dynamic loading conditions due to both wind- and wave-induced motions of the floater.

In the project work, the candidate has performed a literature study on mooring line design, and carried out a preliminary mooring system design for a 5MW semi-submersible floating wind turbine in water depth of 100m, based on the existing mooring design for 200m. The design was obtained by varying the key parameters (such as the line length, the position of anchor and the clump weight), to achieve the same horizontal force-displacement relationship of a single mooring line as that of the 200m design.

In the thesis work, the candidate should extend the same approach to achieve a mooring system design for 50m water depth. In addition, a comparative study should be carried out using Simo/Riflex/AeroDyn considering three mooring designs for three water depths. The corresponding numerical model of the 5 MW semi-submersible wind turbine will be provided to the candidate. Coupled time-domain analysis considering both operational and survival wind and wave conditions should be performed. To facilitate the comparison, the same input of wind and wave conditions should be considered when comparing the responses (such as motions and mooring line tension).

Assignment:
The following tasks should be addressed in the thesis work:

1. Complete the literature review on mooring system design. Also cover the area of coupled methods for global response analysis of floating wind turbines.

2. Use the same approach as for the 100m mooring system, to design equivalent mooring lines for 50m. A similar mooring line characteristic should be aimed for.

3. Using the same numerical model of the semi-submersible floating wind turbine in Simo/Riflex/AeroDyn, perform decay tests considering three mooring designs (200m ,100m and 50m). Compare the results of natural periods of rigid-body motions and damping ratio.

4. For the given operational and survival wind and wave conditions, perform time-domain coupled analysis using Simo/Riflex/AeroDyn, compare the responses of floater motions and mooring line tension via time series, spectral and statistical analyses.

5. Conclude the work and give recommendations for future work.

6. Write the MSc thesis report.

In the thesis the candidate shall present his personal contribution to the resolution of problem within the scope of the thesis work.

Theories and conclusions should be based on mathematical derivations and/or logic reasoning identifying the various steps in the deduction.

The candidate should utilize the existing possibilities for obtaining relevant literature.

The thesis should be organized in a rational manner to give a clear exposition of results, assessments, and conclusions. The text should be brief and to the point, with a clear language. Telegraphic language should be avoided.

The thesis shall contain the following elements: A text defining the scope, preface, list of contents, summary, main body of thesis, conclusions with recommendations for further work, list of symbols and acronyms, reference and (optional) appendices. All figures, tables and equations shall be numerated.

The supervisor may require that the candidate, in an early stage of the work, present a written plan for the completion of the work. The plan should include a budget for the use of computer and laboratory resources that will be charged to the department. Overruns shall be reported to the supervisor.

The original contribution of the candidate and material taken from other sources shall be clearly defined. Work from other sources shall be properly referenced using an acknowledged referencing system.

The thesis shall be submitted in two copies as well as an electronic copy on a CD:

- Signed by the candidate
- The text defining the scope included
- In bound volume(s)
- Drawings and/or computer prints which cannot be bound should be organized in a separate folder.

Supervisors:
Torgeir Moan
Zhen Gao
Constantine Michailides

Deadline for thesis report: 12.06.2015

Acknowledgements

The master thesis herein constitues the Master Degree program of Marine Technology at the Norwegian University of Science and Technology (NTNU).

First of all, I would like to express my sincere gratefulness to Prof. Torgeir Moan for providing me with inspirations and guidance during my thesis work. The thesis will be impossible without his encouragement. A warm thanks is also given to Dr. Zhen Gao. He has during the whole year followed my work and given competent advice. I have benefited a lot from the regular meeting with him. Special appreciation is given to Postdoc Constantine Michailides for the help he offered whenever needed. He has given me much feedback with respect to the analysis tool and result post-processing.

Sincere gratitude also goes to PhD candidates Chenyu Luan for discussing the reference mooring system model with me. In addition, Dr. Erin Elizabeth Bachynski at MARINTEK has given important guidances on Simo-Riflex-AeroDyn code and environmental condition determination. Special thanks is also given to PhD candidate Yuna Zhao for her help in Matlab code and discuss about decay test.

Last but not least, I would also like to thank my family who have always been supporting and comforting me no matter what I have achieved. My girlfriend, Yining Dong , has also given me huge support through the whole master study in Trondheim. The memory I gained here will be the fortune for my whole life.

Kun Xu

Trondheim, Norway

June 10, 2015

Summary

There has been a remarkable development in offshore wind energy. From the view of cost efficiency, floating wind turbine becomes more competitive than bottom fixed wind turbine when the water depth comes above 50 m. Semi-submersible floater concepts have been proposed to be deployed in shallow waters (50 m - 100 m) because of its smaller draft compared to other floater types.

However, mooring system design is extremely challenging for floating structures in shallow water. There is a transition from linearity to nonlinearity in the relationship between mooring line tension and offset at the fairlead, which indicates a potential for extremely large mooring line tension during harsh environment when the floater motions have large offset ranges. Moreover, the nonlinear tension increment in shallow water becomes more critical than deep water. In addition, the degree of tightness of mooring system will influence the tension increment trend as well.

In present thesis, two mooring system design concepts in 100 m and 50 m water depth (shallow water) have been proposed for the use of 5-MW-CSC semi-submersible floating wind turbine. Original mooring system design in 200 m water depth is taken as a reference. Initially, preliminary static design has been carried out in SIMA to determine mooring line properties, mooring system configurations and document static performances of mooring line. Afterwards, free decay tests are carried out to calculate the natural periods of the floating wind turbine with mooring system at six degrees of freedom in the three water depths. At last, fully coupled time-domain dynamic analysis in ultimate limit state and fatigue limit state were performed using Simo-Riflex-AeroDyn. Critical responses have been checked to verify if proposed design concepts satisfy design standards.

In order to achieve desired mooring line pretension and catenary shape in different water depths, studless chain link has been chosen for 50 m and spiral rope has been selected for 100 m. The corresponding clump weights have been enlarged to 60 tonnes for both cases. Moreover, in order to avoid large nonlinear tension increment, mooring system is designed to be soft on purpose in 50 m. Meanwhile, corresponding natural periods have been examined to be close to the reference model, larger than the periods of most relevant waves.

Extreme condition test results indicate that the maximum response of mooring

line tension and floater motion occurs when wave is acting aligned with mooring line configuration. Despite, mooring line strengths are sufficient in the light of utilization factor calculations and floater motions have been successfully limited to a reasonable extent. In accordance with operational condition test, accumulated fatigue damage for chain link is larger than spiral rope, even though the stress ranges do not show big difference. This is because highly contact force between chain links produces significant fatigue damage, which does not apply to spiral rope. Furthermore, there is no protection treatment for chain link like plastic sheathing for wire rope. According to spectrum analysis, wave is dominating the responses during extreme condition, while wind contributes most to the responses by influencing low-frequency motion resonant responses in operational condition.

The strategy to fight against the nonlinear tension increment in 50 m is to design the mooring system to be relatively soft, which will lead to relatively large floater motion at the same time. Nevertheless, the compromise has achieved great effect: extreme mooring line tensions do not exceed the capacities, even though the tension has increased nonlinearly. Meanwhile the compromised floater motions are under reasonable ranges, without mooring line being totally lifted up. Mooring system design for 100 m shows great performance as well without extreme line tension or large floater motion, which could be regarded as a satisfactory design concept.

Nomenclature

Abbreviations

$1P$	Rotational frequency of turbine rotor
$3P$	Blade passing frequency
ALS	Accidental limit state
API	American Petroleum Institute
BEM	Blade element momentum
DLL	Dynamic link library
DNV	Det Norsk Veritas
DOF	Degree of freedom
FFT	Fast Fourier transform
FLS	Fatigue limit state
IEC	International Electrotechnical Commission
$JONSWAP$	Joint North Sea Wave Project
LF	Low frequency
$NREL$	National Renewable Energy Laboratory
$OC3$	Offshore code comparison collaboration, Phase 3
RAO	Response amplitude operator
RPM	Revolutions per minute
SRA	Simo-Riflex-AeroDyn
TLP	Tension leg platform
ULS	Ultimate limit state
WF	Wave frequency

Greek Symbols

α	Attack angle
$\ddot{\eta}$	Body acceleration vector
$\ddot{\eta}$	Rigid body velocity
$\dot{\eta}$	Rigid body motion vector
$\dot{\eta}$	Rigid body acceleration
η	Body motion vector
λ	Wave length
ω	Unit weight of mooring line in water
ϕ_0	Velocity potential
σ	Normal stress
φ	Phase angle
ξ_a	Wave amplitude
ξ	Damping ration
ζ	Free surface elevation

Latin Symbols

A	Added mass matrix
A_w	Water plane area
B	Potential damping matrix
C	Restoring matrix
C_D	Drag coefficient
C_L	Lift coefficient
F_{drag}	Viscous drag force vector
F_D	Diffraction force
$F_{mooring}$	Mooring line force vector
F_{wind}	Wind force vector
g	Acceleration of gravity
$h(\tau)$	Retardation function
H_s	Significant wave height
k	Wave number

l	Mooring line total length
l_s	Suspended length of mooring line in water
M	Mass matrix
M_y	Bending moment about y-axis
M_z	Bending moment about z-axis
$S(\omega)$	Wave spectrum
T_H	Pretension of mooring line
T_p	Wave peak period
x	Horizontal distance from fairlead to contact point of the mooring line with seabed

Contents

List of Figures

List of Tables

1 Introduction

"The Stone Age came to an end, not because we had a lack of stones, and the oil age will come to an end not because we have a lack of oil."

- Sheikh Ahmed Zaki Yamani, Saudi oil minister during the 1970's -

1.1 Offshore Wind Energy

Climate change and atmospheric pollution that are greatly influenced by the energy sector have become a hot topic drawing the attention all over the world. With the purpose to fight against global warming, environmental pollution and even the energy crisis, the demand for renewable and reliable energy was increased significantly [1]. Wind energy is one of the most rapidly growing renewable energy sources with the characteristic of being clean and environmentally friendly. Compared with onshore wind energy, offshore wind power has its promising attributes including greater area availability for arranging large projects, lower intrinsic turbulence intensities and wind shear, almost no visual disturbance or noise to residents [2].

There have been numerous plans in recent years to exploit offshore wind energy on a large scale [3], which leads to a remarkable increase in offshore wind capacity during the last decades. The development of offshore wind farms has generally taken place in European offshore sites accounting for over 70% of the total global installed base, mainly located in the North Sea and Baltic Sea along with southern European. There is much more offshore capacity in the planning stages as well. Figure 1.1 shows the map of existing and planned offshore wind farms in North-West Europe, which illustrates that Denmark, UK, Netherlands and Sweden have greatly contributed to European offshore wind industry with UK being the industry driver.

Behind the booming scene is the experience gained from offshore oil and gas industry, the long term survivability of offshore support structures has been successfully demonstrated in wind energy industry. Presently similar fixed support structures

have been mainly used in the offshore wind industry, e.g. monopole, tripod, gravity base, etc. where the water depth is usually less than 30 meters [4].

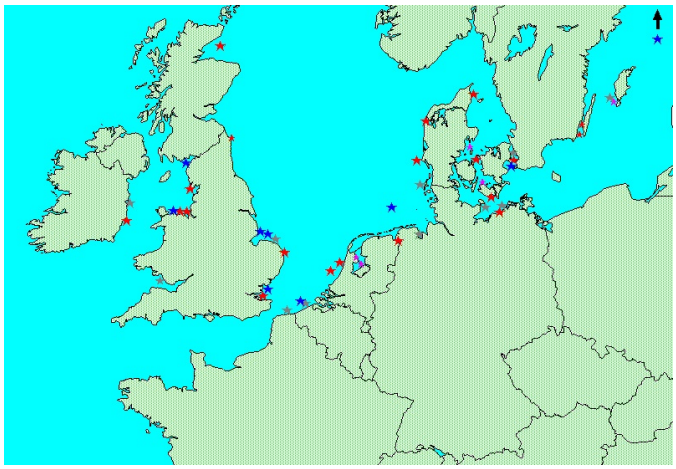

Figure. 1.1 *Map of existing and planned offshore windfarms in North-West Europe. "Stars": red- built MW wind turbines, purple- built small wind turbines, blue- under construction, grey- planned [4]*

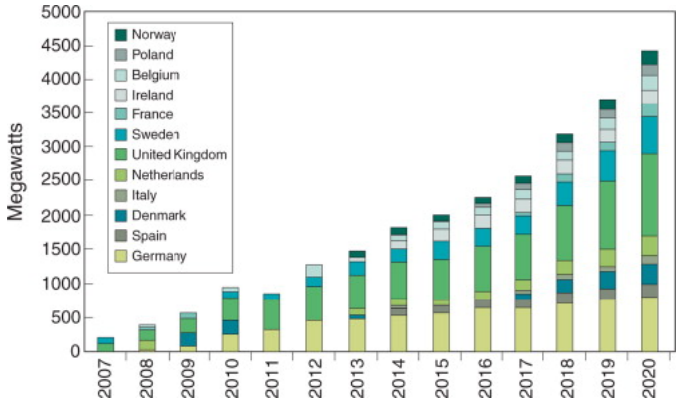

Figure. 1.2 *Europe wind power capacity net additions by country, 2007-2020 [5]*

1.2 Offshore Floating Wind Turbine

1.2.1 State of the Art

In many countries, the best offshore wind resource potential is found at water depths above 100 meters where bottom fixed wind turbine becomes too expensive. Therefore, it is of vital interest to explore floating platforms for mounting wind turbines to harness the wind resources that are available at deep waters. A floating wind turbine is specifically designed to produce power from offshore wind resources in intermediate to deep waters. Currently floating wind turbine is a young field of research and no commercial turbines or parks with more than one unit have been installed at the time. Understanding of the response characteristics of floating wind turbine system under environmental conditions is important for its design, operation, survive and further development.

The concept of floating wind turbine was proposed at the early 1970s, but the realistic industrial product did not come out until mid 1990s. Several milestones have been set up during the industrial development.

- In 2008, Blue H technologies installed the first test floating wind turbine (TLP) in water depth of 113 meters off the Italian coast near the site of future offshore Tricase project with a rated capacity 80 KW. It was finally decommissioned after a year of testing [6].

- In 2008, the Poseidon 37 project went into real sea test at DONG's offshore wind farm off the shores of Lolland in southern Denmark with a 37 meter wide wave energy plant and floating wind turbine foundation [7].

- In 2009, Statoil installed the world's first large scale grid connected floating wind turbine, Hywind, in Norway, with a 2.3 MW Siemens turbine.

- In 2011, the second large scale floating system, WindFloat, developed by Principle Power cooperated with EDP and Repsol, was installed on Portuguese coast.

- SeaTwirl and SWAY tested two floating substructures in 2011 which promoted deep offshore development as well.

- More recently in 2013, Japan has installed the compact semi-submersible floating wind turbine off the coast of Fukushima [8].

There are also a number of ongoing concepts installed with smaller scale in wave basins and in full scale environments all over the world. More and more countries have been devoted to exploring offshore wind energy.

1.2.2 Floater Classification

As indicated in the realistic industry, there could be several different floater configurations based on different design strategy. Generally, the way to achieve static stability is the basis to determine the architecture of the floating platform. A classic classification system based on physical principle was developed by classifying the platforms into three general categories:

1. **Waterplane Area**: Platforms use buoyancy and large free surface for righting moment, typical for semi-submersible and barge platform [9].
2. **Ballast**: Platforms that lower center of gravity below a central buoyancy tank, which create a righting moment in order to minimize heave motion, with Spar buoys as example [10].
3. **Mooring Lines**: Platforms that utilize mooring line tension to guarantee enough righting stability and be anchored on the seabed such as tension leg platform (TLP) [10].

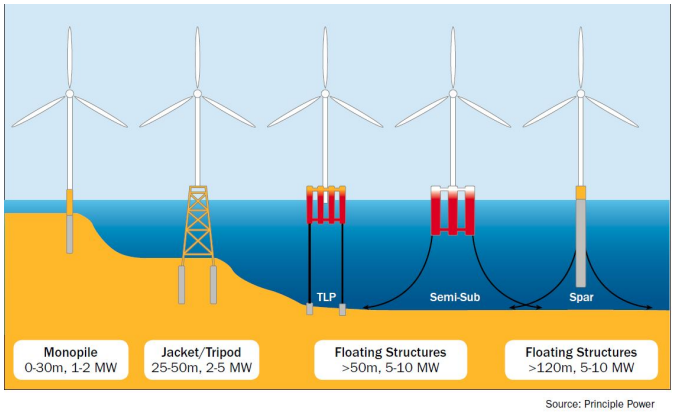

Figure. 1.3 *Offshore wind foundations in different water depths [11]*

1.3 Semi-submersible Wind Turbine Concept

Among the three floating concepts, spar type has better heave performance than semi-submersible because of deep draft and reduced vertical wave-exciting forces, but pitch and roll motions are more significant since the water plane area contribution to stability is reduced. Meanwhile, TLP has good heave and angular motions, but the cost of mooring installation, the tension change in tendon from environmental loading, the structural frequency coupling between the mast and mooring system are main challenges in the design work which do not apply to semi-submersible concept [12]. Semi-submersible floater became popular among

floating wind turbine concepts after the WindFloat project was successfully accomplished. The characteristic of small draft of semi-submersible allows it to be the only floating concept to be deployed in shallow waters (50 m - 100 m).

1.3.1 OO Star Wind Floater

With a strong believe in semi-submersible floating wind turbine and in response to the need for cost efficient solution, a joint project named "OO Star Wind Floater" was carried out with Dr. techn. Olav Olsen being as the project management taking care of the concept, structural design, construction and installation work together with three project partners: IFE focuses on modelling of rotor nacelle, pitch controller etc; Acciona Infraestructuras S.A. takes charge of the access systems and risk analysis; Statoil mainly provides funding and defines the metocean conditions. This has been an innovative concept with great effort from the industry in order to accommodate large wind turbine in harsh environment. The layout of OO Star could be referred to figure 1.4. The OO Star makes itself unique compared to other floating concepts because of its high technology in design, fabrication and installation. First of all, the material could be concrete or steel, or a combination of the two together depending on the turbine size. Several key features of the floater could be summarised as: Design water depth: 50 meters and deeper; Long design life (more than 100 years for concrete); Better fatigue properties of concrete; No maintenance or inspection of the substructure required.

According to the presentation on the EERA DeepWind' 2015 Deep Sea Offshore Wind RD Conference in Trondheim, 2015 [13], the project was divided into two main phases: Define frozen floater configuration and design drawing and load calculations with feasibility of the conceptual design. Based on ultimate condition and fatigue calculation results, mooring line confirmed excess capacity in the two conditions and overall installed cost was estimated to be reduced by 30% with further modification.

Figure. 1.4 *OO concrete star wind floater [14]*

1.3.2 5-MW-CSC Floater

The 5-MW-CSC concept was first proposed by NTNU PhD candidate Chenyu Luan, Postdoc Constantine Michailides, Dr. Zhen Gao and Prof. Torgeir Moan in an article "Modeling and Analysis of a 5 MW Semi-Submersible Wind Turbine Combined With Three Flap-Type Wave Energy Converters [15]" in 33rd International Conference on Ocean, Offshore and Arctic Engineering in 2014 and the project was performed within NOWITECH (Norwegian Research Centre for Offshore Wind Technology)third work package (WP3). Being one of the six work packages in NOWITECH research organization, the main objective of WP3 is to develop novel, cost-effective support structures and floaters for deep-sea wind turbines[16] led by Prof. Torgeir Moan from NTNU.

The 5-MW-CSC semi-submersible floater for a horizontal axis 5 MW wind turbine was one of the greatest achievements in WP3 and the proposed efficient analysis procedures in time domain and frequency domain for floating support structures has been a milestone. After a numerical analysis performed using Simo-Riflex-AeroDyn code focusing on the motion responses, mooring line tension and internal structural loads, an experimental test was carried out in collaboration between MARINTEK and NTNU in order to examine the performance of the floater. An experimental setup to simulate all the aerodynamic loads acting on wind turbine was proposed. Meanwhile, several actuators and load transfer mechanisms are under control by AeroDyn code. This approach is expected to improve the accuracy level of model test for offshore wind turbines.

The physical model of the 5-MW-CSC floater model druing model test can be referred to figure 1.5. It has been chosen as the floater model to carry out mooring system study in current thesis. Detailed dimensions and design strategy can be found in chapter 4.

Figure. 1.5 *5-MW-CSC substructure model test at scale 1:30. MARINTEK [17]*

1.4 Challenge and Motivation - Mooring System

Mooring system is meant for keeping floating structure in position which consists of freely hanging lines connecting the floater to anchors on the seabed. Mooring system design is a common challenge for all stationary offshore floating wind turbines especially when it comes to shallow water (50-100 meters). For one thing, the mooring system should be properly designed so that the natural periods for horizontal motion modes of the floater are sufficiently larger than the periods of most relevant waves. In addition, it should have enough stiffness to limit the offset of the floater under environmental force. The mooring system should limit the maximum platform motion in order to protect the power cable from taking large loads and bending moments. Furthermore, the mooring line should have enough ultimate strength during extreme environmental condition and sufficient fatigue life [18] under cyclic dynamic loading condition.

The challenges to design mooring system in shallow water includes:

1. The relationship between floater offset and mooring line tension becomes nonlinear after a linear part for smaller offsets. And the nonlinear performance in shallow waters becomes more critical than deep water. It could lead to large mooring line tension when the floater experiences large offset during harsh environmental condition, which could have the potential to exceed the capacity of mooring line.

2. Generally, when water depth decreases, the suspended mooring line length becomes short as well, which could influence the pretension directly. Therefore, mooring line material with larger distributed mass should be considered together with additional clump weight. This will increase the complexity of design and further installation work.

3. The degree of tightness of mooring system will influence tension increment trend as well. Normally, mooring system in shallow water will be designed to be soft on purpose in order to avoid large nonlinear tension increment. Yet, this will lead to less control over the floater motion range. To find the balance between tension control and motion control is another challenge to face during the design work.

Last but not least, the reliability of mooring system plays a quite important role in the wind turbine normal operation. The failure of mooring line could lead to considerable economic loss [19]. According to the research work from AMOG [20], single mooring line failure rate in offshore industry is $2.5 \times 10^{-}3$ per line every year since 2000, which roughly equals 0.02 facility every year. At the same time, the multiple lines failure probability in a single event is $3.5 \times 10^{-}3$ facility every year and corresponding frequency is 1 facility every 300 year. These two facility frequencies results shows that the mooring line failure rate in realistic industry is way from satisfactory. Being able to increase the reliability of mooring line would definitely contribute to the development of wind energy industry. In order to achieve that,

the factors that could lead to mooring line failure are of great interest to check, such as mooring system design return period, mooring system break strength and number of mooring lines. It is meaningful but challenging to draw the conclusion about in which way will these factors affect the mooring system performance and how to improve the mooring system design according to these discoveries [21].

1.4.1 Scope of the Thesis

Initially, the 5-MW-CSC semi-submersible floating wind turbine and corresponding mooring system was designed for 200 meter water depth. Motivated by the challenges and benefits discussed before, the main objective of this thesis is to design new mooring systems for 5-MW-CSC floater in 100 meter and 50 meter water depths, shallow water so to speak and perform relevant analysis to check their performances. Mooring system has been decided as the main research focus while the floater model is kept the same in three water depths and the existing mooring system design for 200 meter provides a good reference for comparison and evaluation to the two new design concepts.

The whole thesis could be summarized into two parts: Static design and dynamic analysis.

The static design work that has been carried out includes:

1. Perform preliminary static design of mooring system in 100 m and 50 m. Define mooring system configurations, key properties of mooring lines and corresponding clump weight.

2. Pretension, mooring line catenary shape and horizontal force-displacement relationship are main criteria to respect.

The dynamic analysis work that has been carried out includes:

1. Calculate hydrodynamic loads of the floater in 100 m and 50 m.

2. Perform free decay tests to document the natural periods of the floating wind turbine at 6 degrees of freedom with mooring system included.

3. Coupled time-domain dynamic analysis under extreme condition is carried out to check the performance of the mooring systems with respect to mooring line utilization factor and floater motion range.

4. Coupled time-domain dynamic analysis under operational condition is performed to document the wind turbine performance, floater motion range and fatigue damage to mooring lines and tower base.

5. Compare the performances of the three mooring systems. Sum up the discoveries of mooring system design in shallow water.

1.5 Analysis Software

Floating wind turbine is a complex system consisting of blade, nacelle, tower, floater and mooring system, which is exposed to complicated environment consisting of wind, wave and current etc. Combining the nonlinear and dynamic response from different parts in a coupled manner is the key prerequisite of the whole analysis. At the same time, nonlinear factors such as turbulent wind field, nonlinear wave, nonlinear structural behaviour make the coupled nonlinear dynamic analysis quite necessary.

In order to accomplish different sub-purposes, a number of software have been used in the modelling iteration, as well as in post-processing stage. A flow chart showing the relationship between different software sectors are illustrated in figure 1.6.

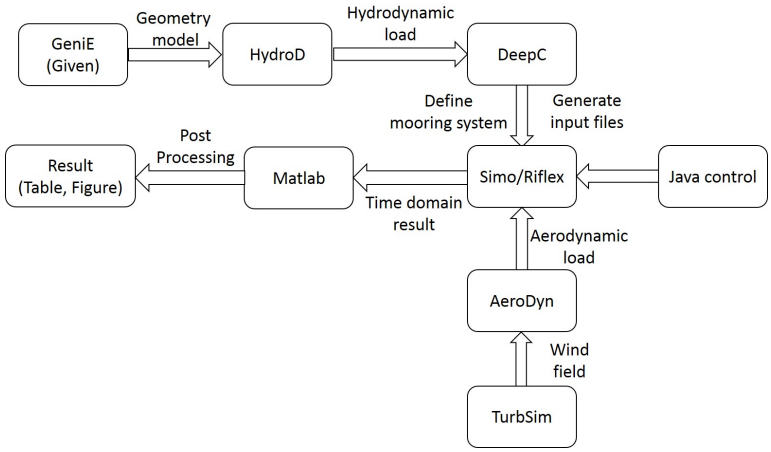

Figure. 1.6 *Software sectors and connections in current thesis*

At first, a 3D panel model of 5-MW-CSC floater built in GeniE was provided. Afterwards, the model was imported to HydroD in order to calculate the hydrodynamic properties of the floater in 100 m and 50 m. In the following, all the results from HydroD are inserted to DeepC to model the mooring system and calculate the retardation function as a preparation for time domain analysis. In addition, DeepC generates necessary input files for wave analysis in Simo/Riflex. As for wind, the wind field is generated by TurbSim for the use of AeroDyn where the aerodynamic force on blades and tower is calculated. Java control module takes control of the rotor speed and blade pitch angle. When the analysis is done by the coupling modules, the time-domain simulation result will be extracted by Matlab for post-processing The final results will be presented in the form of tables or figures.

1.5.1 HydroD

HydroD is an interactive application for ships and offshore structures to calculate hydrostatics, wave loads and motion response etc[22]. Wadam or Wasim are two suites meant for different computation purposes: Wadam uses Morison's equation and first and second order 3D potential theory for wave load calculations in frequency domain, while Wasim calculate 3D diffraction/radiation problem by a Rankine panel method in frequency domain or time domain.

Wadam module has been mainly used in current thesis. Wadam is a based on linear methods for marine hydrodynamic loads in frequency domain. It is an integrated part of the SESAM suite of programs which is designed to calculate wave loads on models created by SESAM preprocessors. 3D panel model is used to evaluate velocity potentials and hydrodynamic coefficients[23], which is based directly on the Wamit program developed by Massachusetts Institute of Technology. HydroD was also used to calculate the second order wave drift forces, which is done through far-field integration (momentum conservation). The final output files from HydroD could be summarized as:

1. Frequency dependent added-mass $A_{ij}(\omega)$ and damping $B_{ij}(\omega)$ as the solution to radiation problem.
2. First order wave excitation forces in forms of transfer function $H_i^D(\omega)$ as the solution to diffraction problem.
3. Mean drift coefficient $\bar{H}_I^{(2)}(\omega)$ as the result of far-field integration.

1.5.2 DeepC

DeepC is an interactive program in SESAM suite, which is used to model floating structures attached to the seabed with mooring systems. Nonlinear time domain finite element simulations are carried out in sub-program Simo and Riflex. The interface supports easy modelling and calculation. DeepC import input from HydrD/Wadam and reads all necessary hydrodynamic results from SESAM Interface File. Additional vessel data are defined directly from DeepC GUI together with mooring and riser system.

DeepC in this thesis is utilized to calculate retardation functions and model mooring system. After the input files are obtained from DeepC, manual modification is required before it is put into computation by Simo-Riflex-Aerodyn.

1.5.3 Simo-Riflex-AeroDyn (SRA)

Simo-Riflex-AeroDyn is developed by MARINTEK/CeSOS and has been used primarily for dynamic analysis of floating wind turbine systems. Three computer codes are coupled together in SRA: Simo, Riflex and AeroDyn.

Simo (Simulation of Marine Operations) is a time domain simulation program for multibody systems [24] which models the rigid body hydrodynamic forces and moments on the floater. It is typically applied for surface vessels and complex marine operations. In the present thesis, Simo is used for environmental modelling and it is able to include wind force from external subroutine. Riflex is based on a nonlinear FE formulation and models the mooring system, tower, shaft and blades as flexible beam elements [25]. Riflex features an extremely efficient nonlinear formulation applicable for irregular wave analysis where the hydrodynamic loading is described by the generalized Morison equation. AeroDyn handles the aerodynamic forces and moments on the blades based on the BEM or GDW theory.

The fully coupled aero-hydro-servo-elastic analysis makes links between separate modules. The local wind velocity from a turbulent wind field box generated by TurbSim is read through DLL to AeroDyn and the hydrodynamic loads on the floater and the aerodynamic loads on the wind turbine blades are passed to Riflex in which the dynamic equations of motions for the entire system are solved. The java control module takes contols of rotor speed and balde pitch angles according to mean wind speed at hub height. The different modules in combined Simo-Riflex simulation are run by a specific order: Riflex inpmod→ Simo stamod→ Riflex stamod→ Simo dynmod→ Riflex dynmod.

Additional modules for post-processing e.g. s2xmod and outmod are run subsequently. The details of the coupling between the codes could be referred to figure 1.7.

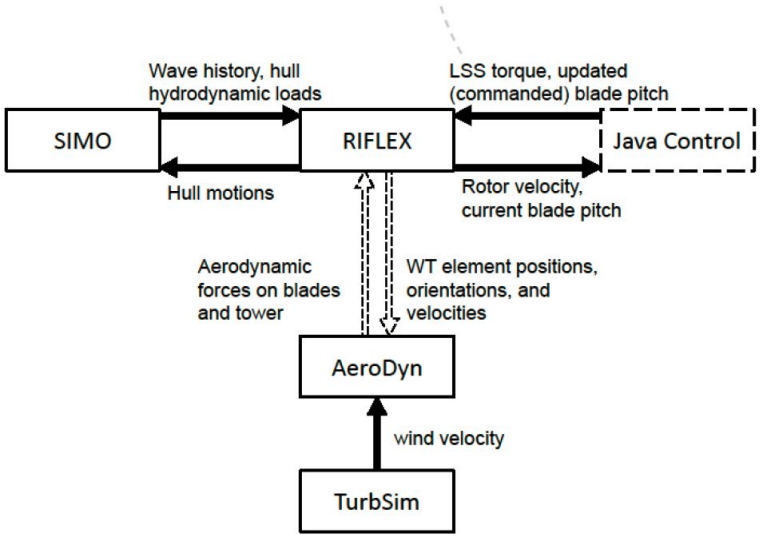

Figure. 1.7 *The coupling between Simo Riflex AeroDyn. MARINTEK [26]*

1.5.4 TurbSim

TurbSim [27] is used to generate full-field wind files which contains coherent turbulence intensity based on wind spectrum. It is a stochastic, full-field, turbulent-wind simulator. Time series of three-component wind-speed vectors in a two-dimensional vertical rectangular grid is produced by a statistical model. TurbSim reads input file where mean wind speed, random wind seed and turbulence intensity etc are defined to execute the simulation. Following IEC guidelines[28], there are several turbulence models available: Normal turbulence model, Extreme turbulence model, Extreme operating gust etc. The wind file generated by TurbSim can be further utilized as input into AeroDyn-based codes.

2 Theory

The hydrodynamic theory described in this chapter is mainly referred to the book "Sea loads on ships and offshore structures" by O. M. Faltinsen [29]. The aerodynamic theory is based on the book " Aerodynamics of Wind Turbines" by Martin O. L. Hansen [30].

Exposed to offshore environment, floating wind turbine experiences complicated loading conditions with a number of possible load combinations with change in time and space. The prerequisite of an accurate structural analysis is to predict the loading sources. Several possible load sources are illustrated in figure 2.1, such as: low-level jet, turbulent wind, icing, lightning, wave, tide, ship impact, current, earthquake, scour, soil mechanics, self gravity and buoyancy etc.

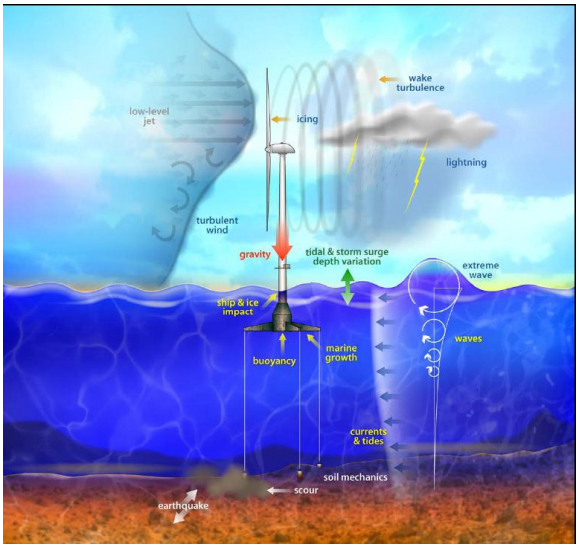

Figure. 2.1 *Offshore wind turbine loading sources [31]*

2.1 Floating Wind Turbine Hydrodynamics

Wave induced force is the most significant loading acting on the floater, which could be the main cause of fatigue and extreme responses. Wave loading models in regular and irregular type provide the fundamental hydrodynamic analysis. Time domain theory is used to simulate ambient wave elevation [31] which takes free surface memory effects into account. The resulting wave loads is the integration of dynamic pressure of wetted surface of the platform. In addition, inertia (added mass), linear drag (radiation), buoyancy (restoring), incident wave scattering (diffraction), current and nonlinear viscous drag effects are included as well.

2.1.1 Linear Wave

Basically, the hydrodynamic analysis carried out in this thesis is based on potential theory (also called Airy wave theory) and the basic assumptions are that the fluid is inviscid and incompressible and fluid motion is irrotational. Sea environment is assumed to be a horizontal sea bottom with a free-surface of infinite horizontal extent.

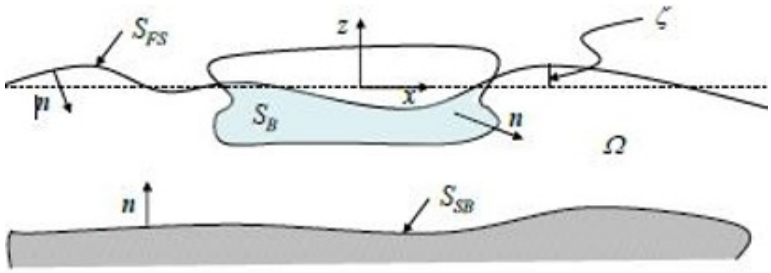

Figure. 2.2 *Linear wave theory [31]*

There is a velocity potential which represents the fluid motion satisfying Laplace equation:

$$\bigtriangledown^2\phi = \frac{\partial\phi^2}{\partial x^2} + \frac{\partial\phi^2}{\partial z^2} = 0 \tag{2.1}$$

Sea-bottom kinematic condition: Impermeability condition on sea bed.

$$\frac{\partial\phi}{\partial n} = 0 \qquad\qquad S_{SB} \tag{2.2}$$

Body kinematic condition: Impermeability condition on body.

$$\frac{\partial\phi}{\partial n} = V_B.n \qquad\qquad S_B \tag{2.3}$$

The relevant boundary conditions are linearised and the free surface condition can be obtained as:

$$(\frac{\partial \phi^2}{\partial x^2} + g\frac{\partial \phi}{\partial z})|_{z=0} = 0 \tag{2.4}$$

Assuming deep water condition and wave propagates in positive x direction, we can obtain the solution for velocity potential as

$$\phi = \frac{g\zeta_a}{\omega} e^{kz} cos(\omega t - kx + \gamma) \tag{2.5}$$

Where

- ζ_a: Wave amplitude
- d: Water depth
- ω: Angular frequency
- k: Wave number
- γ: Arbitrary phase angle

As long as the velocity potential is available, the particle velocities, accelerations can be found by differentiating the particle velocities.

2.1.2 Irregular Wave

In order to describe the real sea state in a more reasonable manner, a random irregular wave is needed. By superimposing separate linear regular waves with different heights, frequencies, directions and phase angles. The one-dimensional wave elevation can be expressed as:

$$\zeta = \sum_{j=1}^{N} A_j sin(\omega_j t - k_j x + \varepsilon_j) \tag{2.6}$$

Where

- A_j: Wave amplitude
- ε_j: Phase angle, uniformly distributed between 0 and 2π and remain constant

The wave amplitude A_j can be expressed by a wave spectrum as:

$$\frac{1}{2} A_j^2 = S(\omega_j) \triangle \omega \tag{2.7}$$

Where

- $\triangle\omega$: Difference between successive frequencies
- A_j: Harmonic wave component, generated by Fast Fourier Transform (FFT)

- $S(\omega_j)$: Wave spectrum, description of sea surface and frequency energy contribution

The wave spectrum is the frequency domain representation of the waves and can be estimated from wave measurements. The commonly used wave spectrum - "Joint North Sea Wave Project (JONSWAP)" is a great representative of North Sea. A sea state can be uniquely described in terms of significant wave height H_s, the peak period T_p and a peakedness parameter γ.

The JONSWAP spectrum can be written as:

$$S_\zeta(\omega_k) = \frac{5.061 H_s^2 (1 - 0.287 ln\gamma) g^2}{T_p^4 \omega_k^5} exp[-1.25(\frac{2\pi}{T_p \omega_k})^4]\gamma^Y \tag{2.8}$$

Where

$$Y = exp[-\frac{(\frac{T_p \omega_k}{2\pi} - 1)^2}{2\sigma\omega^2}] \tag{2.9}$$

and

$$\sigma = \begin{cases} 0.07 for T > T_p \\ 0.09 for T < T_p \end{cases} \tag{2.10}$$

2.1.3 First Order Wave Forces

The linear first order wave body interaction problem could be split into two terms:

$$F_i^{Waves,(1)} = \underbrace{F_i^R}_{\text{Radiation}} + \underbrace{F_i^D}_{\text{Diffraction}} \tag{2.11}$$

- Diffraction problem: the body is fixed and interacting with incident waves;
- Radiation problem: the body is forced to oscillate, no incident waves.

Based on linear theory, the velocity potential ϕ could be written as:

$$\phi(x,y,z,t) = \underbrace{\phi_0(x,y,z,t)}_{incident\,wave} + \underbrace{\phi_D(x,y,z,t)}_{diffration} + \underbrace{\phi_R(x,y,z,t)}_{radiation} \tag{2.12}$$

Diffraction

The diffraction problem consists of two velocity potentials: $\phi_0(x,y,z,t)$ is the potential for the incident waves and $\phi_D(x,y,z,t)$ is the diffraction potential. The total excitation forces are obtained from integrating the incident wave dynamic pressure and the diffraction dynamic pressure over the mean wetted surface of the body:

$$F_{exc,k}(t) = -\int_s \frac{\partial \phi_0}{\partial t} n_k dS - \int_s \frac{\partial \phi_D}{\partial t} n_k dS \tag{2.13}$$

Where $k = 1.2...6$ stands for the degree of freedom.

The solution to the diffraction problem is obtained in the frequency domain by the use of HydroD in this thesis. The wave excitation loads are given in terms of force and moment transfer functions:

$$F_i(\omega_k, \beta) = H_i(\omega_k)\tilde{\zeta}(\omega_k) \tag{2.14}$$

Where

- $H_i(\omega_k)$: Complex first order wave force transfer function
- $\tilde{\zeta}(\omega_k)$: Complex harmonic wave component

In order to represent the forces for an irregular wave field and in time domain simulations, a transformation using inverse Fourier transform applied to the transfer function in equation 2.14:

$$h_i(\tau) = \frac{1}{2\pi}\int_{-\infty}^{\infty} H_i(\omega)e^{i\omega\tau}d\omega \tag{2.15}$$

As a result, the excitation load is expressed as the convolution between h_i and ζ.

$$F_i^t = \frac{1}{2\pi}\int_{-\infty}^{\infty} h_i(\tau)\zeta(t-\tau)d\tau \tag{2.16}$$

It is clear to see that the wave excitation forces do not depend on the floater motion, which means the wave excitation forces can be pre-calculated before time simulation.

Radiation

The radiation problem is related to hydrodynamic loads on the body due to forced oscillations of the body in six degrees of freedom. The radiation problem is involved with ϕ_R and hydrostatic pressure while the integration gives the added mass, potential damping and restoring force.

The radiation problem can be expressed as:

$$F_R(t) = \sum_{k=1}^{6} -A_{jk}\ddot{\eta_k}(t) - B_{jk}\dot{\eta_k}(t) - C_{jk}\eta_k \tag{2.17}$$

Where

- $j = 1....6$: Degree of freedom
- B_{jk}: Potential damping coefficient
- C_{jk}: Linear restoring coefficient

The solution to radiation problem could be written as:

$$\phi_R(x, y, z, t) = \Re(\sum_{k=1}^{6} \dot{\eta}_k\varphi_k(x, y, z)) \tag{2.18}$$

Where $\varphi_k(x, y, z)$ is the complex spatial velocity potential. At the same time, A_{jk} and B_{jk} can be split into a summation of the asymptotic values at infinite frequency ($A_{\infty,jk}$ and $B_{\infty,jk}$) and their frequency dependent parts ($a_{jk}(\omega)$ and $b_{jk}(\omega)$):

$$A_{jk}(\omega) = A_{\infty,jk} + a_{jk}(\omega) \tag{2.19}$$

$$B_{jk}(\omega) = B_{\infty,jk} + b_{jk}(\omega) \tag{2.20}$$

The asymptotic value $B_{\infty,jk}$ of the potential damping can be set to zero [31]. By taking the inverse Fourier transform of the radiation forces in the frequency domain, the total force can be described in time domain by:

$$F_j^R(t) = -A_{\infty,jk}\ddot{\eta_k} - \int_0^t h_{jk}(t-\tau)\dot{\eta_k}(t)d\tau \tag{2.21}$$

Where $h_{jk}(\tau)$ is the retardation function found from a transform of the frequency-dependent added-mass and damping:

$$\begin{aligned} h_{jk}(\tau) &= \frac{1}{\pi}\int_0^\infty [b_{jk}(\omega)cos\omega\tau - \omega a_{jk}(\omega)sin\omega\tau]d\omega \\ &= \frac{2}{\pi}\int_0^\infty b_{jk}(\omega)cos\omega\tau d\omega = -\frac{2}{\pi}\int_0^\infty \omega a_{jk}sin\omega\tau d\omega \end{aligned} \tag{2.22}$$

The term involving potential damping is used in Simo to calculate the retardation functions.

By checking the retardation force term $-\int_0^t h_{jk}(t-\tau)\dot{\eta_k}(t)d\tau$ in equation 2.21, we could find out that the history of the motion in all the previous time steps needs to be accounted for when calculating. The total retardation force F_j at time t can be regarded as the summation of the part force impulse responses from all the previous steps value at time t, which is named as the memory effect.

2.1.4 Second Order Wave Forces

For first-order solution, the loads/motions have zero mean value and oscillate with the frequency of the incident waves where the superposition principle is valid. When incident waves become steeper, the higher order effect become more important in estimating the loads and motions. The second-order contributions to the total loads are more difficult to estimate, both experimentally and numerically, since they are relatively small to the first-order contributions. But they may cause resonance excitation due to difference and sum frequency effects which is worthy consideration to several types of structures. The second-order effects caused include: a mean value, a difference wave-frequency oscillatory behaviour and a sum wave-frequency oscillatory behaviour. Slow drift motion can be caused by second order difference frequency effect, which for moored platforms will induce resonant motion in surge, sway and yaw.

In order to calculate the forces acting on a marine structure taking second-order effect into account, there are two methods available:

Direct Pressure Integration

Integrate the pressure along the instantaneous wetted surface of the body

$$F = \int_{S_B} p\mathbf{n}dS \tag{2.23}$$

where p stands for the pressure with expression as:

$$p = -\rho g z - \rho\frac{\partial\phi_1}{\partial t} - \rho\frac{\partial\phi_2}{\partial t} - \rho\frac{1}{2} \bigtriangledown \phi_1 \bigtriangledown \phi_1 \tag{2.24}$$

From the expression of the pressure, the contribution from the first order quantity and second order quantity are separated from each other.

Conservation of Fluid Momentum

The force is calculated by keeping the fluid momentum within a fluid volume constant:

$$F = -\frac{\mathrm{d}}{\mathrm{d}t}(\int_\Omega \rho V d\Omega - \int_{S-S_B} pndS - \int_\Omega \rho g k d\Omega - \int_S \rho V(V_n - U_n)dS) \tag{2.25}$$

The second method with volume integrals is more complicated than first method. However, when it comes to the calculation of the mean loads, the integrals can be simplified on a far-field control surface which can be estimated more simply and correctly.

2.1.5 Viscous Damping

Potential theory is based on the assumption of inviscid fluid which is not true for realistic sea environment. Viscous effects can contribute to large loads and induce damping to the platform motions. The damping term in equation 2.17 only takes the potential damping into account, which indicates the wave generation ability. When it comes to long waves, the generating wave is small which means the potential damping is small. As a result, the resonance could cause large amplification of the motion which lead to the viscous forces become dominating. The region of the dominating force could be found in figure 2.3.

An important viscous load is the drag force which works in-line with the incident wave and current direction in the cross-sectional plane. The force is caused by flow separation and shear stress along the body surface. The effect will be included by the quadratic drag term in the Morison equation. The drag force for a fixed cylinder with a diameter D could be written as:

$$dF_{drag} = \frac{1}{2}\rho C_D D \left|u - \dot{\eta}\right| (u - \dot{\eta}) \tag{2.26}$$

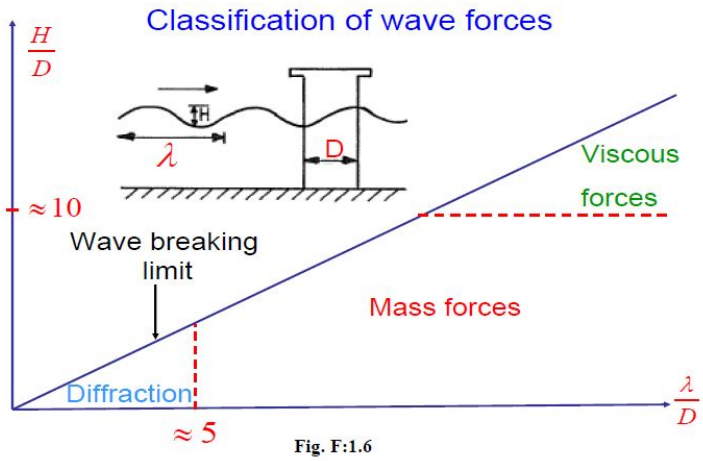

Figure. 2.3 *Classification of wave forces [32]*

2.2 Floating Wind Turbine Aerodynamics

Wind turbine rotor, nacelle and tower are subjected to aerodynamic loads, where the loads acting on nacelle and tower can be defined as drag force, while the force on rotor consists of both lift and drag force. Aerodynamic forces on the rotor can be calculated with different detail level of accuracy: one-dimensional (1-D) momentum balance models, vortex and panel methods and full 3-D blade structure with a Navier-Stokes's solution[2] etc. There are some intermediate methods which are able to model the dynamic effects and aerodynamic loads with acceptable accuracy and reasonable computation time. In general, two typical models are available for modelling wind turbine: Blade Element Momentum (BEM) and Generalized Dynamic Wake (GDW).

In current thesis, AeroDyn code is used to calculate relevant aerodynamic loads utilizing both BEM theory and GDW theory mainly depending mean wind speed. BEM method is used when the mean wind speed is below 8 m/s, otherwise GDW method is switched to by taking advantage of its inherent settings.

2.2.1 Blade Element Momentum Theory

Blade element momentum theory is currently widely used because of its efficient computation time. BEM theory is illustrated by breaking the blades of wind turbine into many elements along the span. When the elements rotate in rotor plane, the annular region it passes is regarded as the place momentum is kept balance. Since the blades and tower are slender structures and the span-wise velocity component is much lower than the stream-wise component, it assumes that the forces at

a specific point on the blades can be calculated based on two-dimensional aerodynamic properties, with lift force, drag force and pitching moment on each element. The lift and drag coefficients are defined as:

$$C_L(\alpha) = \frac{f_L}{\frac{1}{2}\rho V_{rel}^2 c} \tag{2.27}$$

$$C_D(\alpha) = \frac{f_D}{\frac{1}{2}\rho V_{rel}^2 c} \tag{2.28}$$

$$V_{rel} = V\sqrt{(1-a)^2 + (\frac{r\Omega_r}{V}(1+a'))^2} \tag{2.29}$$

$$\alpha = \phi - \beta \tag{2.30}$$

$$tan(\phi) = \frac{V}{r\Omega_r}\frac{1-a}{1+a'} \tag{2.31}$$

Where

- f_D: Drag force per length
- f_L: Lift force per length
- c: Chord of the airfoil
- ρ: Air density
- α: Attacking angle
- V_{rel}: Relative velocity
- a: Axial induction factor
- a':Rotational induction factor

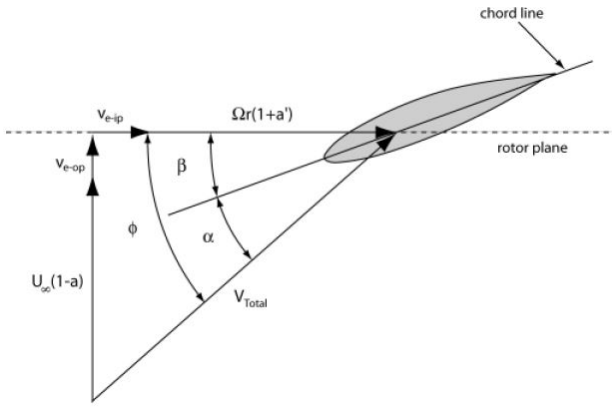

Figure. 2.4 *Local element velocities and flow angles*

Because of the simplicity of the assumption, several inaccuracies are introduced into the theory. For example, the flow over the blades is assumed to be in equilibrium all the time, which disregards the dynamics of the wake. Dynamic wake can be implemented in BEM code via filter for induced velocities. In addition, pressure gradients in the span-wise direction of the blade are ignored and this can make a difference when the tip speed ratios are high. Therefore, in practice, several corrections are applied to make up for the assumptions, such as tip loss, hub loss, high induction factor, skewed wake correction, dynamic stall and dynamic inflow. Moreover, when the deflection of the blade is quite large, BEM theory is no longer valid.

2.2.2 Generalized Dynamic Wake Theory

Generalized dynamic wake theory was initially developed from helicopter theory and is based on potential flow solution of Laplace equation[33]. As notified in the name, GDW takes the wake dynamics into account when inflow angle changes by implementing a time lag in the induced velocities which is created by blades shedding vorticity and being convected downstream. In addition, tip loss, dynamic stall and skewed wake are inherent in GDW. The pressure and induced velocity are solved as infinite series of Legendre functions and Trigonometric functions. The GDW method can achieve a more general pressure distribution on rotor plane by including many flow states.

Even though, GDW method has limitations. It is not valid for highly loaded rotors and low wind speed, when turbulent wake state is approached. Moreover, wake rotation is not inherently included and large aeroelastic deflections or significant coning of rotor blades on wake aerodynamics has not been accurately modeled.

2.2.3 Structural Dynamics Aeroelasticity

Wind turbine structure usually consists of several slender bodies with big difference of dimensions between different components. In order to estimate the response of blades and tower, aero-elasticity should be considered by carrying out simultaneous calculations of aerodynamic loads and the responses of the structure which is modelled as beam elements because of flexible natural modes of tower and blades. The aerodynamics of the turbine system is represented by a thrust force acting on the top of the tower. The thrust can be expressed as:

$$T_H(t) = \frac{1}{2}\pi\rho_a R^2 C_T(U_{rel}(t))U_{rel}(t)|U_{rel}(t)| \tag{2.32}$$

Where

- R: Radius of the rotor
- C_T: Thrust coefficient

- ρ_a: Density of air
- $U_{rel}(t)$: Relative velocity between wind and rotor hub

With application of Euler-Bernoulli beam theory [34] and local to global coordinate system transformation, the dynamic structural equilibrium of a beam element equation can be represented as as the equation of load balance (dF) and moment balance (dM) for each structural component:

$$(\int_a \rho dA\ddot{r})dy = dF + (\int_a \rho dAg)dy + \delta P dy \tag{2.33}$$

$$(\int_a \rho dAr_p \times \ddot{r})dy = dM + dr_e \times (F + dF) + (\int_a \rho dAr_P \times g)dy + r_a \delta P dy \tag{2.34}$$

Where

- A: Cross section
- dy: Width
- δP: Vector of external aerodynamic forces per unit length

In operational condition where the blades are rotating, the aerodynamic forces on wind turbine is quite larger than the force on tower. However, during the extreme condition where the wind turbine is under parked condition, the force acting on blades turns out to be quite smaller compared with the force on the tower. As a result, a drag force standing for the force on the tower is presented as:

$$F_H(t) = \frac{1}{2}\rho_a C_D A U^2_{rel(Z^*)}(t) \tag{2.35}$$

Where

- C_D: Drag coefficient for tower cross section
- $U_{rel(Z^*)}$: Relative velocity between wind and tower

2.2.4 Wind Field

Wind field is a stochastic process that is randomly distributed in time and space. A structure under the influence of wind will experience static wind force as well as dynamic wind force. The wind speed can be divided into a time-independent static velocity and a time-dependent fluctuating velocity. The total velocity in terms of height and time can be expressed as:

$$U(z,t) = U(z) + u(z,t) \tag{2.36}$$

A typical description of the wind speed is shown in figure 2.5. The mean wind speed U_z increases with the height above the sea surface as can be found out in

the figure, while the turbulent component $u_{z,t}$ is defined with a zero expectation value and fluctuate around the mean velocity. The mean wind force will give rise to a steady-state wind force, while the turbulent wind force may excite resonant slow drift motion specially for a moored structure. A simple mean wind velocity

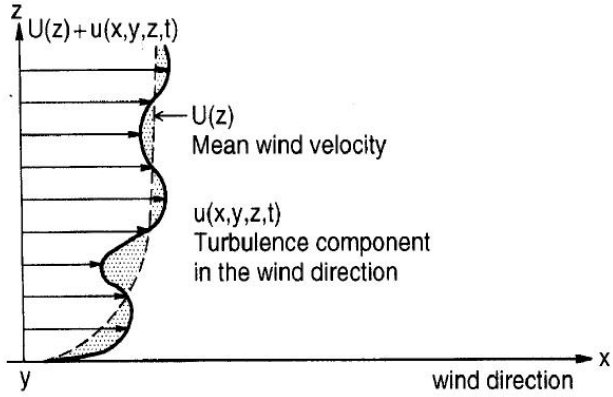

Figure. 2.5 *Wind shear [35]*

model recommended in IEC standard can be written as:

$$U_0(z) = U_0(z_0)(\frac{z}{z_0})^{\alpha} \tag{2.37}$$

For standard wind turbine classes, according to IEC 61400-1, the value for the exponent α should be set to 0.2 for onshore turbine and 0.14 for offshore turbine [36], which is influenced by the surface roughness and atmospheric stability.

Just like the wave spectrum, wind spectrum is utilized to expresses how the energy of the wind turbulence is distributed between different frequencies. The wake effect is taken into account as well [37]. In IEC 61400-1 standard, two turbulence models are provided for the wind spectrum: Mann model and Kaimal model [36]. The Kaimal model is used in TurbSim [27] for generating wind time series. The expression of Kaimal wind spectrum is written as:

$$S_w(f) = 4\sigma_w^2 \frac{L_k/V_{Hub}}{(1+6f\frac{L_k}{V_{Hub}})^{\frac{5}{3}}} \tag{2.38}$$

Where

- V_{Hub}: Mean wind speed at the hub
- f: Frequency
- σ_W: Wind speed standard deviation

- L_k: Length scale parameter, depending on the height of the hub

$$\sigma_u = I_{ref}(0.75V_{Hub} + 5.6) \tag{2.39}$$

and

$$L_k = \begin{cases} 5.67Z, forz < 60m \\ 340.2, forz > 60m \end{cases} \tag{2.40}$$

Since the main task studied in this thesis is the mooring system of the floating wind turbine rather than the response of the blades and the turbine itself. Therefore the research priority is given to the hydrodynamic analysis rather than aerodynamic analysis.

2.3 Coupled Dynamic Time-domain Analysis

Taking the current study objective - offshore floating wind turbine into account, factors such as turbulent wind field, nonlinear wave loading, nonlinear structural behaviour and servo control make it necessary to carry out fully coupled aero-hydro-servo-elastic analysis to capture the nonlinear responses [38]. Therefore fully coupled time-domain analysis is recommended.

Offshore floating wind turbines are constructed to operate in harsh environments and the main sources of the loads acting on the floater include wave, wind, and current. The total force vector for a rigid platform with catenary mooring system and a turbine in a coupled model, contains non-linear restoring, inertia and damping from mooring lines, wave forces, wind forces and inertia and damping forces from the turbine can be expressed by:

$$F(t) = F^{Mooring}(t) + F^{Waves}(t) + F^{Wind}(t) + F^{Turb}(t) \tag{2.41}$$

All the forces are functions of floater motions, velocities and acceleration, in addition to time. The hydrodynamic loads mainly come from first order and second order wave forces together with viscous effects. The aerodynamic loads acting on the nacelle and the tower are primarily drag forces, which are easily modelled. However, both lift and drag forces are important for rotor, which could be calculated using Blade Element Momentum (BEM) method and Generalized Dynamic Wake (GDW) method. The aerodynamic and hydrodynamic loads and corresponding structural responses are considered simultaneously in the coupled time-domain analysis, including the wind turbine controller.

The solution in time domain can be obtained by dividing the time period into a number of time steps and perform equilibrium iterations at each time step. Every sub-solution is calculated by utilizing the start condition from previous time step and assuming a new motion pattern, which will make the solution become the start condition for the following time step. The practical time-domain analysis has

been carried out in agreement with Newton-Raphson equilibrium iteration which recalculating the tangential mass, damping and stiffness matrices at each iteration cycle. The solution provides a quadratic convergence rate which is based on modified Euclidean displacement norm as a criterion to make sure the summation of displacements is below a certain acceptable value.

The numerical integration solution is based on Newmark β-family methods. The velocity and displacement at time step $t + \Delta\tau$ is calculated as:

$$\dot{r}_{t+\Delta\tau} = \ddot{r}_t + (1-\gamma)\ddot{r}_{t+\Delta\tau}\Delta\tau + \gamma\ddot{r}_{t+\Delta\tau}\Delta\tau \tag{2.42}$$

$$r_{t+\Delta\tau} = r_t + \dot{r}_t\Delta\tau + (\frac{1}{2} - \beta)\ddot{r}_t\Delta\tau^2 + \beta\ddot{r}_{t+\Delta\tau}\Delta\tau^2 \tag{2.43}$$

Where β and γ are setting parameter, while $\Delta\tau$ stands for the time step increment.

The main benefits of this method is that the phases between wind and wave excitations and structural responses are reasonably considered. Meanwhile, all sources of damping, e.g. aerodynamic, hydrodynamic, soil and structural damping can be included correctly. Moreover, the variation of wind turbine loads due to the change of rotor speed or blade pitch angle through the controller could be properly considered as well, which improve the analysis result to a great extent[1].

3 Mooring System

When the floating wind turbine is displaced away from the equilibrium position due to wind and wave forces, mooring system will operate to keep it in position. Precise positioning and long term motion control of the floating wind turbine is critical for relevant operations. Station-keeping system is required to restrict the horizontal excursions of floater within acceptable limits, as well as to provide directional control since the orientation of wind turbine is important for operational considerations. In order to provide enough restoring forces, mooring system, dynamic positioning (DP) system or a combination of these two could be utilized. In the perspective of economy, mooring system is much more cost efficient compared with other methods [39] and it has been widely utilized in floating wind turbine.

3.1 Introduction

Mooring system is usually made of several lines with several possible material components (chain, wire or synthetic rope) with upper ends attached to the fairlead on the floating structure and lower ends anchored at the seabed. Mooring lines are constructed by steel chain, rope or a combination of both. Normally, it is suggested to use multi-component mooring line which is composed of two or more different materials in order to get a heavy chain at the sea bed and a lighter rope close to the water surface to fulfil different purpose. This results in an optimal combination of stiffness to limit the range of offset and total weight of mooring line at the same time.

The tension forces in the lines are dependent of the self-weight of the mooring line. In addition, clump weight or buoyancy element could be used to adjust the restoring force and mooring line catenary shape by attaching to mooring lines [40]. Rich experience in designing mooring systems for offshore floating oil and gas platform offers abundant knowledge to the mooring system design for floating wind turbine.

In current industry, typical types of mooring systems could be categorized as:

I. Catenary Line Mooring

It is the earliest and most common mooring systems that are used in current industry. The restoring force is obtained by lifting and lowering the weight of the mooring line in the static perspective. This leads to a hard spring system with a force increasing more than directly proportional to the displacement. In a spread mooring system, several mooring lines are uniformly arranged around the floating structure to keep it in position. For the anchor which is placed on the seabed, it could be easily moved, which means that it could not stand too large vertical force. It is of great meaning to save a significant part of anchor line lying on the seabed to avoid the mooring line is totally lifted up and this is usually regarded as the design criterion to define the total length of the mooring line [41]. It is necessary to note that the part lying on the seabed does not provide restoring force and only the part suspended in the sea water produces stiffness to limit the possible offset. The restoring forces are generated by the self-weight of suspended mooring line. Moreover, the movement of the seabed part on seabed could lead to friction force against the seabed.

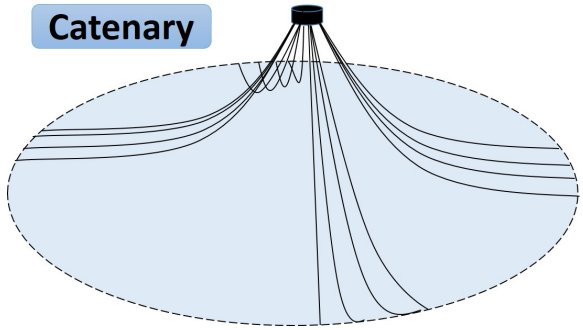

Figure. 3.1 *Catenary line mooring system*

II. Taut Line Mooring

Taut line system consists of a pattern of taut, light-weight lines spreading outward. Taut lines have a relatively low net submerged weight, which means that the catenary properties of the line could be ignored. The restoring force depends on the horizontal displacement from elastic stretch of the line itself. The most common line material used is synthetic fibres. The major difference between a catenary mooring and a taut leg mooring is the position where the mooring line attaches at the seabed horizontally. Taut leg mooring arrives at the seabed at an angle, which means that the anchor have to undertake both horizontal and vertical forces, while for catenary mooring, the anchor is only subjected to horizontal forces [42]. The restoring forces are generated by the elasticity of the mooring line for taut line mooring. Compare taut leg mooring with catenary mooring, there is an advantage of taut line, which is the smaller footprint, i.e. the mooring radius of the taut line

is smaller than the catenary line for a similar application. This could result further in reduction of material quantity, cost and weight of the total mooring system, etc.

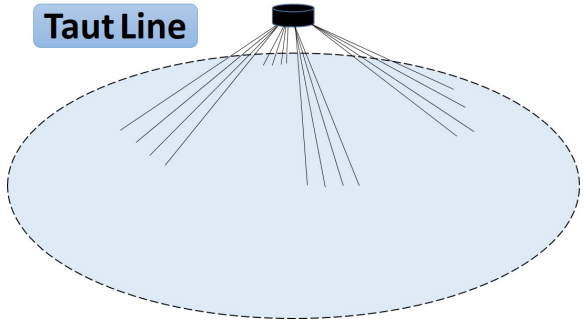

Figure. 3.2 *Taut line mooring system*

III. Tension Leg Mooring

Tension leg mooring system is specially used for tension leg platforms (TLP). Since the buoyancy of the platform exceeds its weight which leads to a downward extra force balanced by the vertical tensioned mooring lines, complied by dead-weight or anchor piles. Total restraint against vertical movements of the platform is guaranteed by these tensioned line. Horizontal component of the mooring line tension function when the floating structure is displaced from its equilibrium position [26]. The pre-tension in the line is often obtained by the use of winches on the floating structure. The winches pull on the cables to get access to the desired cable configuration with different line shape. Since the mooring lines are exposed to unsteady environmental loads, the tension in the mooring line become various as a result. The mooring lines should have an effective stiffness combining the motions of the structure to introduce forces depending on the mooring line characteristics and limit the horizontal motion of the floating structures.

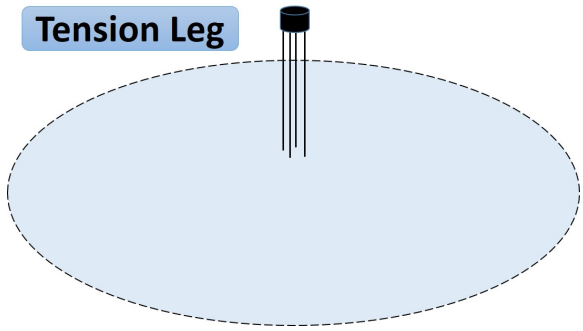

Figure. 3.3 *Tension leg mooring system*

3.2 Mooring Line Material

The most popular mooring line materials that are currently in use in floating offshore structures are chain, wire rope and synthetic fiber rope. Chain is considerably most popular with over half usage of all semi-submersibles for station keeping. In floating production systems, the use of wire rope in combination with chains is popular. The advantage of the combination of wire and chain is to take full use of different advantages of each material type.

To be more precise, chain provides weight and catenary effect while the wire rope provides greater elasticity and significantly reduced cost per unit length. As a result, optimal performance in a wide range of water depths could be achieved by using a combination of wire and chain. For example, the use of chain wire combination can provide initial catenary stiffness with the chain segment and then fulfil high tension requirement through the elasticity of the wire rope. On the other hand, in deeper waters, the use of wire rope could help to reduce the vertical loads and the use of chain at the touchdown avoids bending tension loads on the wire rope. For the same reason, chain material is preferred to wire ropes at the fairleads. As offshore structures and activities go towards deeper water, the benefits of wire moorings will become increasingly apparent. On this point, man-made fibres have the potential to play an increasingly important role in the future because of their superior strength to weight ratios.

3.2.1 Chain

General

Chains are rolled steel bars with the shape of links. The joint in each link is flash butt-welded. There two configurations of the chain link, which are studlink and studless chain. The studlink chain is most commonly used for mooring system which is to going to be reset several times during the service life, while the studless chain is often used for permanent mooring system. The industrial experience shows that the seat of the studs have been considered as the start point for fatigue cracking, which bring studless chain concept up with better fatigue performance.

Five different steel grades of chain are currently in use in the offshore industry. Based on different yield strengths of the steel that are used, different grades of chains are distinguished. The International Association of Classification Society denotes the steel grades with a R followed by a number. Offshore Standard DNV-OS-E302 [43] provides the minimum mechanical properties for the five steel grades listed in Table 3.1. Meanwhile, NS-EN 1993-1-1 [44] standard is only applicable for normal steel with yield stress up to 460 MPa, i.e. $R3$. Additional standard NS-EN 1993-1-12 [45] is applicable for high-strength steel with yield stress up to 700 MPa, i.e. $R3S, R4, R4S$. Grade 5 chain, $R5$ is a even stronger steel with yield strength of 760 MPa, which is about 8.6% increase over $R4S$ and 30% over $R4$.

Table. 3.1 *Minimum mechanical properties for chain cable materials [43]*

Steel grade	Yield stress $[MPa]$	Tensile strength $[MPa]$	Elongation [%]
$R3$	410	690	17
$R3S$	490	770	15
$R4$	580	860	12
$R4S$	700	960	12
$R5$	760	1000	12

Property

Weight and stiffness properties of chain are independent of grade certification. For a mooring line with chain nominal diameter D, the submerged weight per unit length w and axial stiffness per unit length AE of chain are two basic parameters [46].

$$Submerged\ weight\ per\ unit\ length,\ w = 0.1875D^2\ N/m\ (D\ in\ mm) \tag{3.1}$$

$$Axial\ stiffness\ per\ unit\ length,\ AE = 90000D^2\ N\ (D\ in\ mm) \tag{3.2}$$

The stiffness and submerged weight of studless chains are approximately 10% less than those for stud chain of the same diameter.

Breaking strength of chain is a highly uncertain parameter because chain is a series system and the weakest link in the line will determine the strong level of the mooring line. As a result, an extremely high degree of uniformity of chain link strength in order to equate link strength with chain strength is crucial. A majority of the mooring codes link the safety factor requirement to the catalogue break strength (CBS) and proof load. Equation followed defines the CBS and proof load for different grades of stud or studless chain:

$$CBS\ or\ proof\ load = c(44 - 0.08D)D^2\ N\ (D\ in\ mm) \tag{3.3}$$

Where the factor c is selected according to the material grade and whether the CBS or proof load is required. Detailed value could be found in table 3.2. Some experimental data of CBS or proof load is available on some handbooks and manuals, such as "Anchor Manual [42]" from Global Maritime. It provides the practical data for chain with different dimensions and material grades.

Table. 3.2 *Minimum mechanical properties for chain cable materials [43]*

Grade	C value	
	CBS	Proof Load
3	22.3	14.8
3S	24.9	18.0
4	27.4	21.6
5	25.1	31.9

3.2.2 Wire Rope

General

There are three wire rope constructions that are currently used in the mooring application, which are: six strand, spiral strand and multi strand. Among these three, six strand independent wire rope core (IWRC) is the most popular construction for mobile drilling units because of its lateral flexibility and relative cost benefit. Meanwhile, spiral strand construction is more commonly utilized in floating production systems, where it shows great longitudinal stiffness, torque balance and lower spinning loss performance. Multi strand rope construction is not commonly used in offshore industry. Compared with chain, wire rope has a lighter weight and a higher elasticity for same breaking load. Generally wire rope is more prone to damage and corrosion than chain.

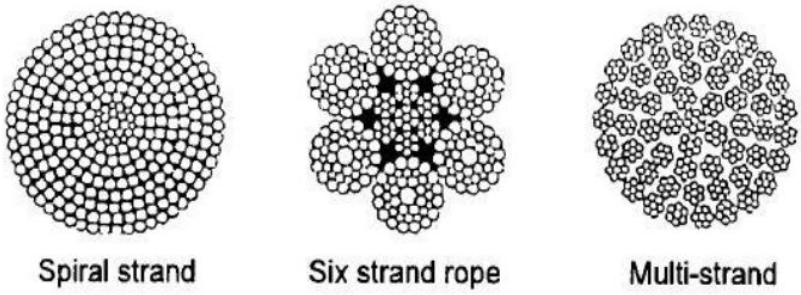

Figure. 3.4 *Typical wire rope constructions*

Property

The weight and stiffness of wire ropes are influenced not only by rope construction but also on the manufacturer's professionalism. Generally, different construction types depend on the nominal diameter of the rope. It is meaningful to notice that the wire rope tends to decrease its stiffness with age after long period of usage, which leads to some uncertainty in the stiffness values to be used in analysis. Multi strand ropes tend to have higher stiffness than spiral strand. The breaking strength is dependent on the construction of the rope and the grade of steel used.

Moreover, when a steel wire rope of a given specification is ordered, the break strength is more explicitly known than that of chain. Because a segment of wire rope is usually tested to destruction and the load at failure is recorded. The test certificate provides the most reliable estimate of the break strengths for standard independent wire rope core constructions with different grades of steel. Table 3.3 provides the generic standard for six strand and spiral strand ropes.

Table. 3.3 *Nominal breaking strengths of steel wire mooring ropes*

	Six strand	Spiral strand
Submerged weight / length (N/m)	0.034 d^2	0.043 d^2
Stiffness / length (N/m)	45000 d^2	90000 d^2
Ultimate tensile stress (N/mm)	1770	1570
Breaking strength (N)	525 d^2	900 d^2

Corrosion is considered as the major cause of degradation of wire mooring lines which can affect the performance both externally and internally. The loss of lubricant and blocking compound or dissolution of the zinc coating can accelerate corrosion damage. High density polyethylene sheaths are often used on spiral strand ropes destined for long term operations. Internally, inter-wire pressure and friction could be the reason leads to wire breaks. Externally, several operational abuses could also lead to significant damage to wire ropes, for example: inappropriate fairleads, kinking, inadequate care during rope handling, incorrect tensioning, chasing or incorrect pulley sizing can cause major damage.

3.2.3 Synthetic Fiber Rope

General

The use of synthetic fiber ropes in mooring line has become popular recently in deep water area. The major advantages of synthetic fiber ropes are the light weight and elasticity of the material, which can absorb imposed dynamic motions through extension without causing excessive dynamic tension. The material used in fiber ropes can be divided into polyesters, aramid, high modulus polyethylene, liquid crystal polyesters, carbon fibers and inorganic fibers. Among all the materials, the first three can be regarded as the primary solutions for mooring application with breaking strengths in the range from 1000 to 4000 N/mm^2.

Property

The axial stiffness of fibre ropes is a more critical parameter in the mooring system performance than that of either chain or wire rope as substantial part. A precise understanding of axial stiffness is critical to the successful use of fibre ropes offshore. Traditional mechanism that develops restoring forces through changes of the catenary shape, while for fiber rope, it could extend from 1.2 to 20 times as much as steel. Polyester tethers display a combination of permanent and visco-elastic extension when loaded. Construction elongation is the extension exhibited due to the bending down of the rope when first loaded. This extension is permanent and is fully accounted for after 5-10 loading cycles. Elastic elongation is the extension of the rope when load is applied which fully recover immediately once the load is removed. Constructional extension ranges between 1.6 % and 3.6 % of total length and elastic elongation varies from 2.5 % to 7.5 % of the total length [47].

3.2.4 Comparison of Mooring Line Materials

Three key parameters are dominating during the selection of the mooring line material, which are breaking strength, elastic modulus and submerged weight per unit length. Elastic modulus and submerged weight often indicate the breaking strength required of a particular mooring configuration. As the relative contribution of dynamic and static loads varies greatly in different conditions, it is not possible to identify the optimal mooring material according to a specific standard. However, a comparative review of the important mooring material characteristics should give an indication of the conditions under which a particular mooring is likely to perform optimally. The final choice of the mooring line material should be based on the integral analysis.

Figure 3.5 provides a direct comparison between the three mooring line materials with the range of breaking strength, elastic modulus and submerged weight per unit length after being normalized by square of nominal diameter of mooring line.

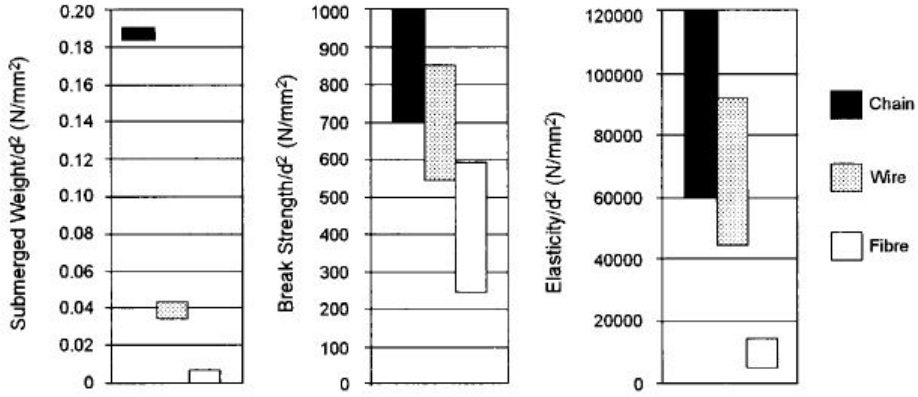

Figure. 3.5 *Comparison between different mooring line materials*

3.3 Mooring System Analysis

3.3.1 Overall Design Considerations

Generally, the mooring system for a floating wind turbine should satisfy the following requirements:

- Maintain the position of the wind turbine within a specific limit from its reference position.
- Control the directional heading of the wind turbine, since the orientation is important for safety and operational considerations.
- Assist in maintaining the acceleration and the tilting angle at tower top within a specific limit.

Mooring system design work should take into account all conditions relevant to pre-service operations during installation and commissioning, in-service conditions including operations, maintenance and repair operations. The floating support structures of un-manned floating wind turbine are typically designed to have a minimum safety level equivalent to the medium (L2) exposure level as defined in ISO 19904-1 for un-manned, medium consequence floating offshore structures used in the oil and gas industry. The design life of the mooring system for floating wind turbine should be generally at least 20 years, while shorter design life could be acceptable for testing model.

Wind turbine stability is also an important issue to be considered when design the mooring system, mooring system should be able to provide sufficient yaw stiffness to mitigate the yaw motion of floating support structure. Meanwhile rotor nacelle assembly yaw control effects on the floating support structure should be taken as a modification as well.

Protection against corrosion and wear to the mooring line is ensured by increasing diameters for chain link. Current industry practice is to increase chain diameter by 0.2 mm to 0.4 mm per service year in splash zone and thrash zone on the hard seabed. Corrosions of wire rope at connections to sockets could be severe due to the wire acting as an anode for adjacent components. For permanent systems, the protection method could be electrically isolated from socket. It is also recommended to add sacrificial anodes to this area.

3.3.2 Time-domain VS Frequency-domain

There are four primary nonlinear effects that could affect mooring line behaviour:

- *Nonlinear stretching behaviour of the mooring line.* The strain or tangential stretch of the mooring line is a function of the tension magnitude. Nonlinearity occurs mostly in synthetic materials like polyester.

- *Changes in geometry.* The geometric non-linearity is associated with large variations of the mooring line shape.
- *Fluid loading.* Morison equation is frequently used to represent fluid loading effects on mooring lines. The drag force on the line is nonlinear since it is proportional to the square of the relative velocity.
- *Bottom effects.* The part of the mooring line lying on the seafloor has interaction with the seabed, which is considered to be a nonlinear frictional process. Moreover, the length of grounded line segment constantly changes causing interaction between bottom non-linearity and geometric non-linearity.

Frequency-domain

Frequency-domain method is always linear because of the linear superposition principle. As a result, all sources of non-linearity should be simplified by either a direct linearisation approach or an iterative linearisation approach. When utilizing frequency-domain analysis method, the mean position of the floater is first determined from static equilibrium calculations for surge, sway and yaw. The motion responses to wave and low-frequency excitation are then calculated and superimposed to the mean position.

Time-domain

Time-domain method is able to model the nonlinear effects showed above: Elastic stretch can be mathematically modelled; full Morison equation can be implemented; the position of the mooring line can be updated at each time step; and the bottom interaction can be simulated using a frictional model. Such time-domain analysis requires recalculating mass, damping and stiffness matrices and loading at each time step. Hence the computation can be complex and time consuming. In general, the fully coupled integrated analysis approach is recommended for the following two important advantages:

- Low-frequency damping from the hull structure, mooring lines can be internally generated in the simulation.
- Coupling between floating support structure, the turbine rotor nacelle assembly, control system and mooring system can be fully accounted for.

3.3.3 Uncoupled Analysis VS Coupled analysis

Mooring system analysis consists of both floater motion analysis and mooring line tension analysis. The wave-induced response of the wind turbine normally can be divided into three main categories of response, wave frequency motions, low frequency motions and steady drift motions.

- *Wave frequency motions.* These motions have six degrees of freedom (surge, sway, heave, roll, pitch, yaw) at wave frequencies that can be obtained from

model tests in regular or random waves or by numerical analysis in the frequency or time domain.

- *Low frequency motions.* These motions are induced by low frequency components of second order wave forces. The low frequency motions of surge, sway and yaw can be substantial, especially at frequencies near the natural frequency of the floating support structure. The low frequency motion-induced loads on mooring lines could be dominant design loads for mooring system.
- *Steady drift motions.* Mean offset due to environmental force (waves, wind and current).

Coupled analysis where both the vessel motion and mooring line tension responses are simultaneously calculated in the time domain, however, uncoupled analysis is usually carried out in the frequency domain in an uncoupled way. The paper from H. Ormberg and K. Larsen [48] studied the differences between performing a uncoupled and coupled analysis when designing a mooring system.

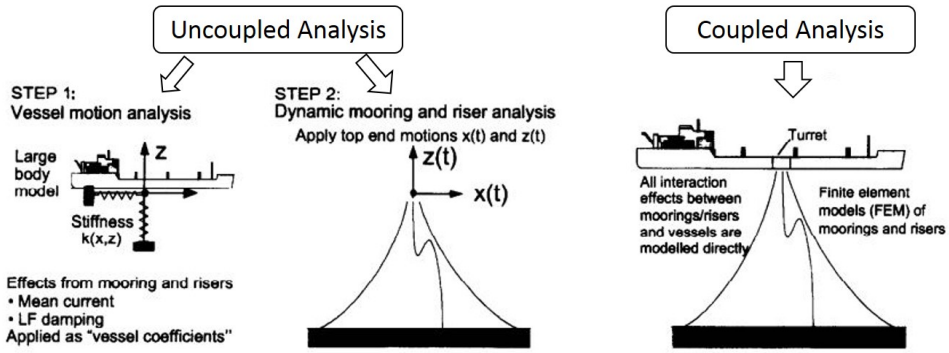

Figure. 3.6 *Uncoupled and coupled mooring system analysis*

Uncoupled Analysis

Traditional global response analysis of moored floating structures are carried out in two separated steps: calculations of floater motions, and dynamic response analysis of mooring lines utilizing the top end motions estimated in the first steps. This is referred to as the uncoupled analysis. Mean current, low frequency damping and mass are applied as vessel coefficients in the analysis. Because of the simplification, there are some resulting disadvantages of the method: neglect and simplification of current forces and low frequency damping contribution from mooring lines.

Coupled Analysis

For a coupled analysis, these effects mentioned above are accounted for, which will increase the accuracy of the final result for sure. The floater motions and mooring line dynamics are included simultaneously. All interaction between mooring lines and floater are modelled directly. The advantage become obvious when the water

depth increase where the mean offset and low-frequency motions is governing the total motion. Meanwhile, the coupled analysis shows good results when compared with experiment test. According to the result from a case study carried out in the article, for a turret moored ship at 2000 m water depth, 62% of the surge damping is due to slender structures, which makes the low-frequency damping coefficients quite important. Therefore, coupled analysis is preferable in deep waters even though it might be time consuming.

3.4 Analysis Types

3.4.1 Static Test

Normally, the mooring system for floating wind turbine consists of three or four mooring lines. The performance of single mooring line determines the overall performance of whole mooring system. The classic catenary equation proposed by O. M. Faltinsen [29] provides a good example to study mooring line behaviour in the manner of linear static analysis where the elasticity of the mooring line is neglected.

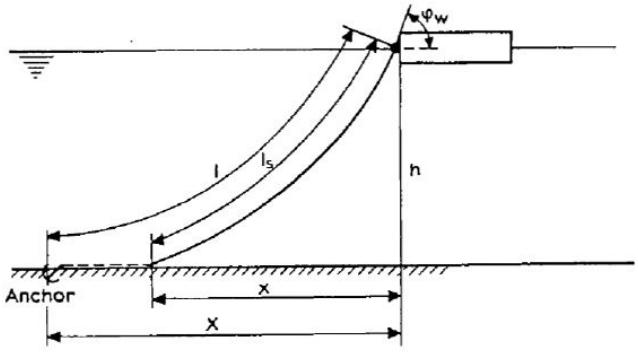

Figure. 3.7 *Vessel moored with one anchor line*

In the figure 3.7:

- h: Water depth from fairlead to seabed
- x: Horizontal distance from fairlead to contact point between mooring line and seabed
- X: Horizontal distance between fairlead and anchor position
- l_s: Mooring line length suspended in water
- l: Mooring line total length
- φ_w: Mooring line angle at the fairlead position.

The catenary theory could derive several important results:

$$l_s = asinh(\frac{x}{a}) \tag{3.4}$$

$$h = a[cosh(\frac{x}{a}) - 1] \tag{3.5}$$

where

$$a = \frac{T_H}{\omega} \tag{3.6}$$

T_H is the pretension of the mooring line when there is no offset given to the vessel, corresponding to the horizontal component of the maximum tension T_{max} at fairlead, while ω is the unit weight of mooring line in water:

$$T_{max} = T_H + \omega h \tag{3.7}$$

The horizontal distance X could be expressed as:

$$X = l - l_s + x \tag{3.8}$$

As a result,

$$l_s^2 = h^2 + 2ha \tag{3.9}$$

If there is no vertical force is allowed at anchor, the limit value is available for a:

$$a_{limit} = \frac{l^2 - h^2}{2h} \tag{3.10}$$

So the corresponding limit value for horizontal distance X could be obtained by utilizing $X = x$ in the extreme case:

$$X_{limit} = a_{limit} sinh^{-1}(\frac{l_s}{a}) \tag{3.11}$$

Then the allowable offset of the vessel could be obtained:

$$\Delta x = X_{limit} - X \tag{3.12}$$

In the case where only linear restoring effect is taken into account, the restoring coefficient of the spread mooring system could be written into:

$$C_{11} = \sum_{i=1}^{n} k_i cos^2 \varphi_i \tag{3.13}$$

The linear restoring coefficient for one mooring line k_i could be written as:

$$k_i = \omega[\frac{-2}{(1 + 2\frac{a}{h})^{\frac{1}{2}}} + cosh^{-1}(1 + \frac{h}{a})]^{-1} \tag{3.14}$$

According to the catenary equation mentioned above, a preliminary design procedure could be determined if there is no clump weight or buoyancy element used.

1. Assume a reasonable natural period for surge (around 80s) and calculate the required restoring coefficient C_{11}.
2. Utilize equation (3.14) to calculate the linear restoring coefficient for one mooring line k_i after the number of mooring lines and angles between mooring lines have been decided.
3. An unstreched mooring line length l is determined based on the water depth according to some reference models.
4. Afterwards, the uplimit value a_{lim} and X_{lim} can be obtained. Then in order to ensure an adequate offset, a proper value of a is chosen. An allowable offset around 20% of the water depth is normal to use.
5. Referred to equation (3.15), the required weight ω is calculated, thereafter the mooring line properties, e.g. material, nominal diameter, stiffness and breaking strength can be decided.
6. Based on equation (3.7) and (3.8), the pretension and maximum tension can be decided.
7. Following the calculation, a decay test should be performed to check the realistic natural period of the system.

3.4.2 Free Decay Test

In order to check if the natural periods calculated from catenary equation is realistically reasonable, free decay tests are normally performed in order to document about natural periods at six degrees of freedom, together with added mass and damping of the system to get an image of the basic information of the system. There are two popular methods to determine the linear damping and quadratic damping of the mooring system.

Equivalent Linearisation Method[49]

One degree of freedom system with nonlinear damping is considered as an example. The differential equation describing the system motion can be expressed as:

$$M\ddot{x} + B_1\dot{x} + B_2\dot{x}|\dot{x}| + Cx = 0 \tag{3.15}$$

Where

- M: Body mass (including added mass)
- C: Restoring stiffness
- B_1: Linear damping term
- B_2: Quadratic damping term

Accordingly, the natural frequency for the undamped system is given as:

$$\omega_0 = \sqrt{\frac{C}{M}} \tag{3.16}$$

Under the condition that the natural period of the system is measured and the restoring stiffness is available, the total mass can be calculated. The added mass term is determined by subtracting the structural mass of the system.

The calculation of the linear and nonlinear damping term is carried out afterwards. Firstly, the motion equation is modified by dividing M term at both sides of the equation:

$$\ddot{x}p_1\dot{x} + p_2\dot{x}|\dot{x}| + p_3x = 0 \tag{3.17}$$

The following analysis of the equation is based on solution of a linear oscillating system in combination with the equivalent linearisation method, which means that the nonlinear damping term is replaced by a linear term which satisfies the equal damping energy per cycle requirement:

$$p_{EQ} = p_1 + \frac{8}{3\pi}\omega x_0 p_2 \tag{3.18}$$

Where

- x_0: Motion amplitude of relevant cycle

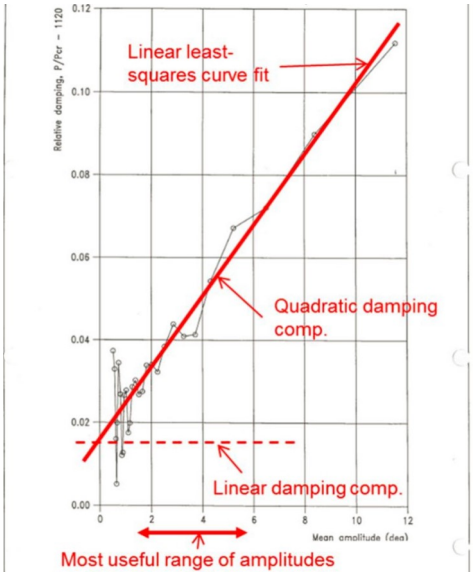

Figure. 3.8 *Equivalent linearisation method[49]*

- ω: Oscillation frequency

In the following, the linearized equation can be modified as:

$$\ddot{x} + p_{EQ}\dot{x}|\dot{x}| + p_3 x = 0 \tag{3.19}$$

The equivalent damping coefficient, p_{EQ} is given as:

$$p_{EQ} = 2M\omega_0\xi = \frac{2C\xi}{\omega_0} \tag{3.20}$$

Where ξ is the damping ratio defined as the ratio between actual and critical damping. The general relation between logarithmic decrement and the damping ratio is calculated as:

$$\Lambda = \xi\omega_0 T_d = 2\pi\frac{\xi}{\sqrt{1-\xi^2}} \tag{3.21}$$

Then p_{EQ} and λ can be obtained for each cycle from the measured logarithmic decrement. The final plot of λ is showed versus the mean amplitude (mean of two successive amplitudes) in one figure with reference to figure 3.8 below. The linear damping p_1 term is determined by the intersection with the abscissa and nonlienar term p_2 is found from the slope of the curve. The first few oscillation should be avoided due to transient effect and the tail part of the motion due to small amplitudes.

Finally, the natural frequency of the damped, freely oscillating system, ω_d is calculated by:

$$\omega_d = \omega_0\sqrt{1-\xi^2} \tag{3.22}$$

where ω_0 is the natural frequency of the undamped system defined before.

Energy Slope Method[50]

A theoretical approach for establishing the linear and nonlinear damping from decay tests has been proposed by Roberts [51]. An energy slope is established accordingly.

Based on a free-decay test result, preprocessing in order to remove mean drift is carried out. This is achieved by fitting separate cubic splines to the positive and negative peaks. The corrected values for positive and negative peaks are expressed as:

$$\varphi_j^+ = \frac{\phi_j^+ + \hat{\phi}_j^+}{2} \tag{3.23}$$

$$\varphi_j^- = \frac{\phi_j^- + \hat{\phi}_j^-}{2} \tag{3.24}$$

In the case of a linear and a quadratic damping term are going to be decided, the relevant energy slope $V(t)$ is defined by :

$$V(t) = \frac{1}{2}\dot{\phi}^2 + U(\phi) \tag{3.25}$$

The averaged rate of energy loss per cycle $L(V)$ is expressed as:

$$L(V) = \frac{\beta}{T(V)} \int_0^{T(V)} F(\dot{\phi})\dot{\phi} dt \tag{3.26}$$

A non-dimensional function $Q(V)$ is defined by:

$$Q(V) = \frac{L(V)}{2\omega_0 V} = b_1^* A(V) + b_2^* D(V) \tag{3.27}$$

where

$$b_1^* = \frac{\beta b_1}{2\omega_0} \tag{3.28}$$

$$b_2^* = \frac{\beta b_2}{2} \tag{3.29}$$

$$D(V) = \frac{\sqrt{V}B)}{\omega_0} \tag{3.30}$$

Minimize the overall least square difference between result from equation (6.13) and the estimates for $Q(V)$ obtained from the cubic spline interpolation:

$$e = \sum_{i=1}^{N} [Q(V_i) - \hat{Q}(V_i)]^2 \tag{3.31}$$

e is minimized if b_1^* and b_2^* are found so that:

$$\frac{\partial e}{\partial b_1^*} = \frac{\partial e}{\partial b_2^*} = 0 \tag{3.32}$$

This will lead to the solution for b_1^* and b_2^*:

$$b_1^* = \frac{S_3 S_4 - S_2 S_5}{S_1 S_3 - S_2^2} \tag{3.33}$$

$$b_2^* = \frac{S_1 S_5 - S_2 S_4}{S_1 S_3 - S_2^2} \tag{3.34}$$

where

$$S_1 = \sum_{i=1}^{N} A^2(V_i) \tag{3.35}$$

$$S_2 = \sum_{i=1}^{N} A(V_i) D(V_i) \tag{3.36}$$

$$S_3 = \sum_{i=1}^{N} D^2(V_i) \tag{3.37}$$

$$S_4 = \sum_{i=1}^{N} A(V_i) \hat{Q}(V_i)) \tag{3.38}$$

$$S_5 = \sum_{i=1}^{N} D(V_i) \hat{Q}(V_i) \tag{3.39}$$

3.4.3 Ultimate Limit State Test

Ultimate limit state (ULS) corresponds to the resistance to maximum applied loads. It is required that all foreseen loads can be resisted with an adequate margin. Control against loss of station keeping is emphasized here. ULS check is introduced to ensure that individual mooring lines have sufficient strength to withstand the load effects imposed by extreme environmental conditions. Extreme mooring line tension as well as floater motion responses are interesting parameters to look at. The requirement of mooring system performance under extreme condition includes:

- Limit the offset of the floater in order to protect the power cable from taking large tension and bending moment.
- Ensure the tension in the mooring line does not exceed the capacity.
- Guarantee there is no vertical forces acting on the anchors i.e. mooring line can not be totally lifted up.

Mooring Line Tension

Based on standard DNV-OS-E301 [52], mooring line tension consists of:

- T_{C-mean} - The characteristic mooring line mean tension, due to pretension and mean environmental loads.
- T_{C-dyn} - The characteristic mooring line dynamic tension, influenced by low-frequency and wave-frequency motions.

Take one time domain simulation result as an example, the mean tension is calculated as the mean value of the tension in time series. Dynamic line tension is taken as the difference between the MPM tension and the mean tension, where MPM stands for most probable max tension which can be fitted to the extreme value distribution (Gumbel distribution).

The mooring system failure can be summarized into two categories depending on the consequences of failure:

- Mooring system failure is unlikely to lead to unacceptable consequences such as loss of life, collision with adjacent platform, capsize or sinking.
- Mooring system failure may lead to unacceptable consequences of those types mentioned.

In current study, consequence class 1 has been selected with corresponding safety factors.

In agreement with the standard, the design equation in form of utilization factor can be expressed as:

$$u = \frac{T_{C-mean}\gamma_{mean} + T_{C-dyn}\gamma_{dyn}}{S_C} \leq 1 \tag{3.40}$$

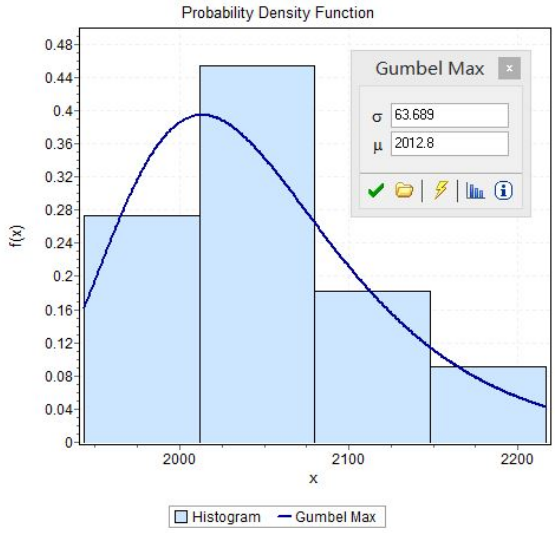

Figure. 3.9 *Gumbel distribution fit of maximum mooring line tension*

Where

- S_C: Characteristic mooring line strength, 0.95 × CBS
- γ_{mean}: Safety factor for mooring line mean tension
- γ_{dyn}: Safety factor for mooring line dynamic tension

Table. 3.4 *Partial safety factors*

Consequence class	Safety factor for mean tension γ_{mean}	Safety factor for dynamic tension γ_{dyn}
1	1.10	1.50
2	1.40	2.10

Floater Motion

The safety of power cable is greatly influenced by the floater motion range, especially in horizontal plane. In the realistic wind turbine design, power cable design is carried out after the mooring system configuration and the maximum offset is determined. Power cable is then designed to accommodate the possible maximum offset. This design philosophy determines that the floater motion should be limited to a reasonable range to accomplish the power cable design afterwards. Moreover, the floater motion should be limited so that the movement of one wind turbine will not affect the normal performance of the adjacent wind turbines.

3.4.4 Fatigue Limit State Test

Offshore structures are in general subjected to cyclic dynamic loads which could lead to undesired result, even though the load stays below the allowable stress. Fatigue cracks can be initiated by any possible environmental conditions, characterized by wave height, peak period and wind speed. Fatigue cracks tend to grow at an accelerating rate and may become a hazard to structural integrity. Fatigue damage has been identified as one of the significant consideration in the design work, especially for the mooring system in floating wind turbine which is subjected to highly cyclic, nonlinear load conditions[53].

Fatigue performance can be improved by ensuring abundant fatigue strength during design or by frequent inspection and repair[54]. Because of similar design philosophy, the units in one wind farm normally have similar fatigue strength and common cause, which makes it meaningful to make a good fatigue estimates in the early design phase. In the mooring fatigue analysis, consideration should be given to: dynamic wind and wave loads; transient effects due to start-up and shut-down of the rotor nacelle assembly and coupling effects among the subsystems of the wind turbine.

Time Domain VS Frequency Domain

Normally, in order to achieve good accuracy in fatigue analysis, fully coupled time domain is used for floating wind turbine. The nonlinearity due to viscous damping, catenary mooring line behaviour, interaction between rotor and platform motion make time domain simulation necessary to capture the nonlinearity. Time domain fatigue analysis is based on the time series of stress history focusing on the local maxima and minima. The cycle counting methods include: peak counting, range counting, level crossing counting and rainflow counting, where rainflow counting method is proved to be the most satisfactory method for estimating fatigue damage. It considers the fatigue damage caused by each individual load cycle by counting the stress ranges corresponding to individual hysteresis loops of the component material[53]. Details about how rainflow counting method works can be referred to Gao's PhD thesis[39].

Frequency domain methods have already achieved satisfactory result for the fatigue analysis of bottom fixed wind turbines. The accuracy level is acceptable compared to time domain simulations and full scale measurements. The frequency domain method deals with the wind and wave loads separately, which will greatly influence the accuracy since there is a strong interaction between wave induced response and wind induced response. Frequency domain methods are computationally efficient. But there is not a closed form solution of rainflow counting method that can be utilized in frequency domain. Therefore, spectral type and random process has to be determined at first, such as narrow-band, bimodal, trimodal and multimodal process. Different analysis method should be applied aiming at different cases. Among them, mooring system response usually can be categorized

to bimodal process where wave frequency and motion resonant frequency are the two main contributions. If VIV is included, the process will become a trimodal process[39]. The calculation for bimodal fatigue damage has been proposed by Jiao and Moan[55] with a composition of high frequency damage and an equivalent process for high frequency envelope together with the low frequency process.

Fracture Mechanics Method VS S-N Curve Method

Fatigue crack growth model is based on fracture mechanics. It examines the fracture behaviour of mechanical elements under dynamic loading. The dominant cracks growth is the criterion to determine whether failure has occurred or not. However, because the crack growth rate is not available and the initial crack size is hardly to quantitatively define, the crack growth models are not popularly applied.

S-N Curve approach known as stress-life cumulative damage models is more practical to predict fatigue life, which calculates the cumulative fatigue damage when a number of loading cycles at a particular stress range have occurred. The approach is in agreement with linear damage accumulation assumption, which ignore the load sequence and crack growth behaviour in the elastic-plastic fracture regime. In current thesis, S-N curve method is utilized in time domain. The procedure to perform cumulative damage calculation is introduced in the following.

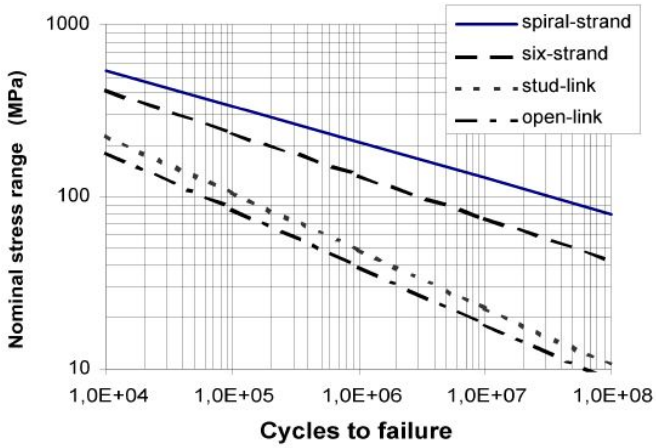

Figure. 3.10 *Design S-N curves for mooring line*

The accumulated fatigue damage in a mooring line component because of cyclic loading, is summed up from fatigue damage arising in a set of environmental states chosen to represent the long term environmental condition[52].

$$d_c = \sum_{i=1}^{i=n} d_i \tag{3.41}$$

Where d_i is the fatigue damage to component arising in state i. The probability of occurrence P_i is required for each environmental state as well.

When the mean tension effect is neglected, the equation for an individual state could be written as:

$$d_i = n_i \int_0^\infty \frac{f_{Si}(s)}{n_c(s)} ds \tag{3.42}$$

Where

- n_i: Number of stress cycles counted during design life
- $f_{Si}(s)$: Probability density of nominal magnitudes (from peak to trough) of the stress cycles

The nominal cross sectional area is used for computing the nominal magnitudes of stress cycles: $\frac{2\pi d^2}{4}$ for chain link and $\frac{\pi d^2}{4}$ for steel wire rope, where d is the component diameter.

The component capacity against fatigue could be expressed as:

$$n_c(s) = a_D s^{-m} \tag{3.43}$$

Where

- $n_c(s)$: Number of cycles
- s: Stress range
- a_D: Intercept parameter in S-N curve
- m: Slope of the S-N curve

It is meaningful to notice that there is only one slope in the S-N curve and the intercept parameter and the slope parameter depends on the material that is being used.

Table. 3.5 *S-N curve parameters*

	a_D	m
Stud chain	1.2 E11	3.0
Studless chain	6.0 E10	3.0
Stranded rope	3.4 E14	4.0
Spiral rope	1.7 E17	4.8

Tower Base

Take the whole floating wind turbine into account, the part that is most sensitive to fatigue damage is the tower base. Therefore, short-term fatigue damage at the tower base due to axial stress is calculated as well beside the fatigue for mooring line.

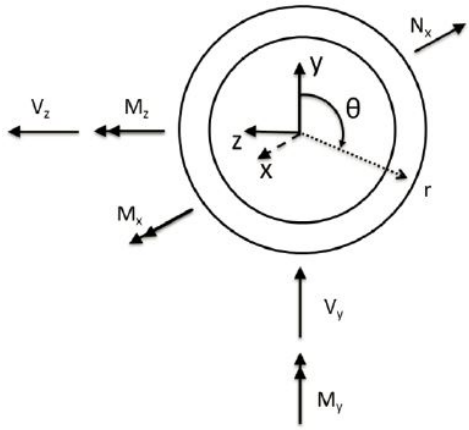

Figure. 3.11 *Coordinate system for tower base fatigue damage calculation*

Where

- N_x: Axial force
- M_y: Moment about local y-axis, -1×DOF 3
- M_z: Moment about local z-axis, DOF 5

Thereafter, the axial stress for the cross section of the tower base can be calculated according to:

$$\sigma = \frac{N_x}{A} + \frac{M_y}{I_y} r sin\theta + \frac{M_z}{I_z} r cos\theta \tag{3.44}$$

S-N curve D from DNV-RP-C 203[56] is applied in order to compute the damage for tower base:

$$logN = log\bar{a} - mlog(\Delta\sigma(\frac{t}{t_{ref}})^k) \tag{3.45}$$

Where

- N: Number of cycles
- t: Plate thickness
- $\Delta\sigma$: Stress range

The stress concentration factor is set to 1 for simplicity and the other parameters are defined below:

Table. 3.6 *S-N curve for tower base*

$N \leq 10^7$		$N > 10^7$		Fatigue limit	k	t_{ref}
m	loga	m	loga			
3.0	12.164	5.0	15.606	52.63 MPa	0.20	0.025 mm

4 5-MW-CSC Semi-submersible Wind Turbine

4.1 Global Layout

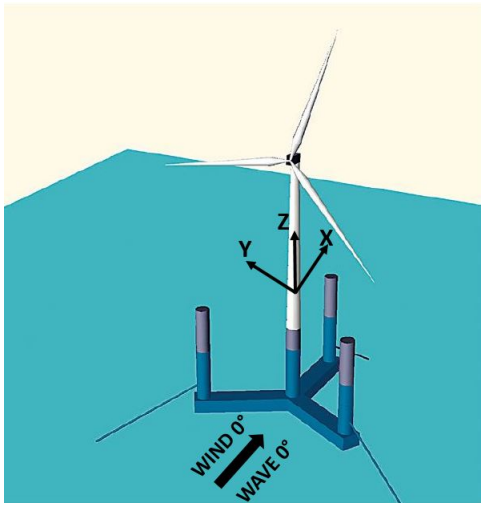

Figure. 4.1 *Layout of the 5-MW-CSC floating wind turbine[16]*

The floating wind turbine that has been selected for study in this thesis is the 5-MW-CSC Semi-submersible floating wind turbine [15]. The background information could be referred to in section 1.3.2.

The 5-MW-CSC semi-submersible floating wind turbine includes a wind turbine, a tower, a semi hull and three catenary mooring lines, shown in figure 4.1. The origin of the coordinate system is placed at the still water level with wave and wind direction illustrated in the figure 4.1. The semi hull consists of three pontoons, three

side columns and one central column supporting the tower and the wind turbine [57]. Enough restoring stiffness is provided by the side columns while the pontoons are used to provide buoyancy and connect the columns. The wind turbine in the study is the NREL 5 MW reference wind turbine [58] mounted on the OC3 Hywind wind tower [59] which starts from 10 meters above the waterline. One important feature to be noticed is that: no brace structure is used, which is favourable for floating structures considering fabrication and fatigue failure potential.

4.2 NREL 5-MW Wind Turbine

NREL 5-MW wind turbine is designed by National Wind Technology Center (NWTC), sponsored by the U.S. Department of Energy's National Renewable Energy Laboratory. The purpose of the project is to assess offshore wind technology in shallow water and deep water off the U.S. offshore continental shelf and other sites worldwide. The NREL offshore 5-MW baseline wind turbine is a conventional three bladed upwind turbine with variable-speed and variable blade-pitch-to-feather control. The general properties of the turbine could be found in the table below. The NREL 5-MW wind turbine has been the most popular turbine model in current research. The corresponding power and thrust curves for NREL 5-MW turbine are shown in figure 4.2.

Table. 4.1 *Gross properties of NREL 5-MW baseline wind turbine [58]*

Rating	5 MW
Configuration	Upwind, 3 Blades
Control	Collective Pitch
Drive train	Multiple-Stage Gearbox
Rated Wind Speed	11.4 m/s
Cut-in, Cut-out Wind Speed	3 m/s, 25 m/s
Cut-in, Rated Rotor Speed	6.9 rpm, 12.1 rpm
Rated Tip Speed	80 m/s
Overall CM	(-0.2m, 0.0m, 64.0m)
Rotor Mass	110t
Nacelle Mass	240t

The tower that supports NREL 5-MW wind turbine is OC3 Hywind wind tower, whose properties have been defined in the article "Definition of the Floating System for Phase IV of OC3" authored by J. Jonkman [59].

The base of the tower is coincident with the floater top and is located at 10m above the still water level (SWL). The tower top supports the yaw bearing with a height of 87.6 m above the SWL. The distributed tower is constructed with base diameter of 6.5 m to match the top diameter of the central column, and the tower base thickness is 0.027 m. The tower top diameter is designed as 3.87 m together

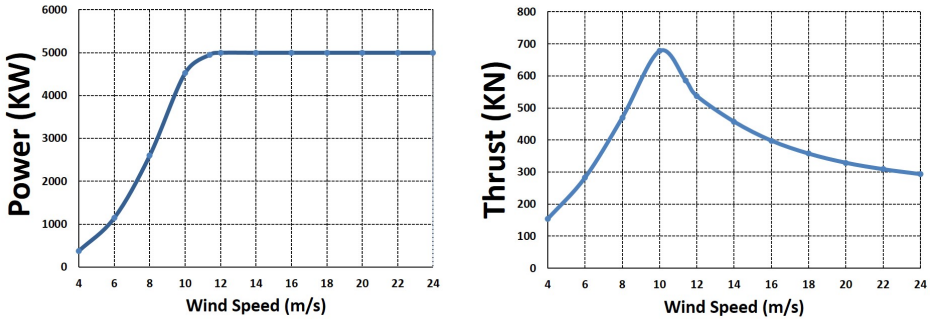

Figure. 4.2 *Power and thrust performance of NREL 5-MW Wind Turbine [60]*

with 0.019 m thickness. The Young's modulus was chosen to be 210 GPa while the shear modulus was 80.8 GPa. The effective density of the steel was selected to be 8500 kg/m^3 which includes and increase above steel's typical value of 7850 kg/m^3 in order to take into account paint, bolts, welds and flanges.

4.3 5-MW-CSC Floater

The semi hull is composed of a central column supporting the tower and wind turbine together with three side columns and three pontoons. There is no traditional bracing structure between column considering fatigue damage of the connection. The angle between each pontoon is 120°.

Table. 4.2 *5 MW-CSC floater properties [61]*

Hull steel mass	1686	t
COG	(0, 0, -24.53)	m
COB	(0, 0, -22.42)	m
Draft	30	m
Pontoon length	41	m
Pontoon height	6.0	m
Column length	24	m
Column diameter	6.5	m
Floater draft	30	m

4.4 Site Condition

The floating wind turbine should be designed to withstand specific operational and environmental conditions at the site. Based on the paper from Lin li [62], Norway

5 site has been selected as a representative site for floating wind turbine. The location is referred to No.14 in the figure.

Figure. 4.3 *Location of Norway 5 site (No.14 in the figure)*

The long-term wind and wave data can be described using a joint distribution of 1-hour mean wind speed at 10 m above sea water level (U_ω), the significant wave height (H_s) and the peak period (T_p). Utilizing the environmental data generated by a numerical hindcast model, Li established a long-term joint probabilistic numerical model for wind and wave condition. Attention should be paid to the mean wind speed, since the one in the joint distribution is the speed at the height of 10 meters above the sea level. However, in order to accomplish the power estimation of the wind turbine, the wind speed should be used is the one at hub height, i.e. 89 m in the current study. The speed in-need can be derived according to a power law with the exponent value equal to 0.1.

$$U(z) = U_{10}(\frac{z}{10})^{\alpha} \tag{4.1}$$

where z stands for the height, U_{10} represents the mean wind speed at the reference height of 10 meters.

The wind field used in this thesis work is generated by TurbSim [63] based on the Kaimal spectral model. The turbulence intensity is defined in IEC 61400 standard [28]. Class C is selected in current study for offshore condition. Meanwhile, Normal Turbulence Model is used for operating condition and Extreme Wind Model is used for extreme condition for parked model.

There are two different status of the wind turbine based on different environmental conditions. For wind speed below 3 m/s and above 25 m/s, parked (idling) model is used where the blades are pitched to feather and the turbine is shut down without

rotor rotating [64]. When the wind speed is between 3 m/s and 25 m/s, operational model is used for power production with blade rotating, control system functioning.

Two typical extreme environmental conditions are provided for Norway 5 site suggested by Li[62] with one refers to the condition with maximum mean wind speed and one condition with maximum significant wave height.

Table. 4.3 *Load cases for extreme condition[62]*

Condition	Mean wind speed at hub height	Significant wave height	Wave peak period	Turbine status
	[m/s]	[m]	[s]	
ULS-1	41.86	13.4	13.1	Parked
ULS-2	38.87	15.6	14.5	Parked

Based on the knowledge from Johannessen's long-term distribution formulas [65] and Dudgeon park condition, Erin Bachynski [66] has proposed an environmental condition for an idealized installation location which contains fifteen different conditions with significant wave height, peak period, wind speed at hub position, turbulence intensity and probability. The wind and waves are both assumed to travel in positive x direction and the wind turbine is assumed to have 95% availability, which could be seen in the summation of the total probability. These fifteen conditions have been considered as the operational conditions to perform fatigue limit state check.

Table. 4.4 *Load cases for operational condition[67]*

Condition	Hs (m)	Tp (s)	Uw (m/s) at 90m	Turbulence Intensity	Probability
1	1.25	4	4	30.1	0.168
2	1.25	6	6	23.6	0.227
3	1.25	8	4	30.1	0.132
4	2.75	6	6	23.6	0.178
5	2.75	8	8	20.3	0.098
6	2.75	10	8	20.3	0.025
7	2.75	12	10	18.3	0.021
8	3.75	6	12	17.0	0.005
9	3.75	8	10	18.3	0.057
10	3.75	10	12	17.0	0.015
11	3.75	12	14	16.1	0.002
12	5.25	8	18	14.9	0.009
13	5.25	10	18	14.9	0.010
14	5.25	12	18	14.9	0.002
15	6.75	12	20	14.4	0.004
Sum					0.9530

5 Preliminary Static Design Result

The main criteria in the preliminary design for mooring system to follow includes:

1. **Stiffness criterion:** The horizontal stiffness of the mooring system should be sufficient enough to keep the platform within a specific range. Moreover, there should not be vertical force acting on the anchor in order to prevent lifting up the anchor.
2. **Strength criterion:** The mooring lines should be strong enough to ensure normal operation, in other words, the maximum line tension should not exceed the capacity of the mooring line.

There are two factors that could influence mooring line tension increment significantly, which could help to better understand mooring line behaviour and propose satisfactory design concepts in shallow water:

1. **Degree of tightness**: Generally, mooring line tension increase faster in stiff mooring system than soft mooring system, because mooring line is vulnerable to be stretched to straight line, losing catenary shape fast in the first case.
2. **Nonlinear increment**: Mooring line tension increment becomes nonlinear when the offset at fairlead exceed a specific range, which means the tension afterwards will increase extraordinary.

5.1 Reference Mooring System Model - 200 m

The initial 5-MW-CSC floating wind turbine is designed for 200 m water depth, which has been utilized as a reference model in order to carry out the study for shallow water - 100 m and 50 m.

The mooring system consists of three catenary mooring lines which are made of spiral rope and positioned with 120 degrees angle between the mooring lines. Each mooring line is attached at the outer columns of the semi at a water depth of 18 meter, where the fairlead is located. The distance from fairlead to the center of the

central column is 44.25 m. The mooring line is divided into two parts by connecting a clump weight between. The clump mass weights 17.25 tonnes and is positioned at a distance of 240 m from the fairlead position.

The configuration of upper part is close to a straight line because of the clump weight, while the lower part has a catenary shape. The anchor used here is a conventional fluke anchor which is mounted into the seabed. The total length of one mooring line is 873.105 m with the diameter to be 0.137 m. The distributed mooring line mass is 115 kg/m, which is kept constant along the whole line. The coordinates of the fairleads and anchors could be referred to table 5.1 and the basic properties of the mooring lines are showed in table 5.2.

Table. 5.1 *Coordinates of the fairleads and anchors for 200 m*

Farilead	X	Y	Z
Line 1	44.25	0	-18
Line 2	-22.125	38.3216	-18
Line 3	-22.125	-38.3216	-18
Anchor	X	Y	Z
Line 1	884.362	0	-200
Line 2	-442.181	765.88	-200
Line 3	-442.181	-765.88	-200

Table. 5.2 *Properties of mooring line for 200 m*

Property	Upper Line	Lower Line	Clump Weight
Length (m)	240	633.105	-
Diameter (m)	0.137	0.137	-
Mass/length (kg/m)	115	115	17250
Material	Spiral rope	Spiral rope	Steel

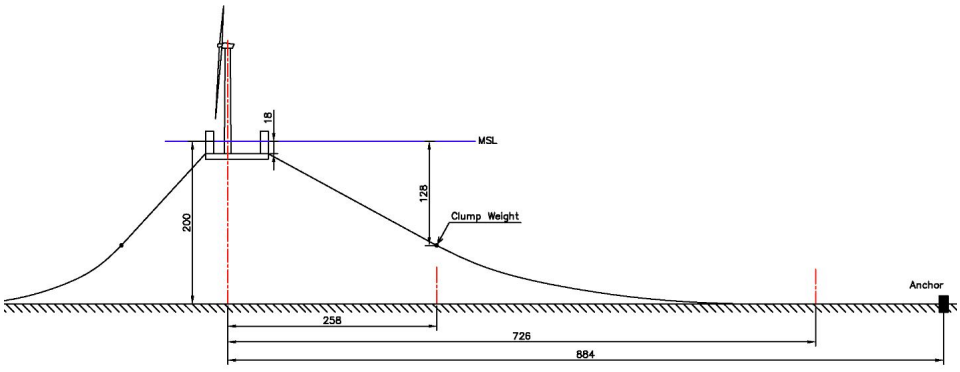

Figure. 5.1 *Mooring system configuration sideview - 200 m*

5.2 Static Design for 100 m and 50 m in SIMA

According to the reference model of mooring system for 200 m water depth, two new mooring system intended for 100 m and 50 m water depths have been designed in SIMA.

5.2.1 Design Basis - 200 m

The mooring system for 200 m water depth has been studied in SIMA in order to document the mooring system performance in aspect of configuration (catenary mooring line shape), pretension, horizontal tension and horizontal mooring line stiffness. The properties of the three mooring lines holds the same, so only one mooring line has been studied as an example.

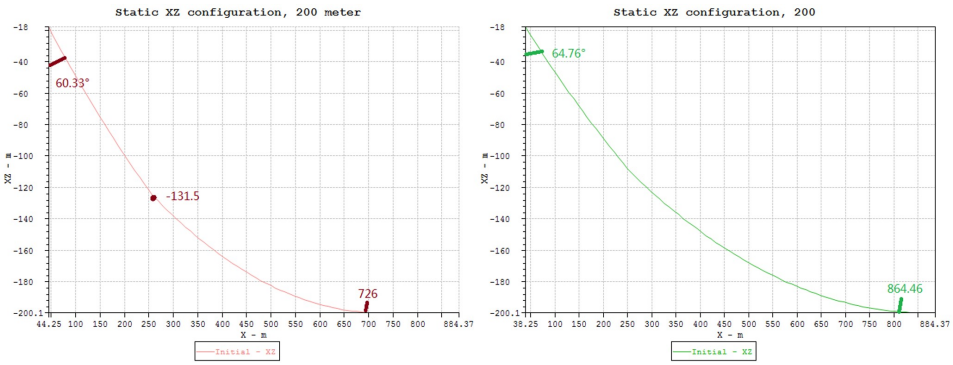

Figure. 5.2 *Static mooring line configuration - 200 m (Initial condition - left and Limit condition - right)*

Left sub-figure in figure 5.2 shows the initial mooring line configuration with self mass and clump weight taken into account. The anchor is placed at 884 m in the global coordinate system, while the first contact point between mooring line and seabed is 725 m away from the center of the central column, which means that there are about 159 m long mooring line lying on the seabed. The water depth of the clump weight position is 131.5 m below the sea level. The angle at the fairlead is 60.33 degree. The initial pretension at fairlead is 1683.1 KN.

By applying continuous offsets to the fairlead, the extreme limit mooring line configuration when mooring line is about to be totally lifted up can be determined as shown in the right sub-figure in figure 5.2. The results demonstrate that when the offset at fairlead is larger than 6 m, there will be no more mooring line lying on the seabed with tension at fairlead position to be 2269.47 KN. In conclusion, in order to prevent anchor from taking vertical loads, the floater motion should be limited around 6 m.

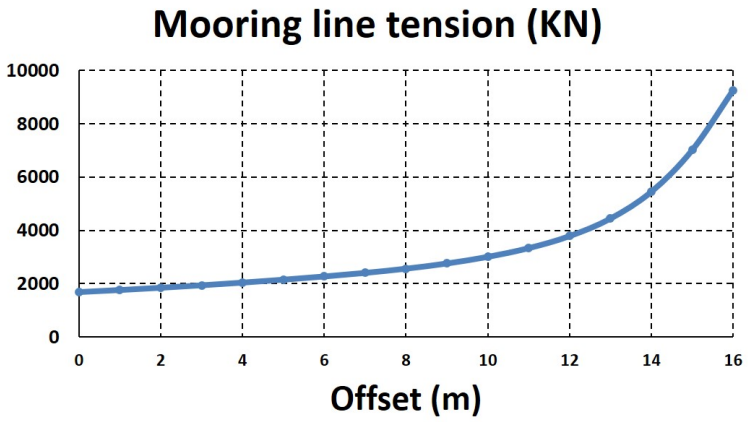

Figure. 5.3 *Mooring line tension with different offsets - 200 m*

Followed by the initial condition, the mooring line is then given certain magnitude of offsets in order to check the stiffness relationship between horizontal force and offsets. The mooring line tension does not reach the break strength until the offset at fairlead comes to 17 meters. Therefore, the tension before mooring line failure together with its corresponding offsets have been recorded. From the fitting figure 5.3, the nonlinear tension increment appears as expected: the horizontal stiffness become nonlinear after a linear part and the transition occurs when the offset is larger than 10 meters. The fitted numerical relationship for the linear part could be expressed as:

$$y = 121.92x + 1381.9 \tag{5.1}$$

Where

- y: Mooring line horizontal tension
- x: Offset at fairlead

5.2.2 Static Design for 100 m and 50 m

Since the mooring system design for 200 m water depth has already achieved satisfactory result, the evaluation criteria of preliminary design for 100 m and 50 m is to achieve the similar stiffness result, catenary shape and pretension as in 200 m.

Configuration

Since the same floating wind turbine is utilized for 100 m and 50 m, the general mooring line configurations are kept the same as the reference model: Three catenary mooring lines are used and the angel between adjacent lines are 120 degree.

The fairlead position is 18 m below water line and the radius from fairlead to floater center is 44.25 m as before.

The radius from anchors to platform center is 698 m for 100 m depth and 600 m for 50 m depth. The unstretched mooring line length for 100 m is 671.66 m in total with 311.95 m lying on the seabed. For 50 m water depth, the total length of one single mooring line is 566.65 m with 483 m lying on the seabed. The initial mooring line configuration for 100 m can be referred to figure 5.5 and figure 5.6 and figure 5.7 and figure 5.8 shows the configuration for 50 m water depth. The longer part lying on the seabed for shallower water is under expectation in order to prevent mooring line from being totally lifted up and prevent vertical force acting on the anchor. Moreover, saving long mooring line lying on the seabed could decrease the degree of tightness of the mooring system, which furthermore could help to slow down the nonlinear tension increment in shallow water.

Besides, the extreme configurations when the mooring line is about to be totally lifted up has also been calculated in order to set the offset limit for the three water depth: the offset limit for 100 m depth is 10 m and the offset limit for 50 m depth is 14 m. Relevant figure could be referred in appendix B.

Table. 5.3 *Mooring system configuration for 200 m, 100 m and 50 m*

Water Depth (m)		200	100	50
Mooring line number		3	3	3
Angle between adjacent lines (deg)		120	120	120
Depth from fairlead to seabed (m)		182	82	32
Radius from fairlead to platform center (m)		44.25	44.25	44.25
Radius from anchor to platform center (m)		884.36	698	600
Initial Configuration	Offset at fairlead (m)	0	0	0
	Angle at fairlead (deg)	60.33	57.5	39.4
	Total length (m)	873.11	671.66	566.65
	Suspended length (m)	714.74	359.71	83.56
	Touchdown length (m)	158.37	311.95	483
Extreme Configuration	Offset at fairlead (m)	6	10	14
	Angle at fairlead (deg)	64.76	70.35	81.46
	Total length (m)	873.11	671.66	566.65
	Suspended length (m)	853.2	661.64	489.91
	Touchdown length (m)	19.91	10.02	76.74

Mooring Line Material

With water depth decrease, the suspended length of mooring line decreases as well, which will further influence the pretension which is mainly determined by self-weight of suspended mooring line and clump weight. In order to make a compensate, heavier mooring line material - studless chain $R4 - RQ4$ is selected for 50 m and wire rope, spiral rope to be specific, is selected for 100 m. Generally,

the weight of chain is about five times of the wire rope, which could be benefited to achieve desired pretension in 50 m. According to "Anchor Manual [42] ", when the required service lift of mooring system is more than 20 years, spiral strand is recommended to use. Therefore, spiral rope is chosen rather than the popular six strand type. In addition, corresponding clump weights in 100 m and 50 m have been enlarged as well, which will explained later. Furthermore, in order to improve the fatigue performance, a HDPE plastic sheathing is used for spiral rope and no stud is utilized to connect chain links.

The nominal diameter for spiral rope is 0.1365 m while the diameter for the chain link is 0.18 m. The distributed unit mass in water is 115.02 kg/m for spiral rope and 648 kg/m for chain with corresponding axial stiffness to be 3.08 E9 N and 2.92 E9 N. The selection is based on the consideration of the larger catalogue breaking load for chain link, which will help to withstand possible large induced tension in shallow water. The corresponding catalogue breaking loads are 16769 KN for spiral rope and 26278 KN for studless chain.

In agreement with DNV-OS-E301[52], different drag coefficients are defined based on different mooring line material in both longitudinal and transversal direction. When determining the added mass coefficient, spiral rope is regarded as a cylinder and chain link is considered as two cylinders placed in a row. The exact value could be referred to DNV-RP-C205 standard[68].

Table. 5.4 *Mooring line properties for 200 m, 100 m and 50 m*

Water Depth (m)	200	100	50
Mooring line type	Spiral rope	Spiral rope	Chain R4-RQ4
Nominal diameter (m)	0.1365	0.1365	0.18
Nominal cross-section area (m^2)	0.01465	0.01465	0.0509
Gyration radius (m)	0.03415	0.03415	0.0636
Unit mass in water (kg/m)	115.02	115.02	648
Axial stiffness (KN)	3.08E6	3.08E6	2.92E9
Transversal drag coefficient	1.2	1.2	2.4
Longitudinal drag coefficient	0.02	0.02	1.15
Transversal added-mass coefficient	0	0	1
Longitudinal added-mass coefficient	1	1	2
Catalogue breaking load (KN)	16769	16769	26278

Pretension

Mooring line pretension is influenced by the self weight of mooring line which is suspended in the sea water and the additional clump weight and buoyancy element incorporated into the mooring line. As mentioned before, when water depth decreases, the possible suspended mooring line length is relatively short compared with deep water depth. Therefore, besides the self-weight of suspended mooring line, clump weight is important to increase the pretension as well. Accordingly, the

clump weight used in 100 m and 50 m have been decided to be 60 tonnes in order to achieve similar pretension as in 200 m.

Table. 5.5 *Mooring line pretension for 200 m, 100 m and 50 m*

Water depth (m)	200	100	50
Total pretension (KN)	1683.1	1710.91	1295.35
Horizontal pretension (KN)	1462.4	1442.88	821.16
Clump weight (t)	17.253	60	60

Performance

In order to check the static performance of the new proposed concepts for 100 m and 50 m, a comparative study is carried out with respect to the performance of 200 m design. Total mooring line tension, horizontal tension, horizontal stiffness and offsets have been looked into. According to the result shows in figure 5.4, the same nonlinear tension increment as showed in 200 m is applicable to 100 m and 50 m as well. Meanwhile the transition occurs at smaller offset (6 m offset) for 50 m and larger offset for 200 m and 100 m (10 m offset).

Table. 5.6 *Mooring line tension VS offset for 200 m, 100 m and 50 m*

	Total tension (KN)			Horizontal tension (KN)		
Offset	200	100	50	200	100	50
0	1683.1	1710.91	1295.35	1462.43	1442.88	821.16
1	1760.86	1800.09	1408.01	1540.94	1536.06	953.19
2	1845.49	1900.53	1549.68	1626.09	1641.38	1106.70
3	1937.75	2014.65	1732.32	1719.06	1760.79	1304.61
4	2038.27	2145.49	1975.2	1820.16	1897.11	1562.21
5	2148.54	2290.07	2307.87	1931.27	2048.30	1913.67
6	2269.47	2474.67	2781.51	2052.82	2238.08	2410.16
7	2403.31	2685.45	3481.17	2187.52	2455.67	3131.36
8	2561.9	2939.2	4543.15	2346.5	2716.15	4208.27
9	2757.59	3249.53	6147.25	2541.99	3030.20	5629.57
10	3006.13	3635.55	8443.98	2789.58	3423.91	8144.64
11	3333.51	4154.93	11446.69	3114.65	3950.89	11167.94
12	3784.86	4934.86	15030.87	3561.24	4738.06	14761.25
13	4441.94	6190.3	19033.69	4209.47	5998.49	18762.92
14	5449.86	8257.43	23322	5201.04	8061.52	23063.97
15	7014.78	11328.48		6737.56	11120.3	
16	9258.57	15144.2		8937.14	14916.74	
17	12049.3			11671.12		
CBS	16769	16769	26278			

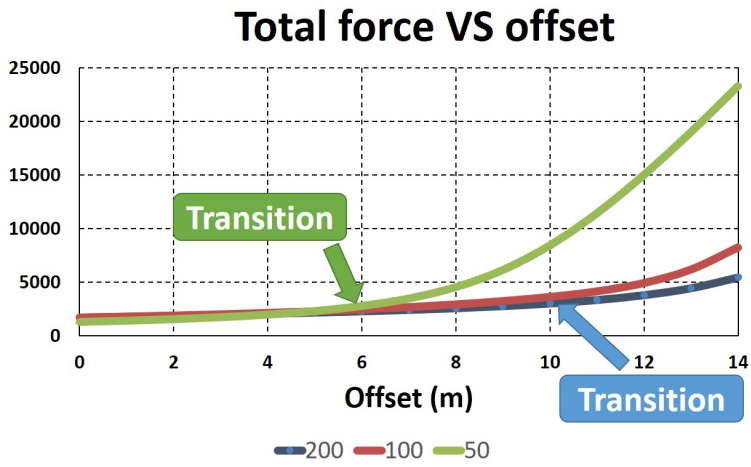

Figure. 5.4 *Mooring line tension VS offset for 200 m, 100 m and 50 m*

The nonlinear tension increment has been taken into consideration by designing large breaking strength of the mooring line. The limit offsets for the three water depths when the mooring line tension is about to reach the catalogue breaking strength are calculated and presented in table 5.6. As calculated, the limit offset for 200 m water depth is 17 m, the limit offset for 100 m water depth is 16 m and the limit offset for 50 m water depth is 14 m. The difference between limit offset and transition offset illustrates that there are large allowable offsets to withstand after the nonlinear transition.

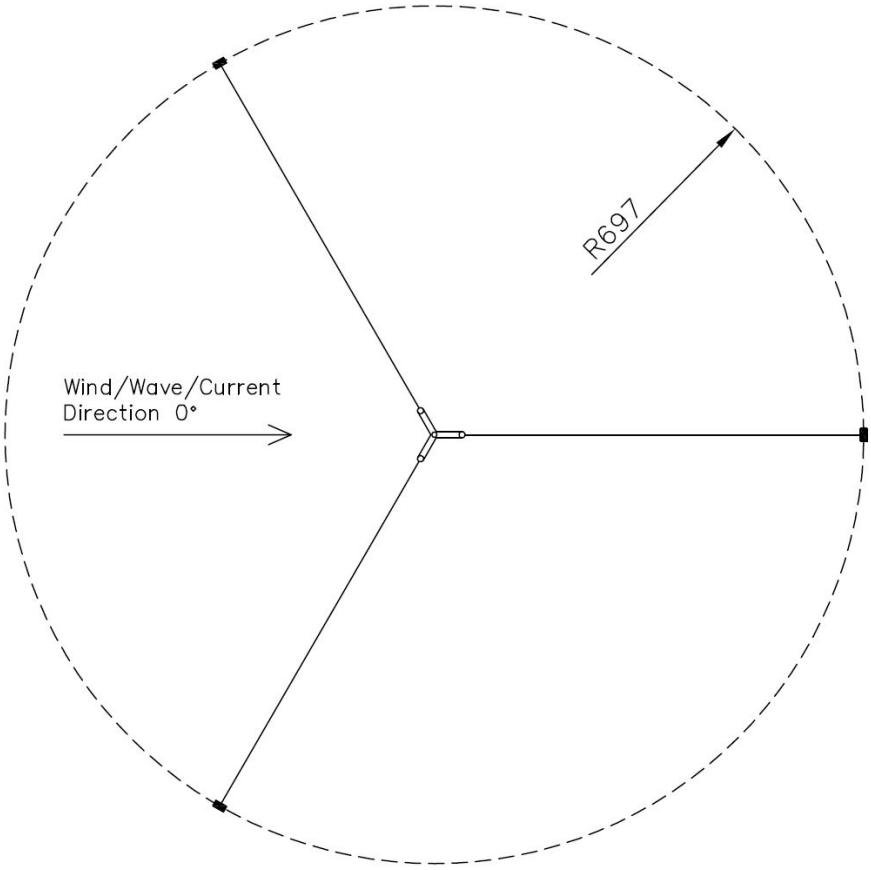

Figure. 5.5 *Mooring system configuration topview - 100 m*

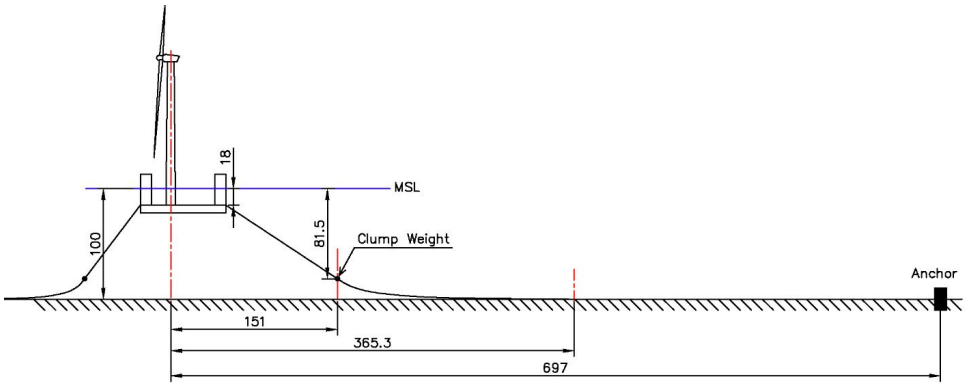

Figure. 5.6 *Mooring system configuration sideview - 100 m*

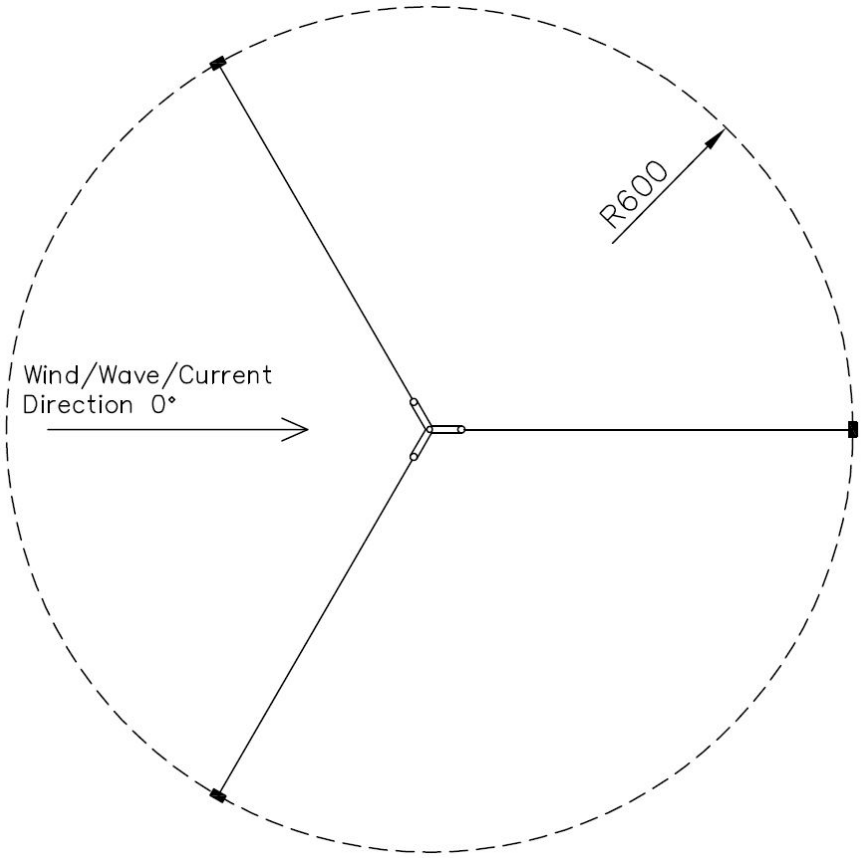

Figure. 5.7 *Mooring system configuration topview - 50 m*

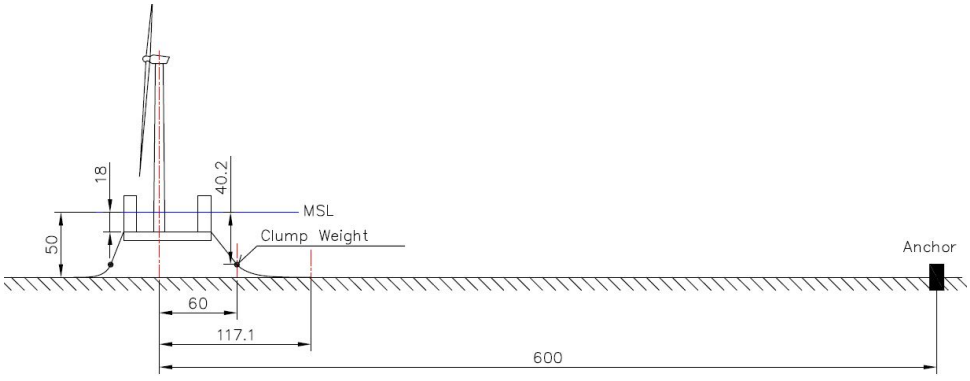

Figure. 5.8 *Mooring system configuration sideview - 50 m*

6 Coupled Dynamic Analysis Result

6.1 Frequency-domain Hydrodynamic Analysis Result

Change of water depth will affect the hydrodynamic properties of the floater, therefore, it is necessary to calculate specific hydrodynamic loads acting on the floater for specific water depths. HydroD (Wadam)[69] in current thesis is used to carry out hydrodynamic analysis of the semi-submersible floating wind turbine without mooring line in 100 m and 50 m water depth. Wadam calculation is based on 3D potential flow theory and utilizes the geometry and meshed panels of floater model which has been constructed in GeniE.

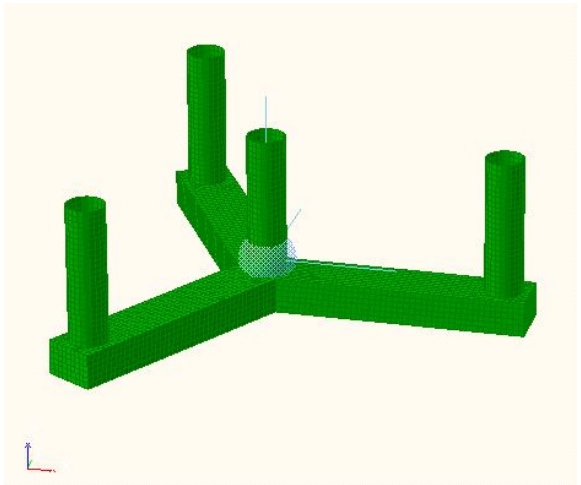

Figure. 6.1 *Hydrodynamic calculation in HydroD*

6.1.1 Eigenfrequency Analysis

The body mass, added mass and stiffness are calculated in HydroD, which could be used to derive the natural frequency of the floater. Because of the symmetry of the floater, pitch and roll motion are of high similarity and horizontal motions are greatly influenced by mooring system, therefore, only heave and pitch motion are of interest to present. The result for 100 m and 50 m water depth are discussed together in order to make a comparison.

The added mass depends on the excitation wave period and converges to a constant value for both heave and pitch, which could be verified by figure 6.2 and figure 6.3.

The natural period of the floater can be calculated according to equation:

$$T_{ni} = 2\pi\sqrt{\frac{M + A_{ii}}{C_{ii}}} \tag{6.1}$$

Where

- M: Body mass, can be read from HydroD result
- A_{ii}: Added mass in i degree of freedom
- C_{ii}: Restoring stiffness

For a typical semi-submersible floater without mooring line, the restoring force mainly comes from large water plane area, which does not change for the two water depth conditions, since the same floater is used. This holds the same for the body mass, while only added mass term change, which is connected with the dynamic pressure caused by the body motions. The natural frequency calculated here can be regarded as a reference to the case with mooring system included in order to check the influence of the mooring system to the floater.

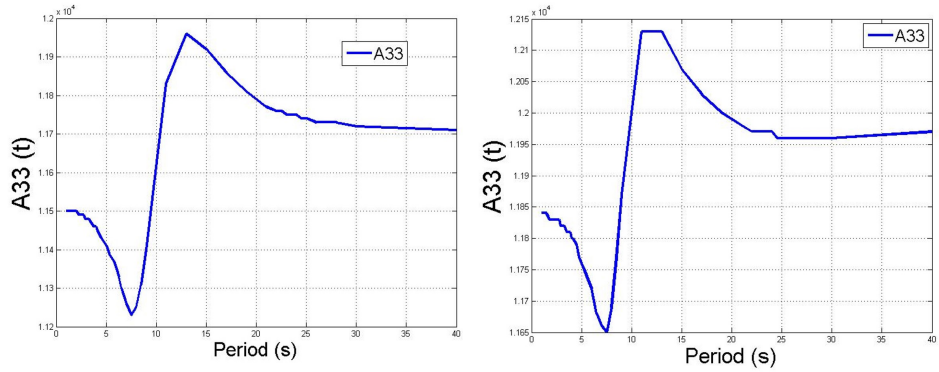

Figure. 6.2 *Added mass of heave motion in head sea for 100 m(left) and 50 m(right) water depth*

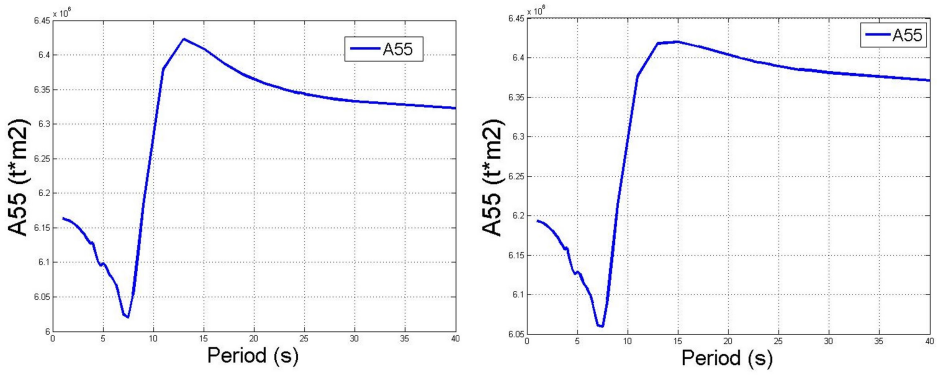

Figure. 6.3 *Added mass of pitch motion in head sea for 100 m(left) and 50 m(right) water depth*

Table. 6.1 *Eigenfrequency calculation for 50 m and 100 m*

Degree of freedom	Heave		Pitch	
Water depth $[m]$	100	50	100	50
Body mass $[kg,\ kg * m^2]$	1.506 E4	1.506 E4	1.066 E7	1.066 E7
Added mass $[kg,\ kg * m^2]$	1.175 E4	1.196 E4	6.336 E6	6.389 E6
Restoring $[N/m,\ N * m]$	1.318 E3	1.318 E3	8.343 E5	8.343 E5
Natural period $[s]$	28.33	28.45	28.36	28.40

6.1.2 Potential Damping

The damping effect plays an important role in limiting the amplitude when the structure is resonating. The potential damping in heave and pitch motion are represented in the figure below. The significant potential damping is located in the wave period between 5 s and 15 s. In the rest range, the potential damping can be neglected.

Theoretically, the potential damping is associated with the capability of the floater to generate waves. When it comes to the long waves case, the behaviour of the floater mainly attempts to follow the wave rather than to interact with the wave. Therefore, the waves generated by the interaction effect are small, which leads to the potential damping at resonance is small. As a result, viscous damping become important to limit the resonant amplitude. The viscous damping can be included based on Morison equation:

$$dF = \underbrace{\rho c_m V \dot{u}}_{\mathrm{F}_I} + \underbrace{\frac{1}{2}\rho C_d A u|u|}_{\mathrm{F}_D} \tag{6.2}$$

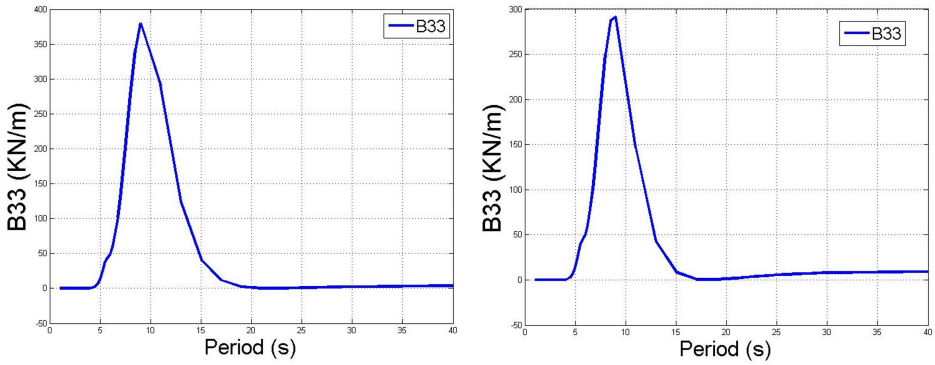

Figure. 6.4 *Potential damping in heave motion in head sea for 100 m(left) and 50 m(right) water depth*

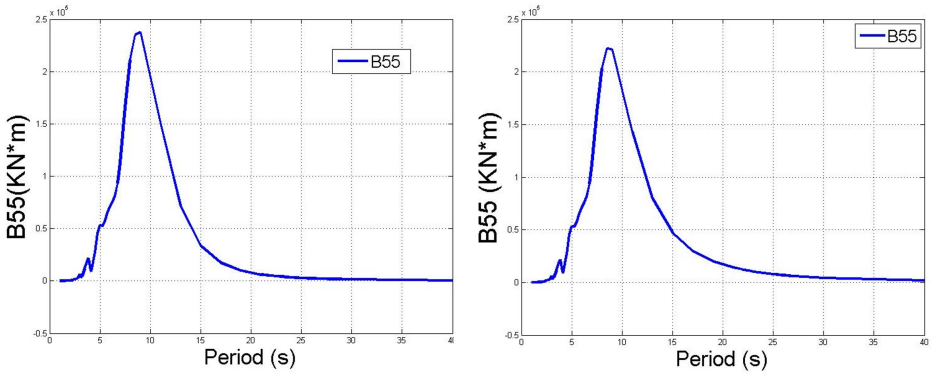

Figure. 6.5 *Potential damping in pitch motion in head sea for 100 m(left) and 50 m(right) water depth*

Where

- C_m: Mass coefficient
- C_d: Drag coefficient

The determination of the coefficient can be referred to DNV standard [68]. The quadratic drag force is added from Simo by attaching elements with Morison force model to the body, where added mass damping and force transfer functions are set to zero and both acceleration terms and quadratic damping terms from Morison equation are included.

6.1.3 Motion RAO

The motion amplitude operator in heave and pitch degrees of freedom shows the resonance occurs at wave period around 25 s to 30 s, which is in accordance with the result of the eigenfrequency analysis. At the same time, the resonant amplitudes do not increase to infinity, which means the potential damping term is functioning to limit the resonant amplitude. In addition, the cancellation effect for heave motion appears in the figure under expectation.

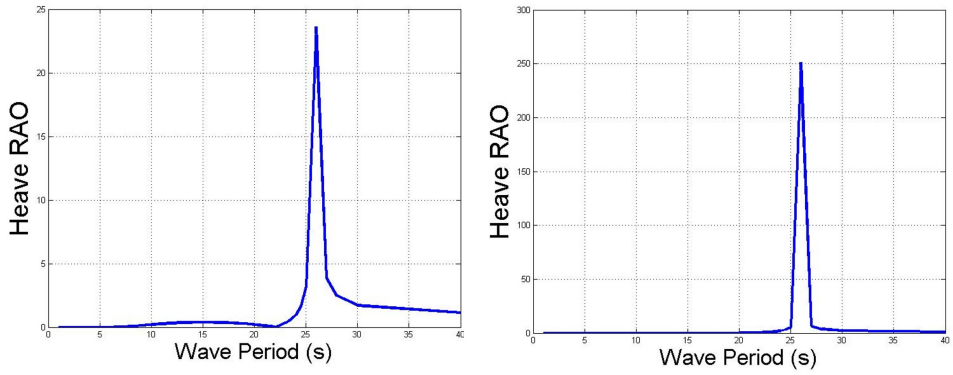

Figure. 6.6 *Heave RAO in head sea for 100 m(left) and 50 m(right) water depth*

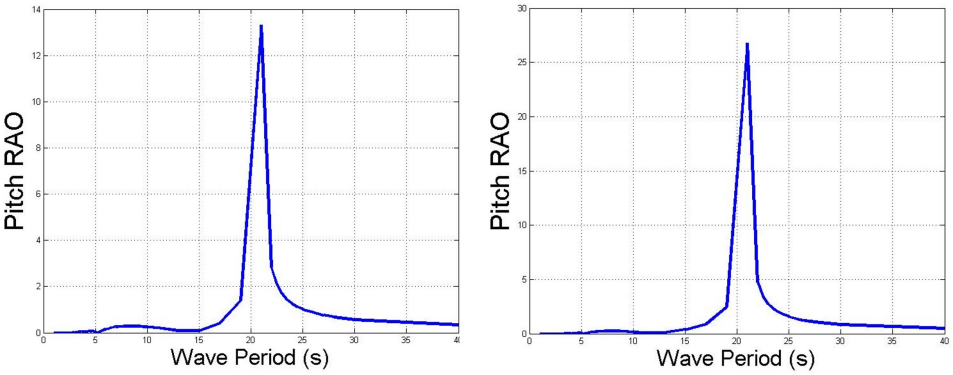

Figure. 6.7 *Pitch RAO in head sea for 100 m(left) and 50 m(right) water depth*

6.1.4 Retardation Function

In order to solve the differential motion equation in time domain, the hydrodynamic interaction effects including the wave excitation forces in both first and second

order and added mass and damping forces should be taken into account. The effects on frequency-dependent added mass and damping forces are included in coupled retardation functions and coupled added mass at infinity frequency. This effect is regarded as the fluid memory effect. Retardation function is computed by a transform of the frequency-dependent added-mass and damping[67]:

$$h(\tau) = \frac{1}{2\pi}\int_{-\infty}^{+\infty}[c(\omega) + i\omega a(\omega)]e^{i\omega t}d\omega = \frac{1}{2\pi}\int_{-\infty}^{+\infty}H(\omega)e^{i\omega t}d\omega \tag{6.3}$$

or

$$H(\omega) = \int_{-\infty}^{+\infty}h(\tau)e^{-i\omega t}d\tau = c(\omega) + i\omega a(\omega) \tag{6.4}$$

This is the Fourier transform of the added-mass and damping:

$$a(\omega) = A(\omega) - A_\infty \tag{6.5}$$

$$b(\omega) = B(\omega) \tag{6.6}$$

A_∞ stands for the asymptotic value of the added mass at infinitely high frequency, while the high frequency limit of the wave damping is assumed to be zero.

DeepC is used in this section to calculate the retardation function by importing the results from HydroD. Figure 6.8 shows the retardation functions for 100 m and 50 m water depths. The retardation function is further kept in sys file which is meant for wave analysis in Simo.

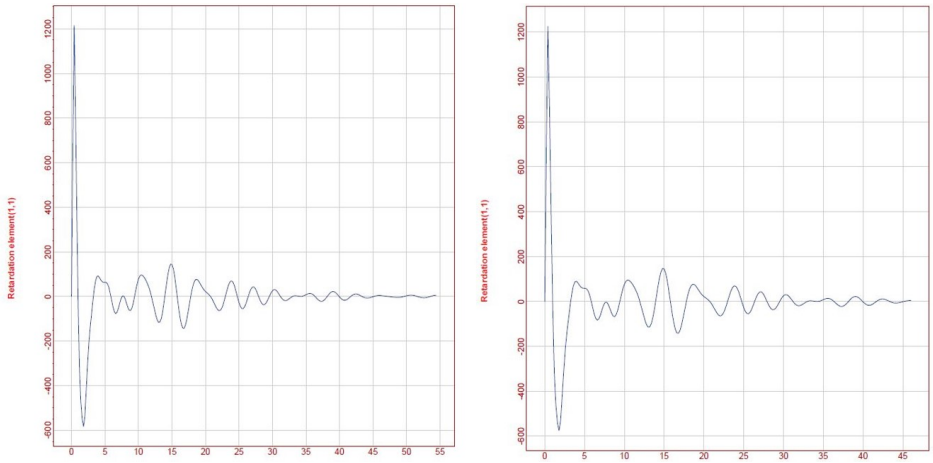

Figure. 6.8 *Retardation functions for 100 m(left) and 50 m(right) water depth*

6.2 Free Decay Analysis Result

Free decay tests are meant to check if the natural periods of floater motions are larger than natural periods for relevant wave in order to avoid large resonant effect due to wave frequency.

The decay tests for 5-MW-CSC floater are performed at the undisturbed position in six degrees of freedom and three water depths. The turbine in under parked condition without rotor rotating. The external environmental loading condition is neglected. The initial displacement of the floater is achieved by applying a ramp force/moment followed by a constant force, which will then be released to let the floater freely oscillate.

The calculation of the linear and nonlinear damping term follows the Energy Slope Method in section 3.4.2 and the simulation is performed in Simo-Riflex-AeroDyn and post-processing is carried out using MATLAB.

Due to the coupling effect between different motions, the platform will always have motions in other degrees of freedom during the decay test, especially for surge-pitch and sway-roll motion. The secondary motion is small compared to the focused motion that it can be neglected. Therefore, the result can be regarded as a pure motion in one degree of freedom.

Table. 6.2 *Natural period and damping of the platform for 50 m, 100 m and 200 m*

Motion	Depth (m)	Natural Period (s)	Linear damping	Quadratic damping
Surge	200	79.43	1.462 E-3	5.063 E-2
	100	78.97	1.670 E-3	3.758 E-2
	50	64.13	1.860 E-3	4.000 E-2
Sway	200	79.43	9.472 E-4	5.290 E-2
	100	74.97	1.780 E-3	3.373 E-2
	50	66.77	1.314 E-3	4.409 E-2
Heave	200	25.34	2.890 E-3	1.905 E-2
	100	25.27	2.426 E-3	1.830 E-2
	50	24.92	2.520 E-3	1.842 E-2
Roll	200	31.14	7.017 E-4	1.703 E-2
	100	30.80	7.986 E-4	1.097 E-2
	50	30.34	1.219 E-3	1.055 E-2
Pitch	200	31.08	2.216 E-4	1.665 E-2
	100	30.74	1.525 E-5	1.054 E-2
	50	30.29	1.418 E-3	7.765 E-3
Yaw	200	57.55	9.468 E-4	4.302 E-2
	100	61.68	1.320 E-3	4.048 E-1
	50	78.43	1.316 E-3	4.800 E-2

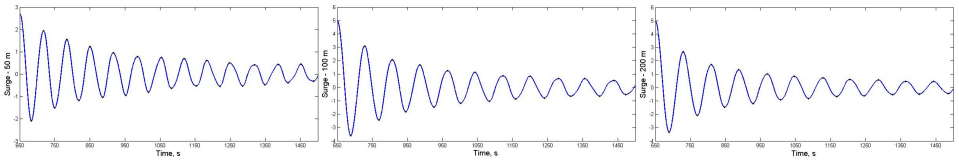

Figure. 6.9 *Surge decay test - 50 m, 100 m and 200 m*

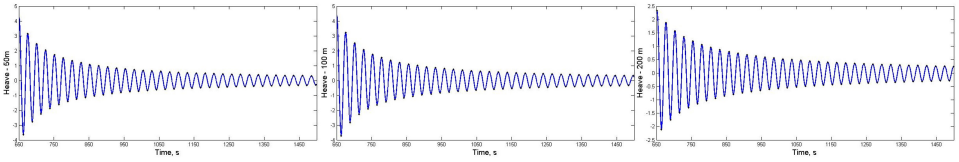

Figure. 6.10 *Heave decay test - 50 m, 100 m and 200 m*

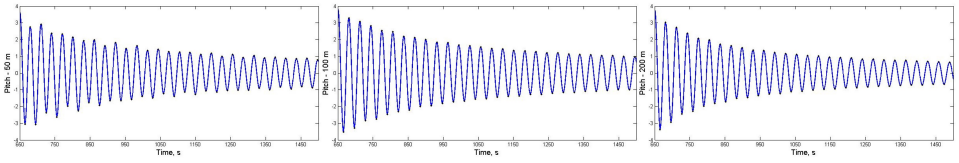

Figure. 6.11 *Pitch decay test - 50 m, 100 m and 200 m*

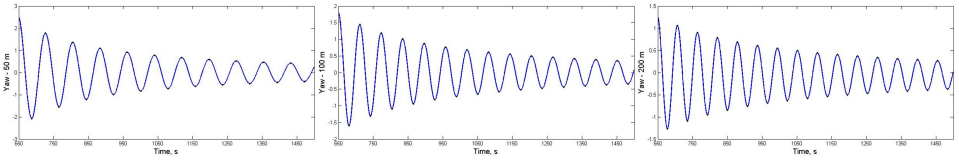

Figure. 6.12 *Yaw decay test - 50 m, 100 m and 200 m*

Generally speaking, all the natural periods in six degrees of freedom for three water depths are within the safe margin. The natural periods in the six degrees of freedom for 50 m and 100 m shows great similarities as those for 200 m with slight difference, which is acceptable. The nonlinear restoring force and elasticity of the mooring line together with the mooring system configuration provides uncertainties during the test, which leads to slight difference between the results for surge, sway motion and roll, pitch motion. Compared the results with those calculated in table 6.1 which is based on pure semi-submersible model, there is difference between them. This results from the influence from mooring system, which provides additional restoring stiffness to the system.

6.3 Ultimate Limit State Analysis Result

In this section, Simo-Riflex-AeroDyn is utilized to perform the extreme condition test, mainly focus on the mooring system performance and the floater responses.

The load condition used in ultimate limit state corresponds to the proposal from Lin Li and has been introduced in section 4.5. Two typical conditions have been selected with one corresponds to maximum mean wind speed and one corresponds to maximum significant wave height. Detailed environmental conditions can be referred to table 4.3. The wind files used here are generated by TurbSim [63] with wind speed corresponding to the hub height using Kaimal turbulence model. In addition, four wave directions have been selected to capture the maximum case: 0°, 45°, 60°, 90°. Moreover, ten different wave and wind seeds have been determined to account for stochastic uncertainty. Accounting for the three water depths, 240 one hour simulations have been carried out in total. The numbering of the mooring line and wave directions are illustrated in the figure 6.13.

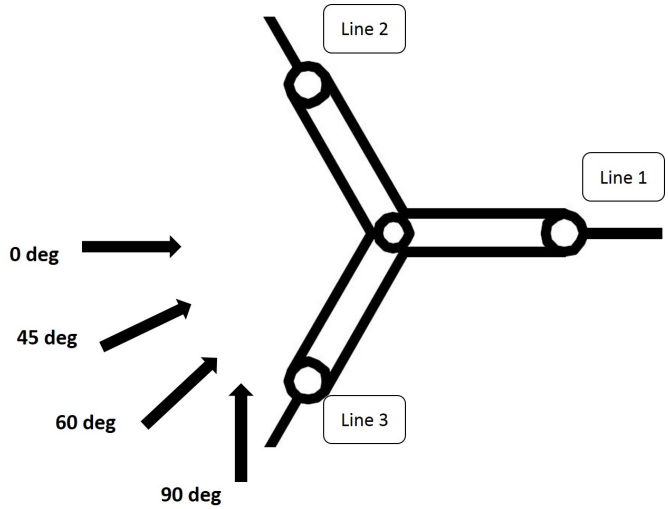

Figure. 6.13 *Numbering of mooring lines and definition of wave directions*

6.3.1 Mooring Line Tension

I. Maximum Wind Speed Condition (ULS-1)

The ULS-1 condition corresponds to the condition with maximum mean wind speed: $U_w = 41.86m/s$ at hub height, $H_s = 13.4m$, $T_p = 13.1s$. The main results are presented in table 6.3 including averaged mean tension (T_{C-mean}), dynamic tension (T_{dyn}), characteristic strength (S_C) and utilization factor (u).

Take the result for one water depth as an example: the maximum mooring line tension occurs in the case when the wave loads are acting directly towards the mooring line, i.e. for mooring line 3 with 60° wave incoming direction. This is because the windward mooring line is in tension with the largest possible offset acting one it while the leeward line is at rest and the offset at the fairlead is relatively small. This discovery applies to all three water depth.

For most cases, the dynamic tension takes smaller part of the total composition compared with mean tension part, which means the mean static force due to wave and wind is dominating and the dynamic behaviour in wave frequency and low frequency are not strong. The utilization factor for mooring line 3 is relatively larger than the other two lines, since it is deployed at windward direction. Despite, the utilization factors for all the cases are on the quite safe side: minimum value is 0.017 and maximum value is 0.321. This evidence shows that the strength of the mooring line is enough to withstand the ULS-1 condition.

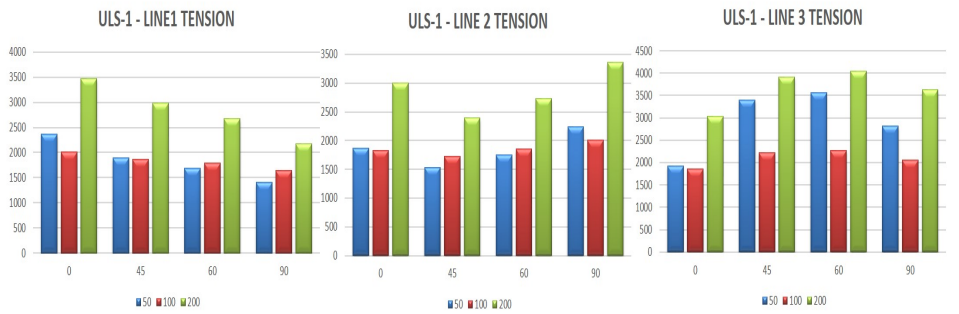

Figure. 6.14 *Average of maximum tension in ULS-1*

Compare the most probable maximum (MPM) mooring line tensions for all three water depths in ULS-1 condition shown in figure 6.14: the tension in 200 m is relatively higher than those in 50 m and 100 m for all wave incoming directions. As discussed in static design section, mooring system design for 200 m is stiffer than 100 m and 50 m. In ULS-1 condition, where environmental condition is not extremely severe so that the tension increment due to degree of tightness in 200 m is more significant than due to nonlinear increment in 50 m i.e. nonlinear tension increment is still in the early stage which greatly influence shallow water depth (50 m). The performance of mooring system in 100 m provides satisfactory result without large tension like 200 m, which indicates the good determination of tightness degree in 100 m.

Table. 6.3 *ULS-1 ($U_w = 41.86m/s$, $H_s = 13.4m$, $T_p = 13.1s$) result - Mooring line tension*

Dir	No.	T_{C-mean}			T_{dyn}			S_C			u		
		50	100	200	50	100	200	50	100	200	50	100	200
0	1	1203.19	1437.94	1597.36	1048.51	539.96	1771.84	2.50E4	1.59E4	1.59E4	0.116	0.150	0.277
	2	1312.98	1552.75	1720.40	503.12	259.65	1204.60	2.50E4	1.59E4	1.59E4	0.088	0.132	0.232
	3	1344.33	1577.47	1744.63	527.37	258.33	207.67	2.50E4	1.59E4	1.59E4	0.091	0.133	0.140
45	1	1216.62	1451.34	1611.77	618.48	383.56	1267.13	2.50E4	1.59E4	1.59E4	0.091	0.136	0.231
	2	1276.43	1517.10	1681.45	237.57	205.90	662.35	2.50E4	1.59E4	1.59E4	0.071	0.124	0.179
	3	1382.74	1602.12	1770.39	1765.36	551.18	1998.71	2.50E4	1.59E4	1.59E4	0.167	0.163	0.310
60	1	1224.09	1460.36	1621.37	426.00	318.04	973.63	2.50E4	1.59E4	1.59E4	0.080	0.131	0.204
	2	1272.34	1509.22	1672.04	436.36	328.68	975.66	2.50E4	1.59E4	1.59E4	0.082	0.135	0.207
	3	1375.58	1599.37	1767.97	1893.82	594.93	2114.63	2.50E4	1.59E4	1.59E4	0.174	0.166	0.321
90	1	1244.51	1481.57	1645.47	145.09	155.53	490.03	2.50E4	1.59E4	1.59E4	0.064	0.117	0.160
	2	1253.76	1491.23	1653.98	885.54	489.47	1596.42	2.50E4	1.59E4	1.59E4	0.109	0.149	0.265
	3	1372.50	1594.56	1762.07	1287.80	418.24	1771.83	2.50E4	1.59E4	1.59E4	0.138	0.150	0.289

II. Maximum Significant Wave Height Condition (ULS-2)

The ULS-2 condition corresponds to the condition with maximum significant wave height: $U_w = 38.87m/s$ at hub height, $H_s = 15.6m$, $T_p = 14.5s$. The main results have been summarized in table 6.4 with respect to mooring line tension and corresponding utilization factors.

Generally speaking, the maximum mooring line tension still happens in the case when the wave acting aligned with the mooring system configuration, i.e. wave direction close to 60°. Moreover, the dynamic behaviour of the mooring line tension becomes competitive compared with the mean static tension, especially in shallow water where the total tension increases significantly.

In ULS-2 condition, mooring line tension and utilization factors are relatively larger than those in ULS-1 condition for all the cases, which indicates that mooring line response is more sensitive to wave condition than wind condition. The maximum utilization in 200 m has been increased to 0.412, while the maximum factors in 50 m is 0.309 and 0.209 for 100 m. However, the maximum tensions still have not exceeded the capacities for all three designs.

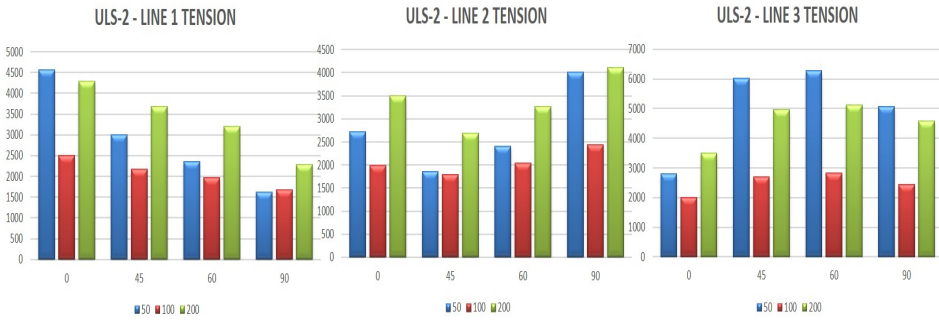

Figure. 6.15 *Average of maximum tension in ULS-2*

In accordance with figure 6.15 where the average of maximum tension in ULS-2 condition have been demonstrated, the tension for 50 m depth increases remarkably to a high amplitude. This is because the environmental condition especially wave condition has become severe enough to give rise to significant nonlinear tension increment. Once the tension enters the nonlinear increment part, it will be more notable in shallow water (50 m) as expected. At the same time, the influence due to degree of tightness plays less important role on the contrast. The mooring system in 100 m shows great performance again without extreme tension increment, which indicates that the nonlinear increment effect is not significant in 100 m water depth.

Table. 6.4 *ULS-2 ($U_w = 38.87m/s$, $H_s = 15.6m$, $T_p = 14.5s$) result - Mooring line tension*

Dir	No.	T_{C-mean}			T_{dyn}			S_C			u		
		50	100	200	50	100	200	50	100	200	50	100	200
0	1	1235.96	1449.55	1605.08	2733.14	942.15	2527.92	2.50E4	1.59E4	1.59E4	0.219	0.188	0.348
	2	1333.06	1553.61	1721.49	1109.04	393.09	1641.40	2.50E4	1.59E4	1.59E4	0.125	0.144	0.273
	3	1357.70	1573.16	1740.75	1132.49	381.84	1621.55	2.50E4	1.59E4	1.59E4	0.128	0.144	0.272
45	1	1245.44	1460.89	1618.13	1481.76	644.31	1887.87	2.50E4	1.59E4	1.59E4	0.143	0.162	0.289
	2	1296.88	1519.55	1681.82	452.51	254.85	898.78	2.50E4	1.59E4	1.59E4	0.084	0.129	0.201
	3	1402.99	1598.57	1769.28	3681.21	944.44	2925.32	2.50E4	1.59E4	1.59E4	0.293	0.199	0.397
60	1	1251.58	1469.76	1628.03	906.72	464.14	1429.77	2.50E4	1.59E4	1.59E4	0.109	0.145	0.247
	2	1293.34	1511.95	1671.79	916.06	482.75	1436.80	2.50E4	1.59E4	1.59E4	0.112	0.149	0.251
	3	1397.89	1596.52	1767.57	4129.51	1048.68	3084.03	2.50E4	1.59E4	1.59E4	0.309	0.209	0.412
90	1	1269.95	1489.44	1652.43	293.24	172.26	584.67	2.50E4	1.59E4	1.59E4	0.074	0.119	0.169
	2	1280.50	1495.44	1654.48	2309.00	857.86	2264.62	2.50E4	1.59E4	1.59E4	0.195	0.184	0.327
	3	1390.87	1591.26	1760.43	3006.03	748.04	2625.87	2.50E4	1.59E4	1.59E4	0.242	0.180	0.368

6.3.2 Floater Motion

In order to focus on the most critical motions, there has been a selection of the motions studied according to wave incoming direction: surge and pitch motions for 0°; surge, sway, roll and pitch motions for 60°; sway and roll motions for 90°. A summary of the mean value and maximum value together with standard deviation is shown in table 6.5.

Table. 6.5 *Floater motion response under extreme condition*

			ULS-1			ULS-2			
Dir	DOF	Depth	Mean	Max	Std	Mean	Max	Std	Unit
0 deg	Surge	50	0.95	8.60	2.01	0.99	12.05	2.91	m
		100	1.34	7.58	1.64	1.26	9.76	2.24	m
		200	1.41	7.82	1.56	1.43	10.21	2.12	m
	Pitch	50	0.69	3.18	0.63	0.59	3.13	0.70	deg
		100	0.77	3.88	0.76	0.66	3.84	0.76	deg
		200	0.75	4.21	0.76	0.66	4.58	0.89	deg
60 deg	Surge	50	0.58	4.03	0.99	0.43	4.81	1.43	m
		100	0.96	4.03	0.81	0.86	4.67	1.10	m
		200	0.98	3.81	0.75	0.91	4.24	1.00	m
	Sway	50	0.43	6.34	1.69	0.27	7.92	2.40	m
		100	0.76	6.07	1.37	0.71	7.34	1.88	m
		200	0.81	5.62	1.28	0.81	6.53	1.71	m
	Roll	50	0.46	2.75	0.58	0.40	3.18	0.73	deg
		100	0.47	3.01	0.66	0.41	3.21	0.71	deg
		200	0.45	3.14	0.71	0.38	3.72	0.86	deg
	Pitch	50	0.64	2.15	0.45	0.54	2.03	0.48	deg
		100	0.70	2.45	0.51	0.59	2.26	0.47	deg
		200	0.68	2.37	0.47	0.56	2.42	0.52	deg
90 deg	Sway	50	0.63	7.87	1.98	0.57	10.30	2.85	m
		100	0.90	7.13	1.61	0.86	8.97	2.20	m
		200	0.95	6.92	1.50	0.99	8.68	2.02	m
	Roll	50	0.60	3.05	0.59	0.52	3.28	0.69	deg
		100	0.56	3.43	0.70	0.49	3.62	0.74	deg
		200	0.52	3.72	0.76	0.45	4.34	0.92	deg

First of all, total motion response is composed of a mean static response due to steady wave and wind together with a dynamic response due to wave frequency and low frequency response, which is same as the composition of tension response. Generally speaking, the motion responses are larger in ULS-2 condition where the wave condition is more severe. This demonstrates that floater motion response is more sensitive to wave condition than wind condition, which is the same as tension response.

The maximum excursion happens in surge motion: 12.05 m for 50 m depth, 9.76

m for 100 m depth and 10.21 m for 200 m depth, when wave comes from 0 ° for all the three water depths. The extreme configuration when the mooring line is about to be totally lifted up according to the static analysis result in table 5.3 shows that the offset limits for the three water depths are: 14 m for 50 m depth, 10 m for 100 m depth and 6 m for 200 m depth. This evidence illustrates that the maximum offsets for 50 m and 100 m are acceptable, while the mooring line for 200 m depth is totally lifted up and there could be a potential of vertical load acting on the anchor. Further improvement could be made by increasing the mooring line length lying on the seabed to make sure of the protection to the anchor. However, if the tension response in 200 m is considered, even though the mooring line has been lifted up, the tension does not show huge increment. This is because the total mooring line length is long, the mooring line still keeps a catenary shape rather than a straight line when experiencing large offset at the fairlead.

6.3.3 Spectrum Analysis

I. Mooring Line Tension

The tension spectrum for three mooring lines in head sea under ULS-1 condition are presented in the figure following. There is great similarity among the three mooring line tension spectrum: The most significant contribution comes from wave frequency ranging from 0.25 to 1 rad/s. Another contribution is wind-induced low frequency effect mainly from surge motion in current case. The low frequency component is not competitive to total response composition, which is because wind turbine is under parked condition and wind induced effect and second order wave force is much smaller compared with first order wave force under extreme condition.

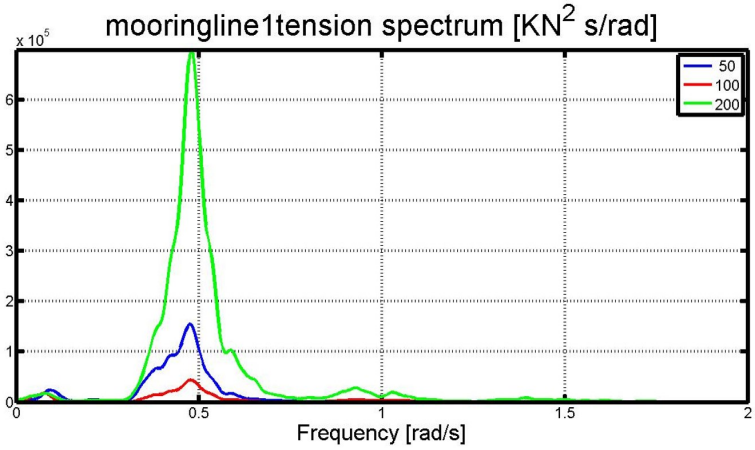

Figure. 6.16 *Mooring line 1 tension spectrum under ULS-1 condition for three water depths*

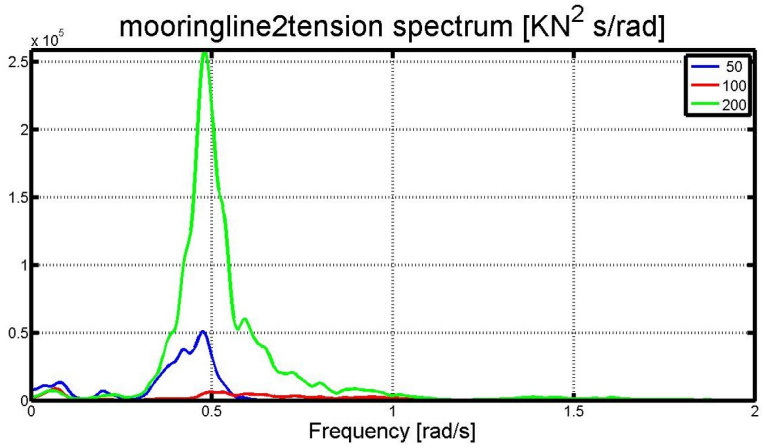

Figure. 6.17 *Mooring line 2 tension spectrum under ULS-1 condition for three water depths*

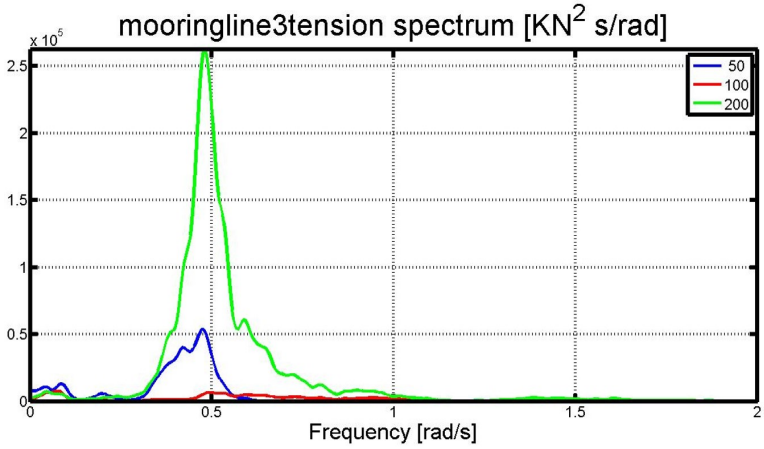

Figure. 6.18 *Mooring line 3 tension spectrum under ULS-1 condition for three water depths*

The spectrum analysis of mooring line tension in ULS-2 condition shows great comparability as in ULS-1 with slight difference in amplitude, because the excitation forces are the same while only the magnitudes of the force are changed. Therefore, no relevant spectrum figures are presented for ULS-2 condition. A collection of all the spectrum can be found in the appendix.

II. Floater Motion

The floater motion response spectrum with 60 deg incoming wave direction in ULS-2 condition are discussed as an example. For surge motion, wave frequency response is dominating ranging from 0.3 to 0.7 rad/s. In addition, there is a low frequency response around 0.07 rad/s, which is due to surge resonance. Moreover, the coupling between surge and pitch also contribute to total motion response. It is notable to find out a small peak located at about 0.2 rad/s which coincides with pitch resonant frequency.

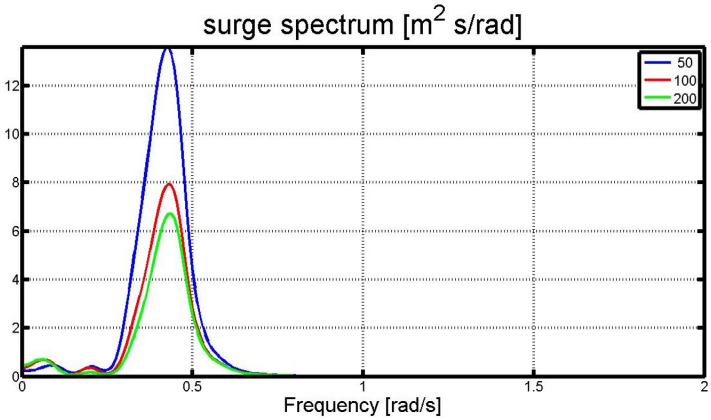

Figure. 6.19 *Surge motion spectrum under ULS-2 condition - 60 deg*

For sway motion, the main contribution comes from wave frequency with a small response due to sway resonance. There is no significant coupling effect detected.

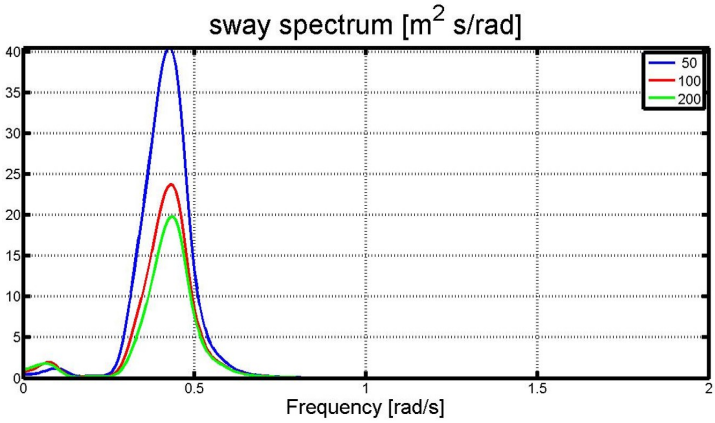

Figure. 6.20 *Sway motion spectrum spectrum under ULS-2 condition - 60 deg*

For roll motion, the roll resonant contribution around 0.19 rad/s becomes larger compared with the first two motion resonant responses, while the main factor is still wave frequency likewise. The coupling effect between sway and roll motion is not obvious as well.

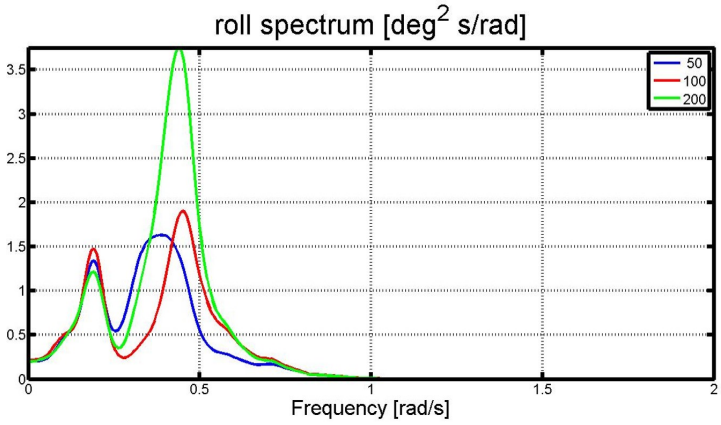

Figure. 6.21 *Roll motion spectrum under ULS-2 condition - 60 deg*

For pitch motion, the pitch resonant contribution is in leading position larger than wave frequency contribution, which makes it different from other responses. This difference is due to the influence from wind force, which increase the pitch resonance significantly and pitch motion is quite sensitive to wind-induced force. Since wind turbine is under parked condition during the ultimate limit state test, the mean pitch motion is quite small. During operational condition large pitch motion due to thrust force can be expected.

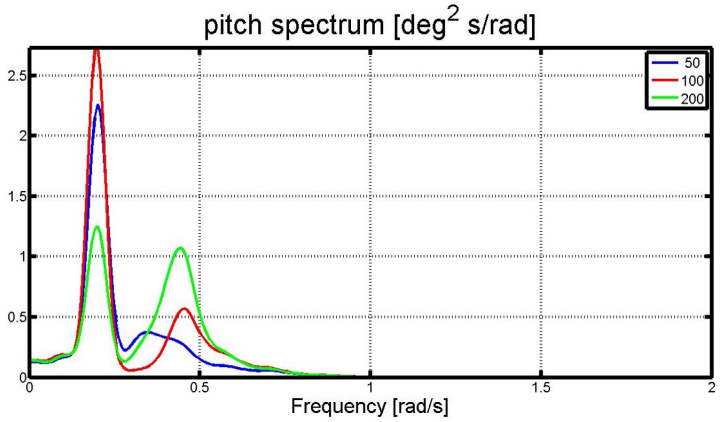

Figure. 6.22 *Pitch motion spectrum under ULS-2 condition - 60 deg*

6.3.4 Comparison between Three Water Depths

The case where mooring line has maximum tension response is mooring line 3 with wave coming from 60°. The tension responses have been summarized in figure 6.23. It is found that nonlinear tension increment becomes significant in shallow water (50 m) as expected, which leads to relatively higher tension amplitude. Despite, all the tension responses do not exceed the breaking strengths.

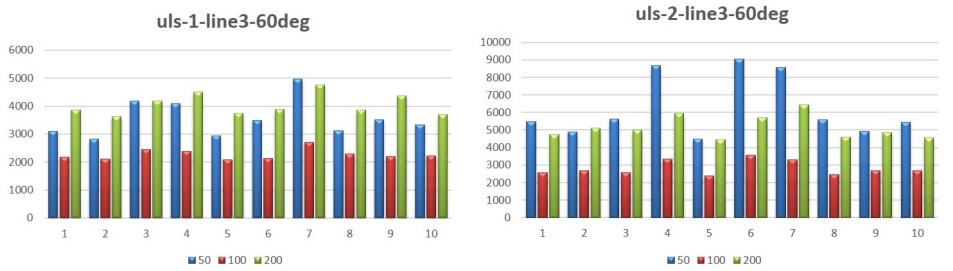

Figure. 6.23 *Maximum mooring line tension case*

The case where floater has maximum offset is surge motion with 0 deg wave direction. Corresponding results have been collected in figure 6.24. It shows that 200 m mooring system has a good control over the floater offset, while the offsets in 50 m water depth are relatively large because of the soft mooring system.

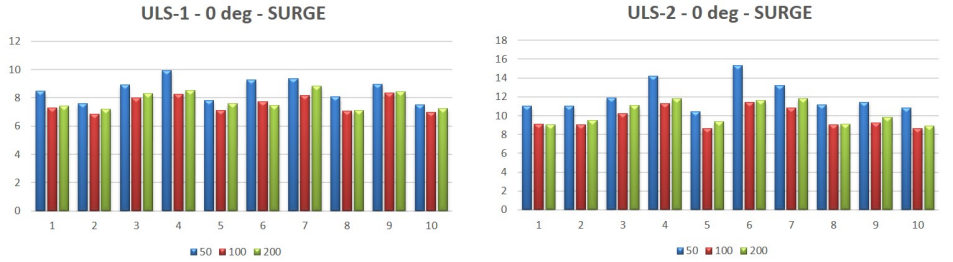

Figure. 6.24 *Maximum motion case: surge - 0 deg*

In conclusion, in order to avoid nonlinear tension increment in shallow water, mooring system for 50 m water depth is designed to be soft on purpose, which leads to relatively large offset range. However, maximum offset is still within acceptable range. Take the tension and motion performance for 200 m into account, there is a great balance between tension control and motion control. Furthermore, the mooring system design concept for 100 m shows most desirable results: tension response is not greatly influenced by the nonlinear tension increment law and resulting offset range is reasonably small.

6.4 Fatigue Limit State Analysis Result

Six one-hour simulations with different wave and wind random seeds are performed for one wave direction in one water depth. One total simulation lasts for 4000 s, while the first 400 s is ignored because the turbine is unstable with large deviation. Together with 3 water depths and 15 conditions, there have been 270 simulations carried out in total. Only one wave direction is chosen here: 0°. Mooring line damage and tower base damage have been calculated: mooring line tension and tower base responses from Riflex results are applied to calculate the stress range. The cycling counting result is based on rainflow counting method by utilizing Matlab Toolbox - WAFO [70]: Function $dat2tp$ extracts the turning point from data and function $tp2rfc$ calculates the rainflow cycles from the sequence of turning points.

The final mooring line fatigue damage result for three water depths together with tower base fatigue damage are showed in table 6.6. The probabilities of the occurrence for each condition are included as well in order to estimate the total damage for 20 years.

6.4.1 Mooring Line Damage

The accumulated fatigue damage in one hour is available for all the three mooring lines in fifteen conditions. Numerically, all the mooring line fatigue damage accumulated in 20 years are acceptable with value smaller than 1, on the safe side.

Figure 6.26 makes it visible to compare the fatigue damage variation in different environmental conditions. The magnitude of fatigue damage for 50 m is almost 1000 times larger than for 100 m and 200 m. Therefore, two y axis is provided with different amplitudes: The blue one on the right is meant for 50 m and the red axis on the left is meant for 100 m and 200 m. Even though the exact amount varies significantly among the three concepts, however, the relative trend in the fifteen conditions are quite similar for the three water depths. The most remarkable fatigue damage happens in condition 8 and 11, where wind speed is close to rated wind speed of the wind turbine and standard deviation in condition 8 ranks the first in figure 6.25, which indicates large stress range.

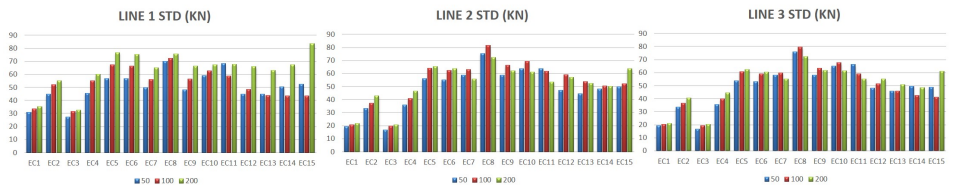

Figure. 6.25 *Comparison of mooring line standard deviation in different conditions*

Normally, large fatigue damage usually accompanies with large stress range. Nevertheless, mooring line tension standard deviations in figure 6.25 do not illustrate huge difference among the three water depths. According to DNV-OS-E301, the chain link is exposed to corrosive influence of sea water without protection measures, while the steel wire rope is equipped with corrosive protection through outer sheathing. This different preprocessing treatment leads to different fatigue properties and different numerical S-N curve parameters as well, which brings about different fatigue damage result in the end.

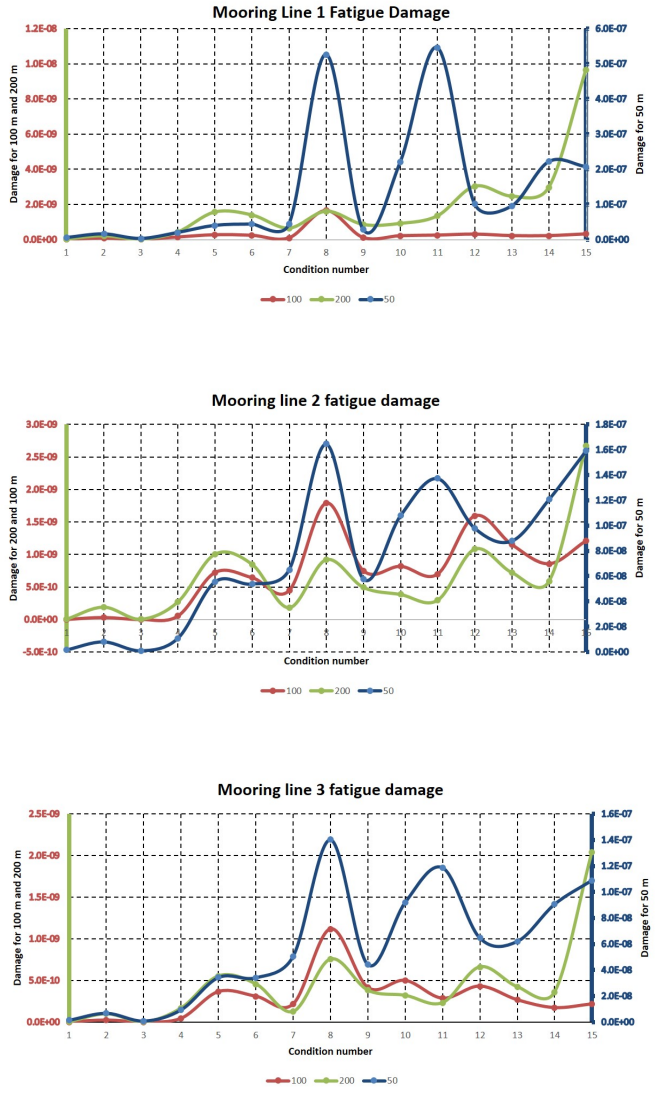

Figure. 6.26 *Mooring line fatigue damage in different conditions and water depths*

Table. 6.6 *Results of fatigue damage for mooring lines and tower base*

	Mooring line 1			Mooring line 2			Mooring line 3			Tower base		
No	50	100	200	50	100	200	50	100	200	50	100	200
EC1	5.61E-9	9.92E-12	1.93E-11	1.61E-9	1.08E-12	3.20E-12	1.45E-9	8.70E-13	2.29E-12	6.89E-7	6.91E-7	6.53E-7
EC2	1.61E-8	7.48E-11	2.04E-10	7.98E-9	3.04E-11	1.88E-10	6.77E-9	2.26E-11	9.78E-11	5.62E-6	5.85E-6	4.07E-6
EC3	3.06E-9	5.85E-12	9.45E-12	9.08E-10	8.48E-13	2.26E-12	8.10E-10	6.77E-13	1.59E-12	3.87E-7	4.13E-7	3.76E-7
EC4	2.01E-8	1.34E-10	4.14E-10	1.07E-8	5.24E-11	2.68E-10	9.44E-9	4.42E-11	1.67E-10	1.58E-5	1.58E-5	1.23E-5
EC5	4.04E-8	2.64E-10	1.55E-9	5.55E-8	7.21E-10	1.00E-9	3.43E-8	3.64E-10	5.52E-10	5.21E-5	5.05E-5	3.11E-5
EC6	4.41E-8	2.34E-10	1.39E-9	5.38E-8	6.42E-10	8.48E-10	3.41E-8	3.08E-10	4.56E-10	4.24E-5	4.01E-5	2.29E-5
EC7	4.37E-8	8.51E-11	6.40E-10	6.50E-8	4.45E-10	1.79E-10	5.05E-8	2.16E-10	1.25E-10	1.09E-5	9.35E-6	8.11E-6
EC8	5.327E-7	1.64E-9	1.60E-9	1.64E-7	1.78E-9	9.19E-10	1.40E-7	1.11E-9	7.55E-10	5.95E-5	5.70E-5	5.38E-5
EC9	2.85E-8	1.07E-10	8.47E-10	5.77E-8	7.48E-10	4.92E-10	4.41E-8	4.13E-10	3.80E-10	2.81E-5	2.65E-5	2.46E-5
EC10	2.21E-7	2.10E-10	9.08E-10	1.07E-7	8.16E-10	3.84E-10	9.19E-8	4.98E-10	3.19E-10	3.19E-5	3.18E-5	3.01E-5
EC11	5.47E-7	2.44E-10	1.33E-9	1.37E-7	6.97E-10	2.94E-10	1.18E-7	2.84E-10	2.31E-10	4.23E-5	4.07E-5	3.61E-5
EC12	1.02E-7	3.01E-10	3.02E-9	9.79E-8	1.59E-9	1.08E-9	6.46E-8	4.30E-10	6.61E-10	1.04E-4	1.00E-4	9.38E-5
EC13	9.56E-8	2.14E-10	2.46E-9	8.78E-8	1.15E-9	7.22E-10	6.19E-8	2.66E-10	4.24E-10	5.89E-5	5.70E-5	5.10E-5
EC14	2.22E-7	2.15E-10	2.96E-9	1.20E-7	8.56E-10	5.84E-10	9.05E-8	1.72E-10	3.56E-10	4.75E-5	4.07E-5	3.52E-5
EC15	2.08E-7	3.12E-10	9.66E-9	1.59E-7	1.21E-9	2.67E-9	1.08E-7	2.16E-10	2.03E-9	6.25E-5	5.09E-5	4.57E-5
20Year	4.62E-3	1.78E-5	8.66E-5	3.66E-3	3.68E-5	4.95E-5	2.71E-3	1.86E-5	2.99E-5	2.631	2.558	1.908

6.4.2 Tower Base Response

Wind turbine tower experiences large axial force and bending moment during operation, which could lead to large fatigue damage. Two different orientated bending moments in global Y direction and global Z direction are caused by wind turbine control strategy [71]. Normally, the variable-speed wind turbine operates in two primary wind speed regimes: below-rated wind speed and above-rated wind speed. When the wind speed is below rated wind speed and generated power is below rated power, control system will operate to adjust the rotor speed to capture the maximum available amount of energy. This is achieved by controlling generator torque without modifying blade pitch angle. In above-rated wind speed condition, the power output is maintained at a steady level to protect rotor system, which is done by holding the generator torque constant and changing blade pitch angle. This control strategy lead to the different trends for thrust and torque along with wind speed, which furthermore influence the bending moment in two directions.

Based on the control theory mentioned just now, figure 6.27 provides a corresponding numerical example: tower base bending moment in Y direction increases to maximum value when the wind speed comes close to the rated wind speed then decreases when the wind speed continues to increase, which follows the same trend as thrust. At the same time, tower base bending moment in Z direction keeps increasing until the wind speed comes close to rated wind speed and become almost constant when the wind speed is above rated speed, which follows the same trend as torque.

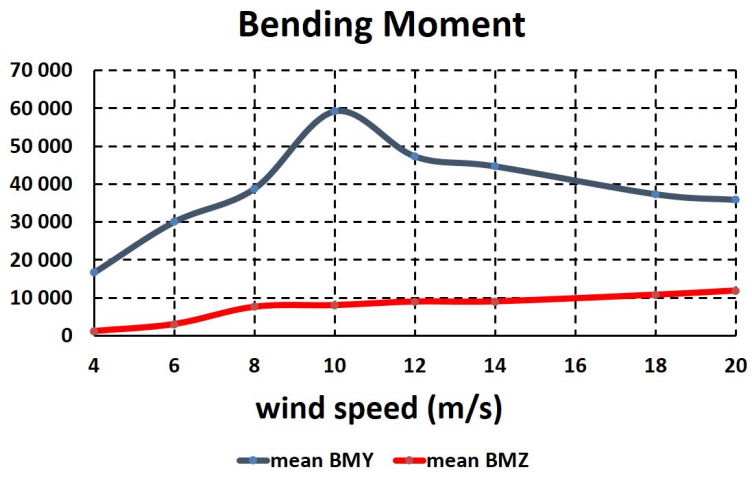

Figure. 6.27 *Bending moment varies with wind speed*

The resulting fatigue damage to tower base is shown in figure 6.28. The fatigue damage for tower base is strongly influenced by the standard deviation of bending

moment acting on it. Moreover, the damage in three concepts are of the same magnitude. The total damages for 20 year are larger than 1 for all three cases, which means there is a potential of fatigue failure for tower base. Improvement method can be increasing the plate thickness of the tower.

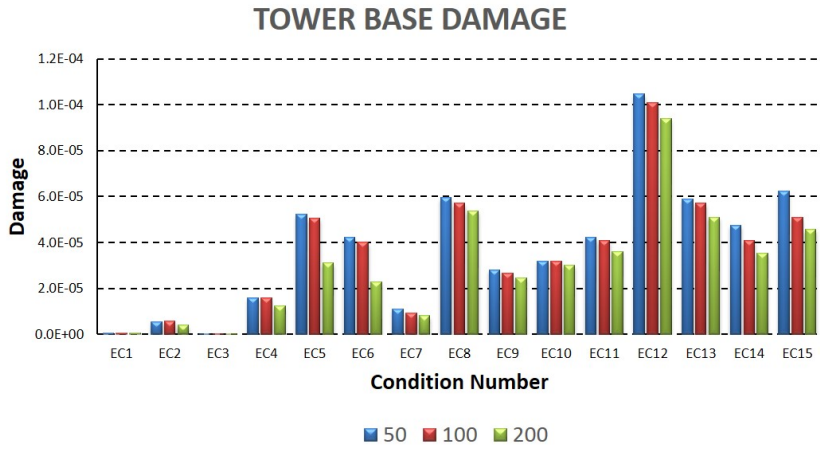

Figure. 6.28 *Fatigue damage for tower base*

6.4.3 Floater Motion Responses

Table. 6.7 *Floater motion responses*

		Mean surge (m)			Mean pitch (deg)			SD surge (m)			SD pitch (deg)		
No	Uw	50	100	200	50	100	200	50	100	200	50	100	200
1	4	0.91	1.38	1.36	1.05	1.12	1.10	0.35	0.53	0.51	0.40	0.42	0.41
2	6	1.60	2.43	2.37	2.07	2.21	2.14	0.56	0.90	0.84	0.67	0.70	0.69
3	4	0.84	1.28	1.24	1.05	1.11	1.08	0.31	0.51	0.48	0.39	0.42	0.41
4	6	1.76	2.67	2.59	2.08	2.23	2.16	0.59	0.93	0.85	0.67	0.71	0.70
5	8	2.73	4.11	4.03	3.53	3.75	3.68	0.81	1.27	1.20	1.02	1.08	1.06
6	8	2.68	4.03	3.97	3.52	3.74	3.67	0.82	1.26	1.19	1.02	1.07	1.01
7	10	4.08	6.11	6.04	5.39	5.73	5.62	0.81	1.21	1.17	0.96	1.03	1.48
8	12	4.52	6.77	6.75	5.54	5.94	5.85	0.95	1.50	1.37	1.42	1.53	1.48
9	10	4.22	6.31	6.24	5.39	5.75	5.63	0.77	1.18	1.15	0.96	1.03	1.01
10	12	4.20	6.32	6.24	5.51	5.89	5.76	0.87	1.33	1.21	1.42	1.53	1.46
11	14	3.40	5.17	5.02	4.56	4.88	4.73	0.96	1.25	1.13	1.62	1.75	1.65
12	18	2.82	4.26	4.16	3.50	3.73	3.65	0.66	0.85	1.74	1.27	1.34	1.24
13	18	2.65	4.02	3.92	3.49	3.72	3.63	0.69	0.80	0.71	1.25	1.32	1.22
14	18	2.58	3.90	3.81	3.48	3.71	3.62	0.82	0.87	0.77	1.24	1.31	1.19
15	20	2.40	3.63	3.56	3.21	3.42	3.34	0.91	0.86	0.78	1.05	1.10	0.99

Floater motion responses are greatly influenced by the performance of mooring system. During operational condition, floater motion has to be limited to an acceptable range to ensure normal operation of wind turbine. It will furthermore influence the safety of power cable.

As mention above, wind turbine control system shifts between torque control and pitch control at rated wind speed which is around 11.4 m/s. Moreover, the adjustment of blade pitch angle will lead to smaller wind force acting on the blade, which furthermore could decrease the horizontal excursion of floater. The result in table 6.7 provides relevant proof where larger surge and pitch motion occurs in condition 7, 8, 9 and 10 when the wind speed is around rated wind speed. When the wind speed continues to increase, the motion responses do not increase. Furthermore, the maximum motion response occurs in condition 8 where the wave height is larger than condition 7 and wave peak period is shorter than condition 9 and 10. This discovery holds the same for all three water depths, which highlights that wind is dominating in operational condition by influencing the mean motion responses.

Compare the surge motion in condition 12, 13 and 14 where the significant wave height and the wind speed are the same and wave peak period vary from 8 s to 12 s, the results confirm that higher wave frequency will lead to larger motion offset. The same discovery can be verified by comparing the mean surge in condition 1, 3; condition 5, 6; and condition 8, 10. As for the standard deviation of motion responses, higher significant wave height (severe wave condition) will give rise to larger deviation, since the fluctuation of the floater motion is mainly introduced by hydrodynamic loads and it becomes significant when wave height increases.

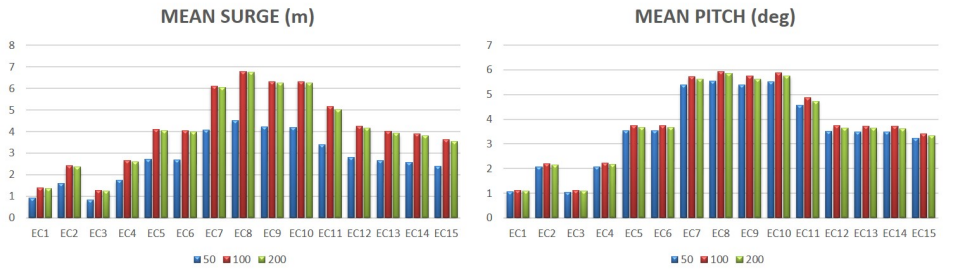

Figure. 6.29 *Floater motion in surge and pitch*

Pitch is a critical motion response in operational condition, since this is the only motion that is larger than extreme condition. With blades rotating, there exists a thrust force acting on the blades, which will induce a large pitch motion. Pitch motion is not significant in extreme condition since wind turbine is under parked condition without blades rotating.

Overall, all the motion excursions in the three water depths are reasonably acceptable. From motion control point of view, all three design concepts provide satisfactory performance.

6.4.4 Wind Turbine Performance

The Wind turbine performance concerning rotor speed and generated power is checked as well to verify if the wind turbine is operating normally.

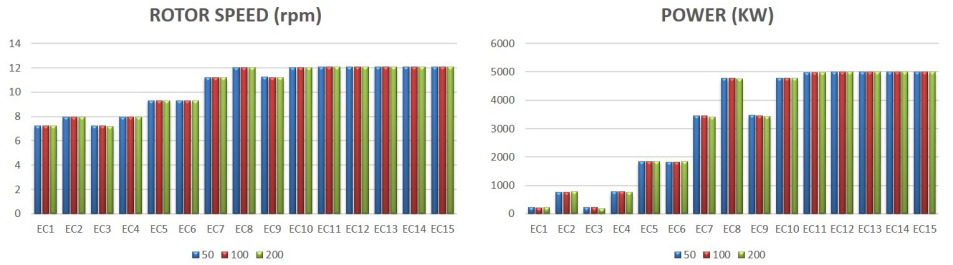

Figure. 6.30 *Wind turbine performance*

Accordingly, rated rotor speed is around 12 rpm and mean rotor speed increases with the wind speed increases with the purpose to maximum the power output. Yet, when the wind speed is over rated wind speed, the blade pitch angle starts to be adjusted by control system in order to keep the speed steady and protect the turbine.

The rated power generating capacity is 5MW as can be seen from figure 6.30. The yearly power generation taking the probabilities of the environmental conditions into account is about 9.64 $E7$ KWh on average. According to statistics of energy consumption of one Norwegian family in 2012[72], annual electricity consumption is about 16000 KWh, which means the 5-MW-CSC floating wind turbine could support nearly 600 Norwegian families for power supply.

6.4.5 Spectrum Analysis

The spectrum explains the frequency distribution of the excitation loads without regard to exact time. It is very useful especially for complex system by providing insight to complicated physical phenomenon. The spectrum in current section are transformed by Fast Fourier Transform of the time series and some post-processing modification has been done using Matlab WAFO toolbox.

Three environmental conditions (condition 6, 8 and 12) corresponding to wind speed below, around and above rated wind speed are selected to represent the results. The frequency distributions for all three water depths are presented in the same figure for comparison. Furthermore, mooring line tension and tower base moment have been chosen as the study focus. Because of the similarity of the excitation force and resulting spectrum, only the response spectrum in condition 12 is presented here. The rest spectrum can be referred to Appendix.

The rated rotor speed is 12 rpm according to figure 6.30, when the wind speed is above rated wind speed, which means the rotational period for one revolution ($1P$) is 5 s and corresponding frequency is 1.26 rad/s. The blade passing frequency ($3P$) is in the range between 2.5 rad/s to 4 rad/s. The wave peak period in this condition is 8 s, with frequency around 0.79 rad/s.

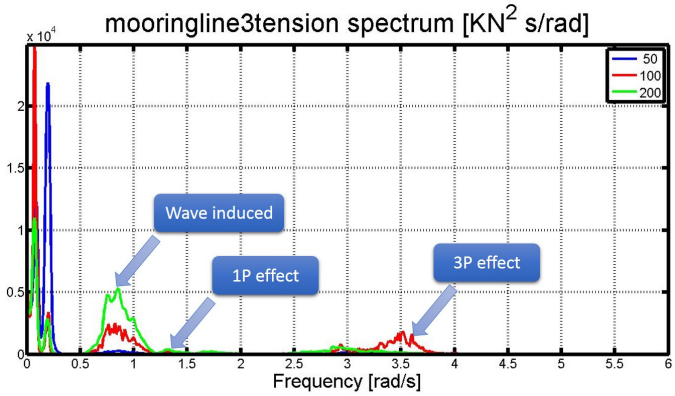

Figure. 6.31 *Mooring line 3 tension spectrum in condition 12 (frequency range 0-6 rad/s)*

According to the mooring line tension spectrum in range 0-6 rad/s in figure 6.31, there is a significant peak between 2.5 to 4 rad/s for all three design concepts, which corresponds to $3P$ blade passing frequency. Moreover, there is a spectral peak at around 1.25 rad/s standing for $1P$ rotor rotational effect induced response. The wave-induced contribution is prominent around 0.79 rad/s, which is in agreement with wave peak period.

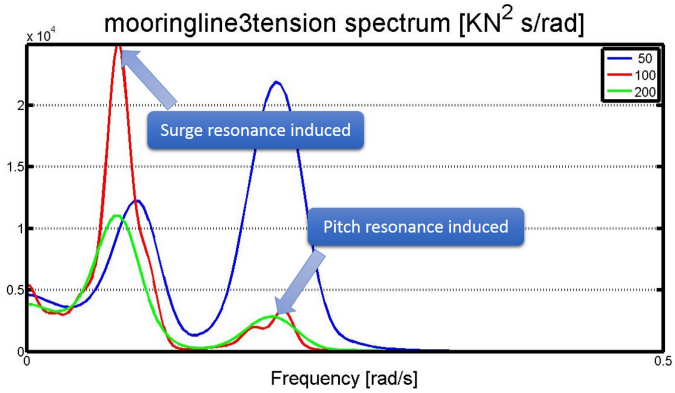

Figure. 6.32 *Mooring line 3 tension spectrum in condition 12 (frequency range 0-0.5 rad/s)*

Besides, there are two more remarkable peaks at the range between 0 to 0.5 rad/s, which could be found in the zoom-in spectrum in figure 6.32. The two peaks correspond to wind-induced low frequency responses: surge resonant effect at 0.08 rad/s and pitch resonant effect at 0.2 rad/s, which are in accordance with the free decay test results in table 6.2.

Take all the excitation contributions into account, the least significant factor is the $1P$ rotational effect, followed by the $3P$ blade passing effect and wave-induced response. The low frequency contributes the most to the total response, which indicates that wind load is dominating in operational condition.

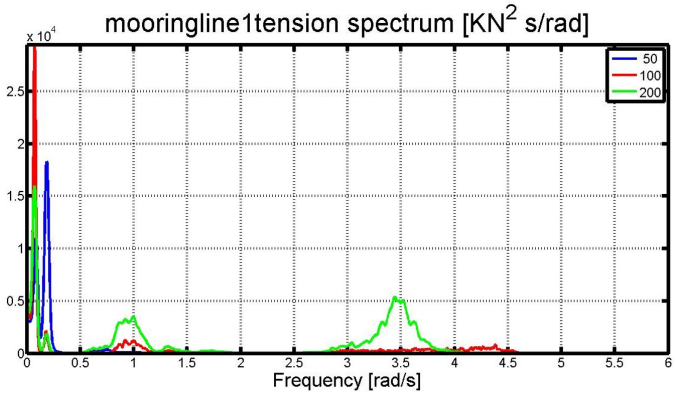

Figure. 6.33 *Mooring line 1 tension spectrum in condition 12*

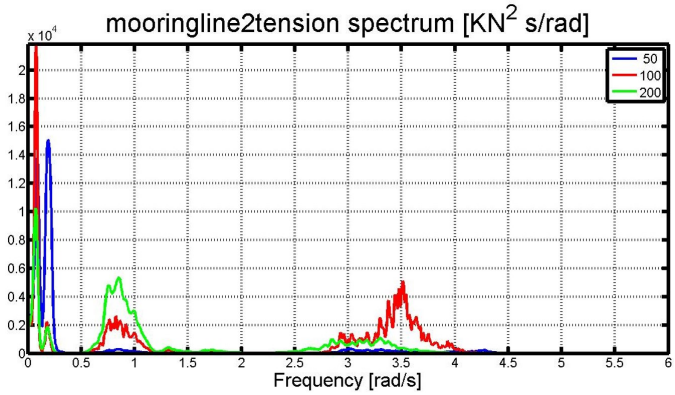

Figure. 6.34 *Mooring line 2 tension spectrum in condition 12*

The same spectrum tendency holds the same for all the three mooring lines with slight difference in the peak magnitudes and peak locations, which could be verified in figure 6.33 and 6.34.

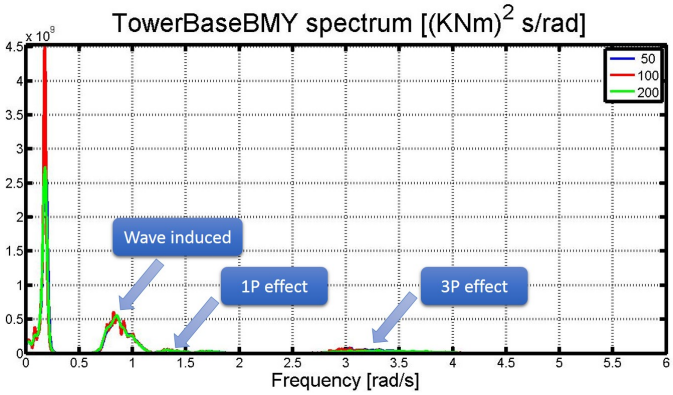

Figure. 6.35 *Spectrum of tower base bending moment in Y direction in condition 12 (frequency range: 0-6 rad/s)*

As for the tower base moment in Y direction shown in figure 6.34, the significant excitation contributions are almost the same as those for the mooring line responses: $3P$ blade passing effect occupies the frequency range from 2.7 rad/s to 4 rad/s, while the slight $1P$ rotor rotational effect is located at 1.3 rad/s. The contribution from wave-induced effect occupies the frequency around 0.8 rad/s.

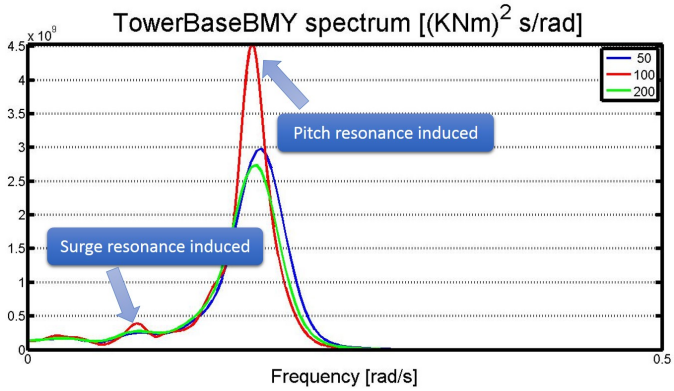

Figure. 6.36 *Spectrum of tower base bending moment in Y direction in condition 12 (frequency range: 0-0.5 rad/s)*

Based on the information offered by spectrum in range 0-0.5 rad/s, the significant response contributions from low frequencies can be roughly regarded as a combination of surge, heave and pitch resonant effects, while pitch resonance is the most remarkable factor followed by surge resonance and heave resonance contributes the least. By comparing the amplitudes of each contributions, wind-induced response takes the largest share again.

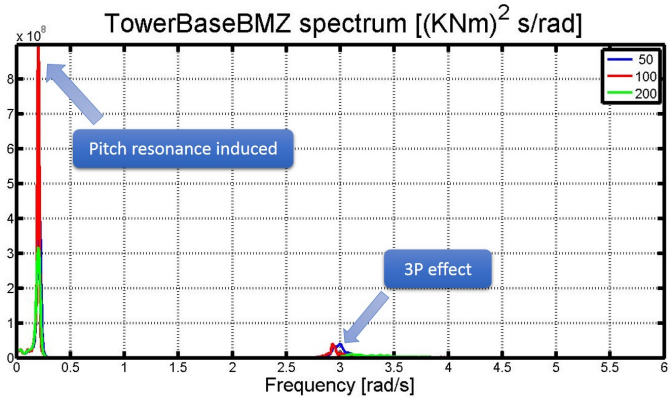

Figure. 6.37 *Spectrum of tower base bending moment in Z direction in condition 12 (frequency range: 0-6 rad/s)*

The notable contributing factors to bending moment in Z direction seems more straightforward because of its side-to-side excitation mechanism. The $3P$ blades passing effect is still functioning while there is on $1P$ rotational effect contribution. In addition, the wave-induced contribution is negligible.

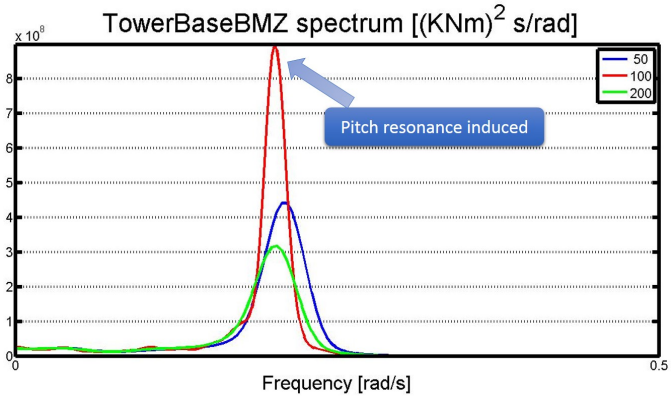

Figure. 6.38 *Spectrum of tower base bending moment in Z direction in condition 12 (frequency range: 0-0.5 rad/s)*

Since tower base bending moment in Z direction is acting aligned with floater pitch motion, when it comes to the wind-induced motion resonant contribution, pitch resonance contribution is in the leading position with nearly no contribution from other motion resonant effects. Figure 6.38 provides the relevant backing information.

The spectral analysis for critical motion response (surge and pitch) under operational condition show great similarity as the spectrum in figure 6.19 - figure 6.22 during extreme condition. However, the difference between them is the proportion of wave-induced response and wind-induced response. In extreme condition where wave condition is dominating, wave-induced response contributes most to total response. In operational condition, main source of response is due to wind-induced motion resonance, where evidence could be found in figure 6.39 and figure 6.40.

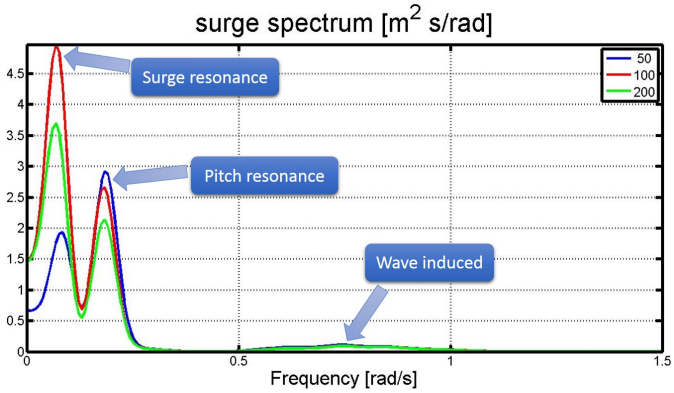

Figure. 6.39 *Spectrum of surge motion in condition 12*

In surge motion spectrum, the maximum response comes from surge resonance, followed by coupling pitch resonance and only a small response from wave frequency.

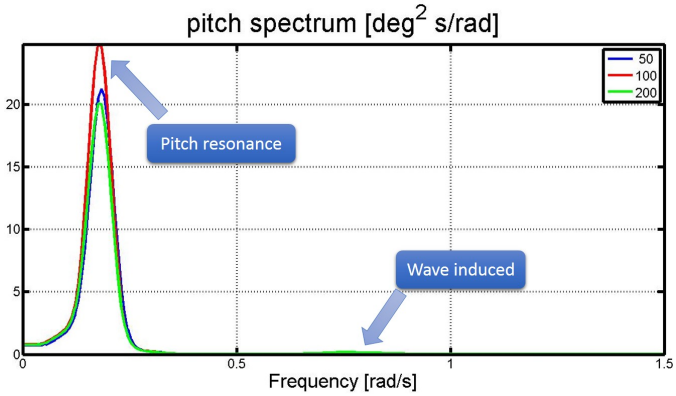

Figure. 6.40 *Spectrum of pitch motion in condition 12*

In pitch motion spectrum, pitch resonance is dominating and contribution from wave effect can hardly be noticed together with coupling effect from surge resonance.

7 Conclusion and Future Work

7.1 Conclusion

Two new mooring system designs have been successfully proposed for 100 m and 50 m water depths (shallow waters) supporting the 5-MW-CSC semi-submersible floating wind turbine based on a reference model in 200 m water depth. Static design and analysis has been carried out in SIMA to determine mooring system configuration, critical mooring line properties and check horizontal tension and offset relationship. Free decay tests have been carried out afterwards to document the natural periods for floater motions in six degrees of freedom. Finally, fully coupled time-domain dynamic analysis has been performed using Simo-Riflex-AeroDyn under ultimate limit state and fatigue limit state. Spectrum analysis has been quite helpful in understanding the response contribution and dominating environmental factors. The performances of the two new mooring systems aiming for shallow water utilizations (100 m and 50 m) are satisfactory.

Numerical Conclusion

Properties of mooring systems for three water depths are summarised in table 7.1.

Table. 7.1 *Mooring system properties for 200 m, 100 m and 50 m*

Water depth (m)	200	100	50
Mooring line number	3	3	3
Mooring line trype	Spiral rope	Spiral rope	Chain R4-RQ4
Fairlead elevation (m)	-18	-18	-18
Unstretched mooring line length (m)	873.11	671.66	566.65
Mooring line nominal diameter (m)	0.1365	0.1365	0.18
Mooring line unit mass in water (kg/m)	115.02	115.02	648
Mooring line axial stiffness (KN)	3.08E6	3.08E6	2.92E6
Pretension (KN)	1683.1	1710.9	1295.4
Clump weight (t)	17.253	60	60

The natural periods for the floating wind turbine in six degrees of freedom with mooring system included are documented in table 7.2.

Table. 7.2 *Natural periods of the floater in 200 m, 100 m and 50 m*

	Natural period (s)					
Depth (m)	Surge	Sway	Heave	Roll	Pitch	Yaw
200	79.43	79.43	25.34	31.14	31.08	57.55
100	78.97	74.97	25.27	30.80	30.74	61.68
50	64.43	66.77	24.92	30.34	30.29	78.43

Static Design Conclusion

1. There are two factors that can influence mooring line tension significantly: degree of tightness of mooring system; nonlinear tension increment during large offset range.

2. In order to achieve desired pretension, mooring line catenary shape and higher breaking strength, two different mooring line materials are selected for different water depths: spiral rope for 100 m depth and studless chain for 50 m depth.

3. Because the suspended length of mooring line is shorter in shallower water, the weight of clump mass has been increased for shallow water.

4. In order to avoid large nonlinear tension increment, the mooring system is designed to be soft on purpose in shallow water (50 m depth).

5. In order to prevent mooring line from being totally lifted up and protect anchor from vertical loads, longer mooring line is lying on the seabed for shallower water depth.

6. The transition from linearity to nonlinearity between mooring line tension and offset occurs at a larger offset value for 200 m and 100 m (10 m offset) and smaller offset value for 50 m (6 m offset).

Dynamic Analysis Conclusion

1. The free decay tests results illustrate that the natural periods of mooring system for 100 m and 50 m are achieved close to those for the reference model in 200 m, sufficiently larger than relevant wave periods.

2. When floating wind turbine is exposed to offshore environment, mooring line tension and floater motion are composed of a mean static component due to mean wave and wind forces and a dynamic component due to first-order wave force and slowly varying wind and wave forces.

3. When the floating wind turbine is exposed to extreme condition, wave is the dominating environmental factor. On the other hand, wind is the dominating factor during operational condition.
4. In ULS condition, the maximum mooring line tension occurs in the case when the wave acting aligned with the mooring line configuration direction. And the utilization factors of mooring line and floater motions are relatively larger in the condition where wave is more severe.
5. Harsh environmental condition will lead to mooring line tension transfer from linear increment to nonlinear increment, especially in shallower water depth.
6. The extreme mooring line tension is great influenced by the degree of tightness of the mooring system. Normally, higher extreme mooring line tension is expected in shallower water depth when similar degrees of stiff are achieved in different water depths. However, if the mooring system is stiffer in deeper water, larger extreme mooring line tension can be expected as well. As for floater motion control, stiffer mooring system could help to limit the offset range. Therefore, there is a compromise between tension control and motion control to decide, when it comes to mooring system design.
7. Numerically, the accumulated fatigue damage of chain link is normally higher than wire rope even though the stress ranges and the number of loading cycles do not show big difference, which is due to different component capacities defined in S-N curve. Corresponding physical reason is that contact force between chain links contributes a lot to fatigue damage, which does not apply to wire rope.
8. In extreme condition, wave-induced effect contributes most to mooring line tension and most of the floater motion except pitch motion. Wind-induced low frequency effect only accounts a small part.
9. In operational condition, wind-induced resonant effect contributes most to mooring line tension and tower base bending moment and floater motion especially pitch and surge motion. Wave-induced effect hardly counts.

7.2 Future Work

Due to limited time and predefined thesis scope, there are some aspects that is meaningful to discuss and have not been fully studied. Moreover, some assumptions have been made during the comparison among the three water depths. Therefore, some possible future work are recommended:

1. More static design concepts consists of different mooring line properties, clump weights, configurations should be proposed to find the optimal concept in different water depths.
2. The nominal diameter of the chain link used in 50 m design is close to the fabrication limit. In addition, the weight of the clump mass used in 100 m and 50 m are 60 t, which turns out to be challenging for fabrication and installation. Innovative weight redistribution strategy is expected to make improvment.
3. Because of the large number of load cases examined in both ULS and FLS condition, the calculation takes too much time and so does the post-processing work. Therefore, a time-saving method which can save computer memory and simulation time would be meaningful.
4. More than one parameters are different when comparing performance of the three mooring systems. Better-defined comparison preconditions are needed in order to make comparison conclusion more persuasive.
5. The reliability analysis, cost estimation study and accidental state condition of mooring system can be interesting to study in the future.

Bibliography

[1] W. Dong, "Time-domain fatigue response and reliability analysis of offshore wind turbines with emphasis on welded tubular joints and gear components," Ph.D. dissertation, NTNU, 2012.

[2] J. F. Manwell, J. G. McGowan, and A. L. Rogers, *Wind Energy Explained: Theory, Design and Application.* Wiley, Chichester, 2009.

[3] M. Etemaddar, "Load and response analysis of wind turbines under atmospheric icing and controller system faults with emphasis on spar type floating wind turbine," Ph.D. dissertation, NTNU, 2013.

[4] J. Twidell and G. Gaudiosi, *Offshore Wind Power*, J. Twidell and G. Gaudiosi, Eds. Multi-Science Publishing Co. Ltd, 2009.

[5] S. Aldock. (2008) Is the offshore wind market poised for scale? [Online]. Available: http://www.renewableenergyfocus.com/view/3339/is-the-offshore-wind-market-poised-for-scale/

[6] A. Williams, "A buoyant future for floating wind turbines?" Tech. Rep., 2011.

[7] (2015) Poseidon floating power. [Online]. Available: http://tethys.pnnl.gov/annex-iv-sites/poseidon-floating-power

[8] B. Publicover. (2015) Fukushima semi-sub floater finished. [Online]. Available: http://www.rechargenews.com/wind/article1365364.ece.

[9] J. N. Newman, *Marine Hydrodynamics*, J. N. Newman, Ed. The MIT Press, 1977.

[10] *Feasibility of Floating Platform Systems for Wind Turbiens.* Reno, Nevada: ASME Wind Energy SYmposium Proceedings, January 2004.

[11] "Deep water - the next step for offshore wind energy," European Wind Energy Association, Tech. Rep., 2013.

[12] D. Roddier, C. Cermelli, A. Aubault, and A. Weinstein1, "Windfloat: A floating foundation for offshore wind turbines," *Joutnal of renewable and sustainable energy 2*, 2010.

[13] T. A. Nygaard, T. Landbo, R. J. Camara, and J. A. Armendariz, Eds., *Design, Analysis and Wave Tand Testing of a Semi-submersible Braceless Concerete Offshore Wind Turbine Platform*, 2015.

[14] (2015) Offshore flytende vindturbin: Oo star wind floater. [Online]. Available: http://www.ife.no/en/ife/ife_images/em/photo_album.2004-11-10.3536561139/oo-star-wind-floater/view

[15] C. Luan, C. Michailides, Z. Gao, and T. Moan, "Modeling and analysis of a 5 mw semi-submersible wind turbine combined with three flap-type wave energy converters," in *33rd International Conference on Ocean, Offshore and Arctic Engineering*.

[16] NOWITECH, "Nowitech annual report, 2013," NOWITECH, Tech. Rep., 2013.

[17] MARINTEK, "Review 2014," MARINTEK Norwegian Marine Technology Research Institute, Tech. Rep., 2014.

[18] C. E. Larsen, "Predicting the fatigue life of offshore structures by the single-moment spectral method. probabilistic engineering mechanics," *Probabilistic Engineering Mechanics*, 1991.

[19] H. Chen and T. Moan, "Safety of dynamic positioning operations on mobile offshore drilling rigs," in *Reliability Engineering and Systems Safety*.

[20] P. Smedley and D. Pertruska, "Comparison of global design requirements and failure rates for industry long term mooring systems," in *Proceedigns of the Offshore Structural Reliability Conference*.

[21] J. Stiff, "How reliable are reliability calculations? (illustrated with station-keeping examples)," in *Proceedigns of the Offshore Structural Reliability Conference*.

[22] *HydroD user manual, Wave load and stability analysis of fixed and floating structures*. DNV, 2013.

[23] *Wadam user manual, Wave analysis by diffractio and morison theory*, 8th ed., DNV, 9 November 2010.

[24] MARINTEK, *SIMO User Manual Version 4.0*, Norwegian Marine Technology Research Insitute, Trondheim, 2012.

[25] Marintek, *RIFLEX User Manual*, Norwegian Marine Technology Research Insitute, Trondheim, Norway, 2013.

[26] E. E. Bachynski, "Design and dynamic analysis of tension leg platform wind turbines," Ph.D. dissertation, NTNU, 2014.

[27] B. Jonkman and L. Kilcher, *TurbSim User's Guide: Version 1.06.00*.

[28] *IEC 61400-1. Wind Turbine - Part 1 : Design requirements.*, International Electrotechnical Commission, 2005.

[29] O. M. Faltinsen, *Sea loads on ships and offshore structures.* Cambridge university press, 1990.

[30] M. O. L. Hansen, *Aerodynamics of Wind Turbines.* Earthscan in the UK and USA, 2008.

[31] S.Butterfield, W. Musial, J. Jonkman, and P. Sclavounos, "Engineerign challenges for floating offshore wind turbines," in *2005 Cohenhagen Offshore Wind Conference*, 2005.

[32] M. Greco, *Lecture note of TMR 4215.* Marine Department. NTNU, 2012.

[33] P. J. Moriarty and A. C. Hansen, *AeroDyn Theory Manual*, National Renewable Energy Laboratory, January 2005.

[34] D. H. Hodegs and E. H. Dowell, "Nonlinear equations of motion for the elastic bending and torsion of twisted nonuniform rotor blades," National Aeronautics and Space Administration, Tech. Rep., 1974.

[35] Z. Gao, *Short-term Wind and Wave Conditions.* Lecture Note for Integrated dynamic analysis of wind turbine, 2014.

[36] IEC, *International IEC 61400-1, Wind turbine- Design requirements*, International Electrotechnical Commission.

[37] DNV, *DNV-OS-J101 - Design of Offshore Wind Turbine Structures*, May 2014.

[38] Z. Jiang, "Long-term response analysis of wind turbines with an emphasis on fault and shutdown consitions," Ph.D. dissertation, NTNU, 2014:266.

[39] Z. Gao, "Stochastic response analysis of mooring systems with emphasis on frequency domain analysis of fatigue due to wid band response processes." Ph.D. dissertation, NTNU, 2008.

[40] J. JournÃŀe and W. Massie, *Offshore Hydrodynamics, First edition.* Delft University of Technology, 2001.

[41] Z. Gao and T. Moan, "Mooring system analysis of multiple wave energy converters in a farm configuration." in *the 8th European Wave and Tidal Energy*, Uppsala, Sweden, 2009.

[42] V. A. Global Maritime, *anchor manual 2015, the guide to anchoring*, Global Maritime, 2015.

[43] DNV, *Offshore Standard DNV-OS-E302, Offshore Mooring Chain*, DNV GL.

[44] *Norsk Standard NS-EN 1993-1-1: 2005+NA: 2008. EUROKODE 3: Prosjektering av stalkonstruksjoner Del 1-1: Allmenne regler og regler for bygninger.*, Standard Norge, 2008.

[45] *Norsk Standard NS-EN 1993-1-12: 2007+NA: 2009. EUROKODE 3: Prosjektering av stalkonstruksjoner Del 1-12: Konstruksjoner med hoyfast stal.*, Standard Norge, 2009.

[46] P. P. Limited, *Floating Structures: a guide for design and anslysis*, N. Barltrop, Ed. Oilfield Publications, Inc, 1998, vol. two.

[47] DeepRope, *Synthetic mooring lines*, Vryhof anchors, 2010.

[48] H. Ormberg and K. Larsen, "Coupled analysis of floater motion and mooring dynamics a turret-moored ship," in *Applied Ocean Research, 20:55-67*, 1998.

[49] S. Steen, *Lecture Notes - TMR7 Experimental Methods in Marine Hydrodynamics*. NTNU, August 2014.

[50] J.R.Hoff, *Estimation of linear and quadratic roll damping from free-decay test*, July 6 2001.

[51] J. B. Roberts, *Estimation of nonlinear ship roll damping from free-decay data*. Journal of ship research, June, pp.127-138 1985, vol. 29, no. 2.

[52] *DNV-OS-E301,Position Mooring*, DNV-GL, October 2013.

[53] P. R. Thies, L. Johanning, V. Harnois, H. C. Smith, and D. N. Parish, "Mooring line fatigue damage evaluation for floating marine energy converters: Field measurements and prediction," *Renewable Energy*, vol. 63, pp. 133–144, 30 August 2013.

[54] M. I. Kvittem, "Modelling and response analysis for fatigue design of a semi-submersible wind turbine," Ph.D. dissertation, NTNU, 2014.

[55] G. Jiao and T. Moan, "Probabilistic analysis of fatigue due to gaussian load processes," *Probabilistic Engineering Mechanics*, vol. 5, no. 2, pp. 76–83, 1990.

[56] *Fatigue Design of Offshore Steel Structures*. Det Norske Veritas, 2010.

[57] M. Constantine, L. Chenyu, G. Zhen, and M. Torgeir, "Effect of flap type wave energy converters on the response of a semi-submersible wind turbine in operational conditions," in *33rd International Conference on Ocean, Offshore and Arctic Engineering*.

[58] J. J., Butterfield, S. Musial, and W. S. G., "Definition of a 5-mw reference wind turbine for offshore system development," NREL, Golden CO USA, Tech. Rep., 2009.

[59] J. Jonkman, "Definition of the floating system for phase iv of oc3," NREL, Tech. Rep., 2010.

[60] K. Xu, Y. Zhao, and S.-P. Cho, "Integrated dynamic analysis of wind turbines-modified windfloat," NTNU-Course Project, Tech. Rep., 2014.

[61] E. Bachynski, V. Chabaud, and T. Sauder, "Real-time hybrid model test of floating wind turbines: sensitivity to limited actuation," in *12th Deep Sea Offshore Wind RD Conference, DeepWind's 2015*, February 4-6 2015.

[62] L. Li, Z. Gao, and T. Moan, "Joint environmental data at five european offshore sites for design of combined wind and wave energy devices," in *Proceed-*

ings of the ASME 2013 32nd International Conference on Ocean Offshore and Arctic Engineering. Nantes, France, June9-14 2013.

[63] B. Jonkman and L. Kilcher, *TurbSim Users' Guide*, draft ed., NREL, September 2012.

[64] E. Bachynski, "Dynamic modeling of floating wind turbines using simo-riflex-aerodyn - lecture notes for course "integrated dynamic analysis of wind turbine"," NTNU, MARINTEK, Tech. Rep., 2013.

[65] K. Johannessen, T. S. Meling, and S. Hayer, "Joint distribution for wind and waves in the northern north sea," in *Proceedings of the Eleventh (2001)International Offshore and Polar Engineering Conference*, no. ISBN 1-880653-51-6 (Set), Stavanger, Norway, June 17-22 2001.

[66] E. Bachynski and Z. Gao, "Course project description: Integrated dynamic analysis of wind turbines, fall 2014," NTNU, Tech. Rep., 2014.

[67] MARINTEK, *Simo- Theory Manual.* SINTEF, 12.15 2009.

[68] *DNV-RP-C205,Environmental Conditions and Environmental Loads*, DNV-GL, October 201.

[69] *Wadam User Manual, Wave analysis by diffraction and morison theory.* DNVGL, january 2 2010.

[70] *A Matlab Toolbox for Analysis of Random Waves and Loads.* the WAFO group, 2011,Version 2.5.

[71] L. Lupu, B. Boukhezzar, and H. Siguerdidjane, "Pitch and torque control strategy for variable speed wind turbines."

[72] B. Bergesen, L. H. Groth, B. Langseth, I. H. Magnussen, D. Spilde, and J. E. W. Toutain, "Energy consumption 2012 - household energy consumption," Norwegian Water Resources and Energy Directorate, Tech. Rep. ISBN 978-82-410-0884-9, 2013.

A Drawings of the Mooring Systems

A.1 Drawing of the Mooring System for 200 m - Top View

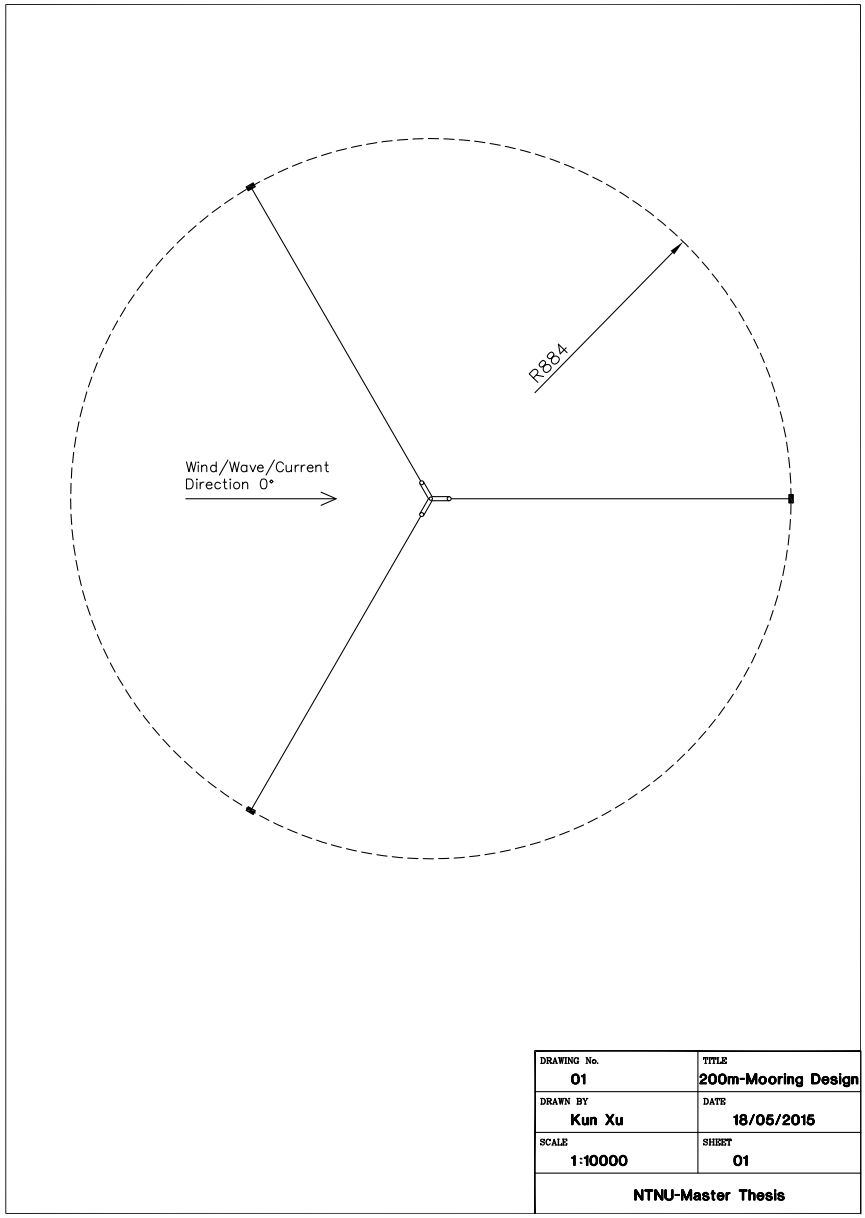

A.2 Drawing of the Mooring System for 200 m - Side View

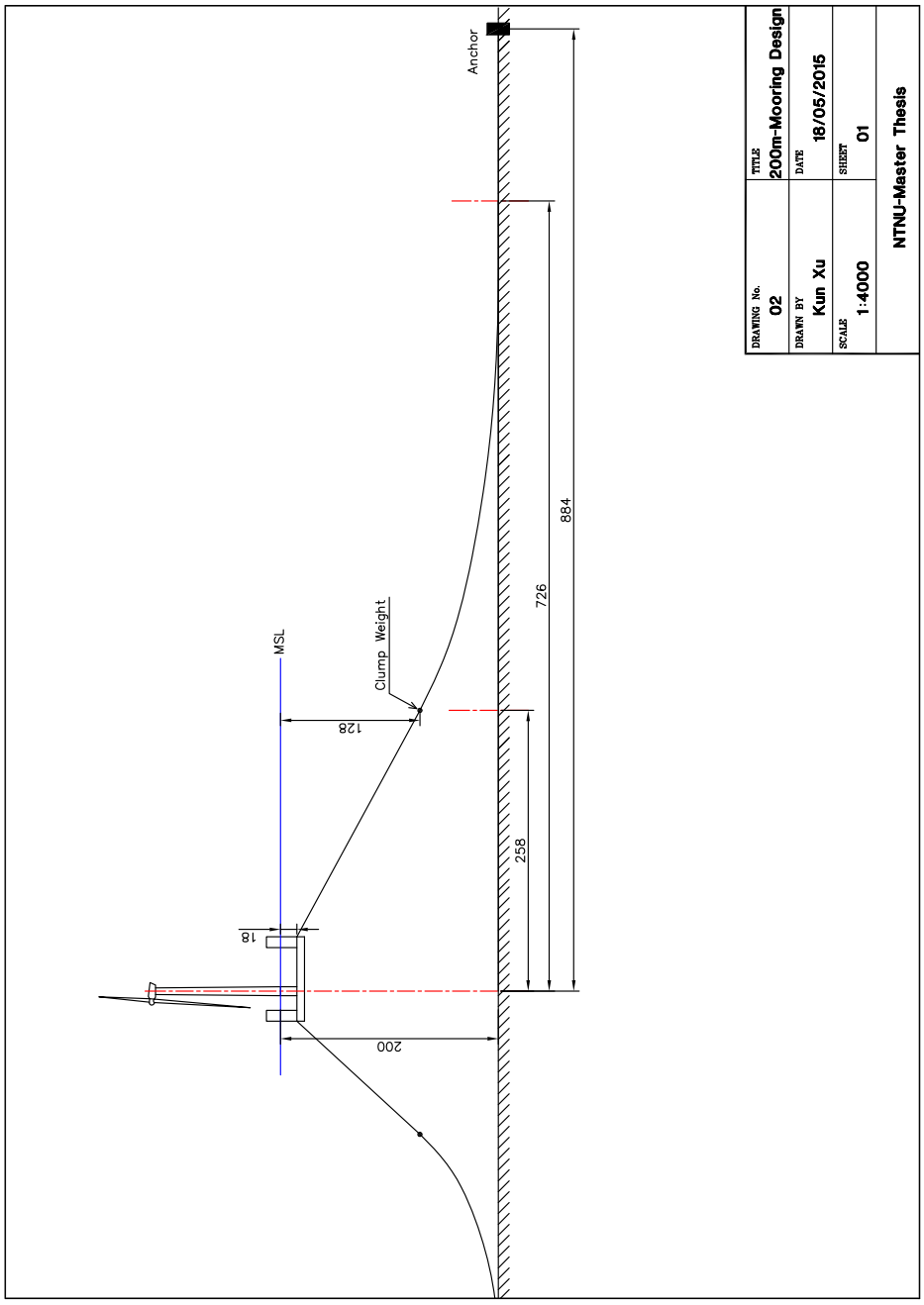

A.3 Drawing of the Mooring System for 100 m - Top View

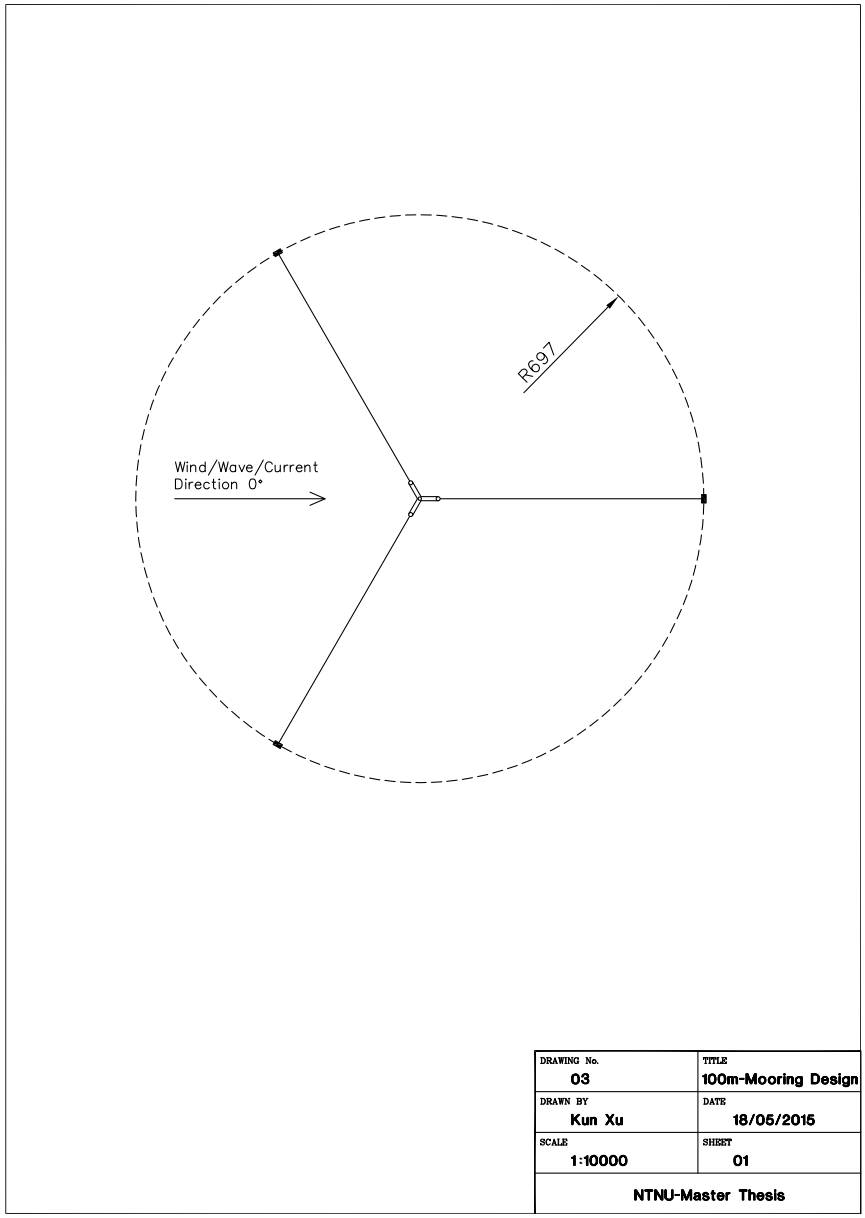

A.4 Drawing of the Mooring System for 100 m - Side View

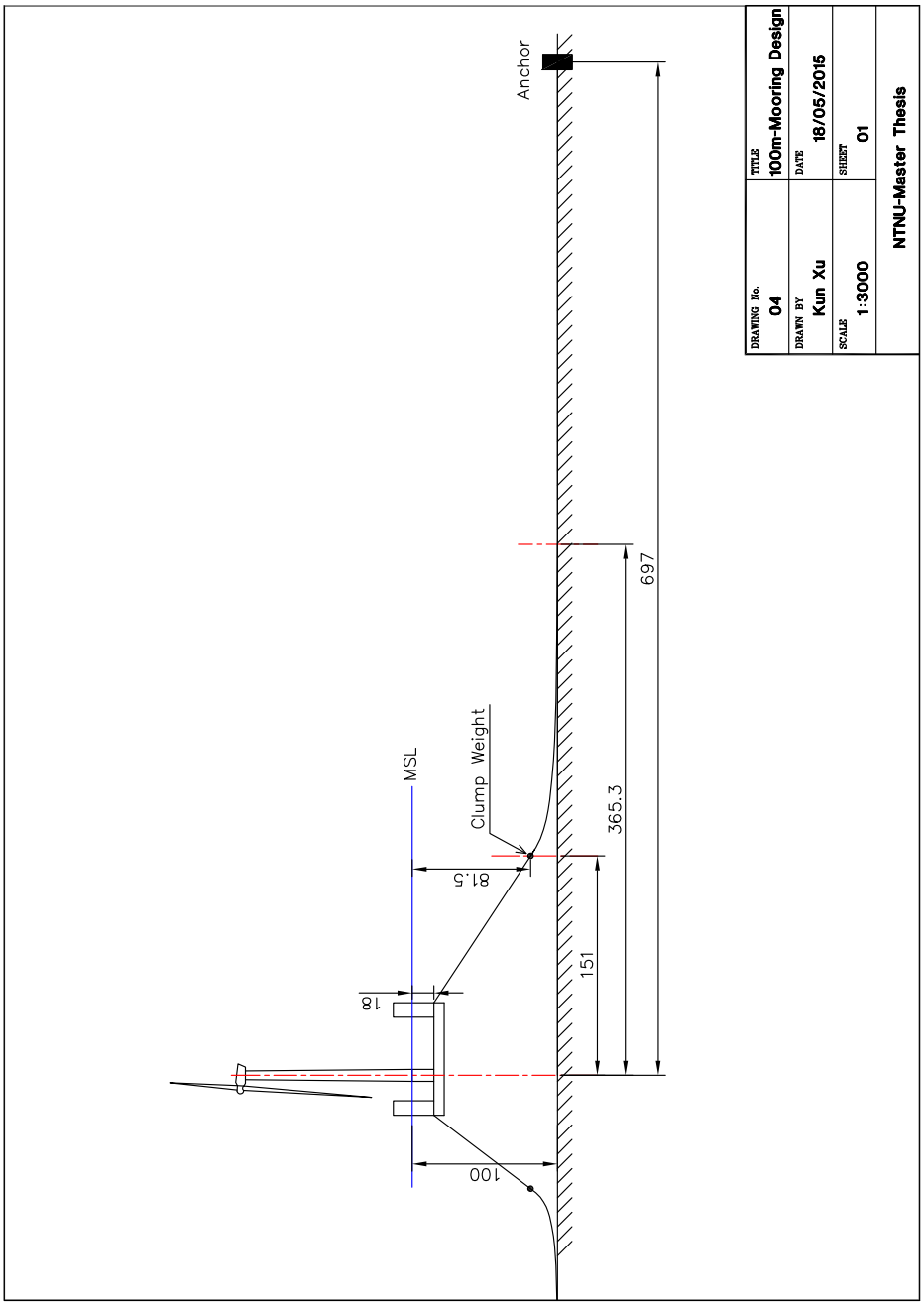

A.5 Drawing of the Mooring System for 50 m - Top View

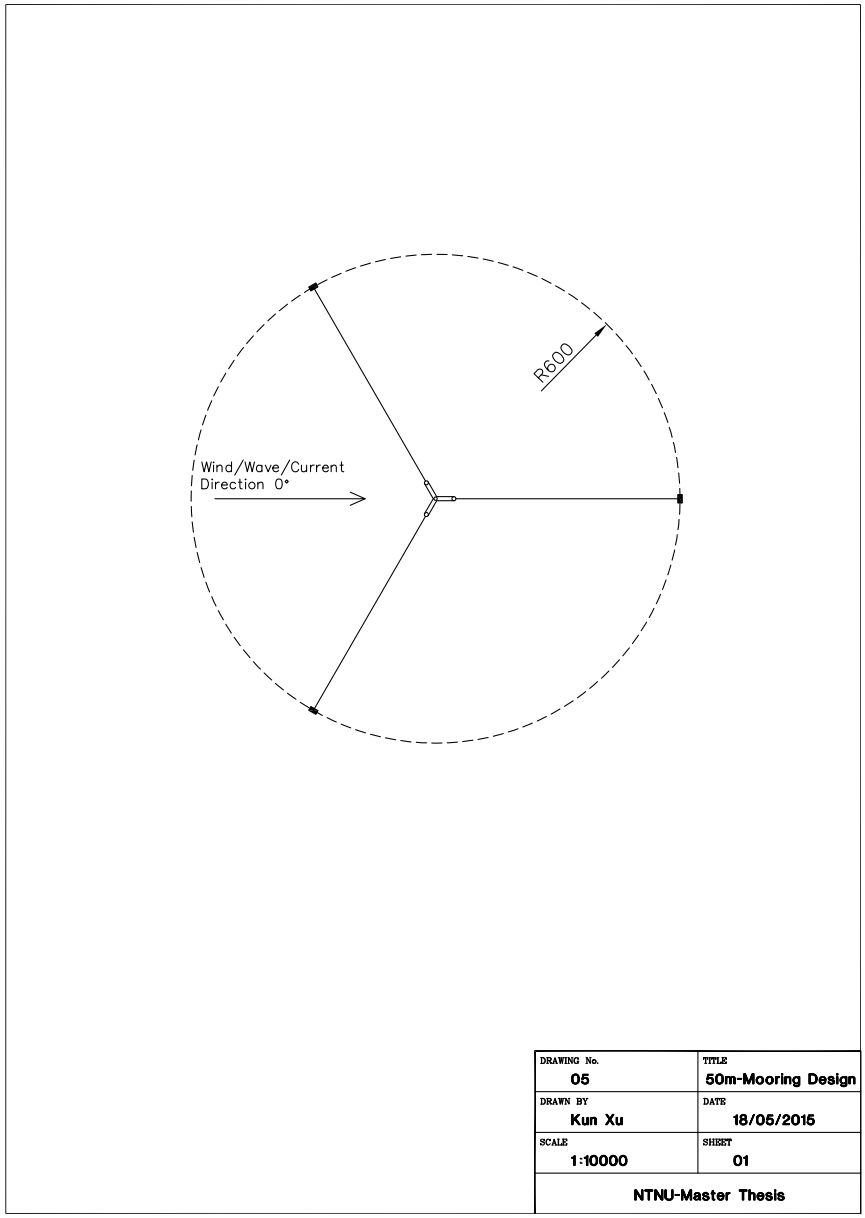

A.6 Drawing of the Mooring System for 50 m - Side View

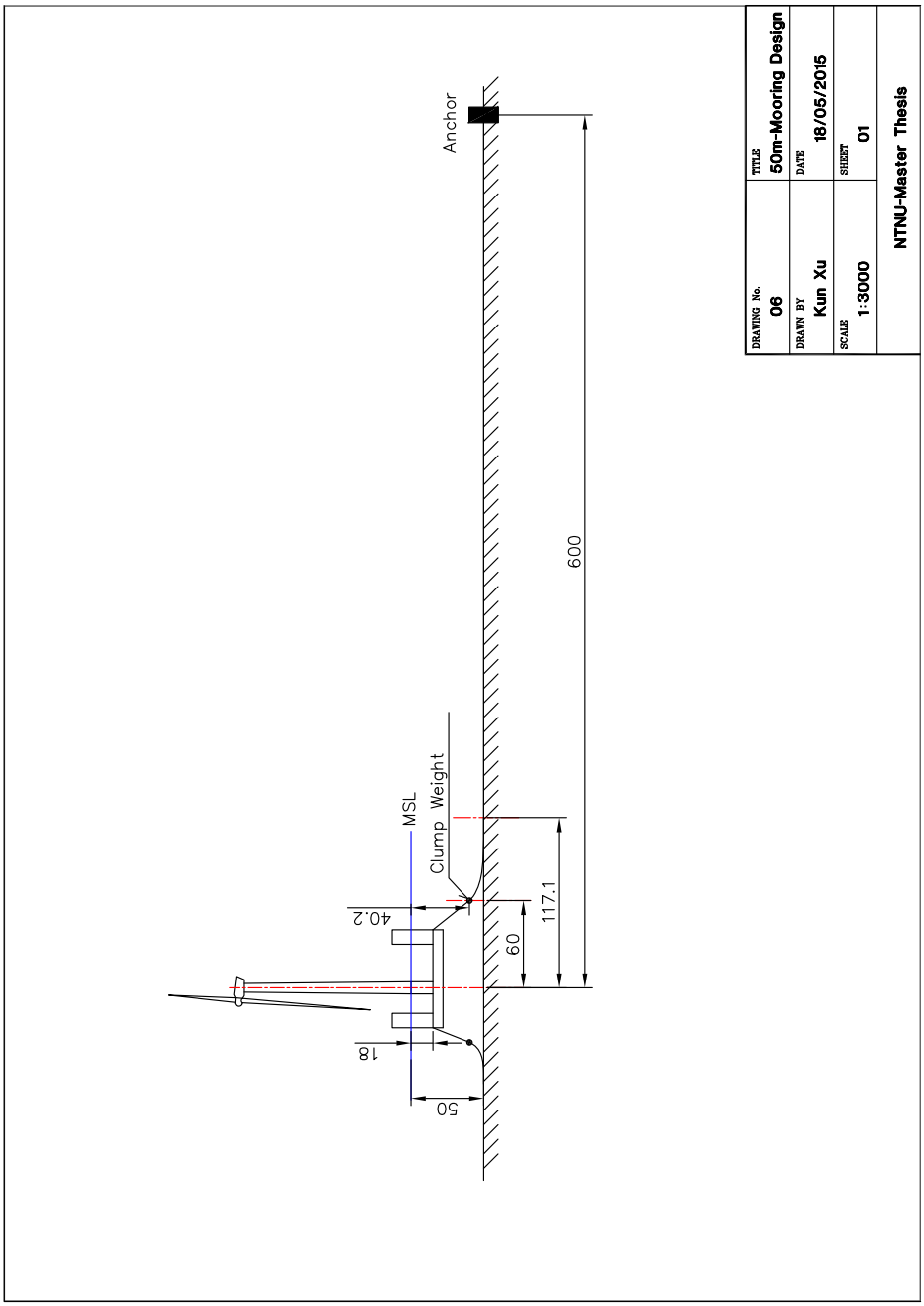

B Mooring Line Static Configuration and Force

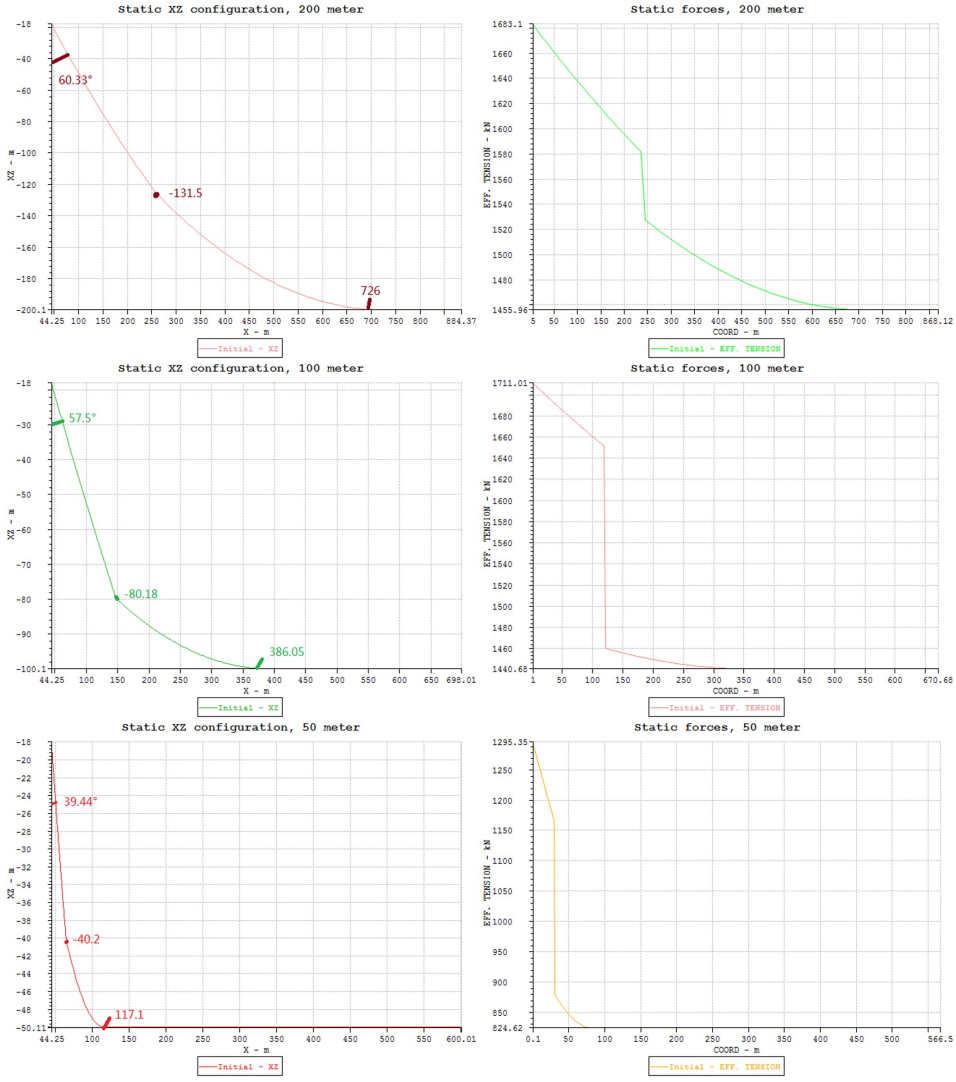

Figure. B.1 *Initial static configurations and forces of mooring lines for 200 m (up,* ***offset = 0 m****), 100 m (middle,* ***offset = 0 m****) and 50 m (low,* ***offset = 0 m****).*

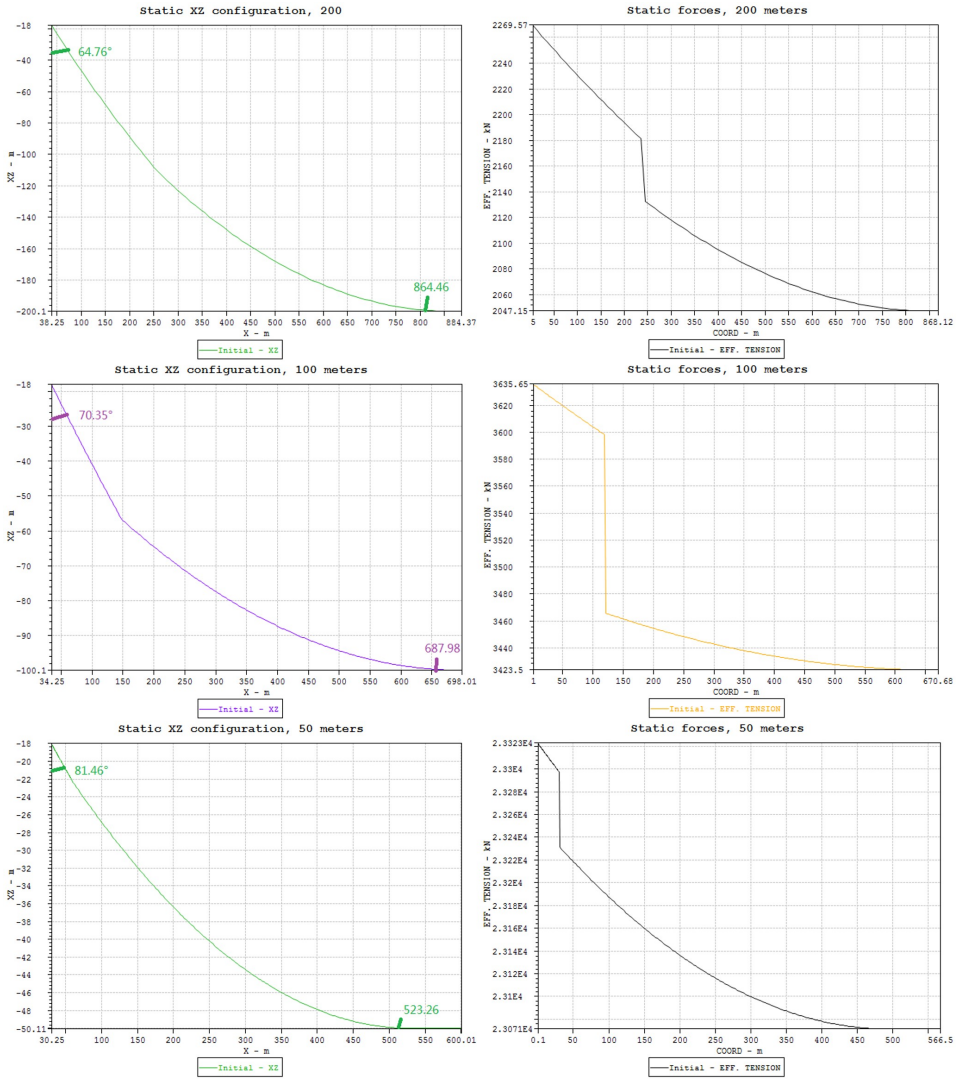

Figure. B.2 *Extreme static configurations and forces of mooring lines for 200 m (up,* ***offset = 6 m****), 100 m (middle,* ***offset = 10 m****) and 50 m (low,* ***offset = 14 m****).*

C Response in Extreme Condition Test

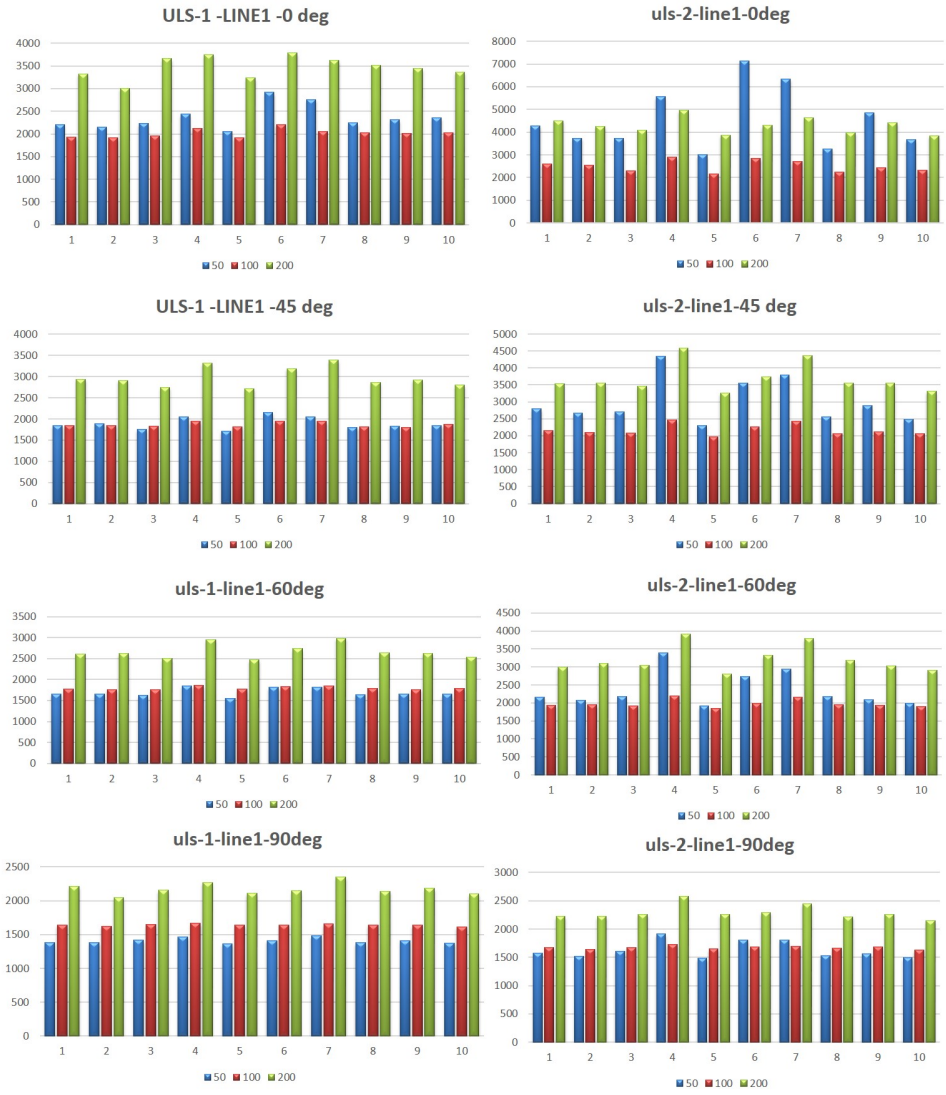

Figure. C.1 *Mooring lines 1 tension for 200 m, 100 m and 50 m in two extreme conditions with four wave directions (0 deg in first row, 45 deg in second row, 60 deg in third row and 90 deg in last row) (ULS-1 condition in left column, ULS-2 condition in right column)*

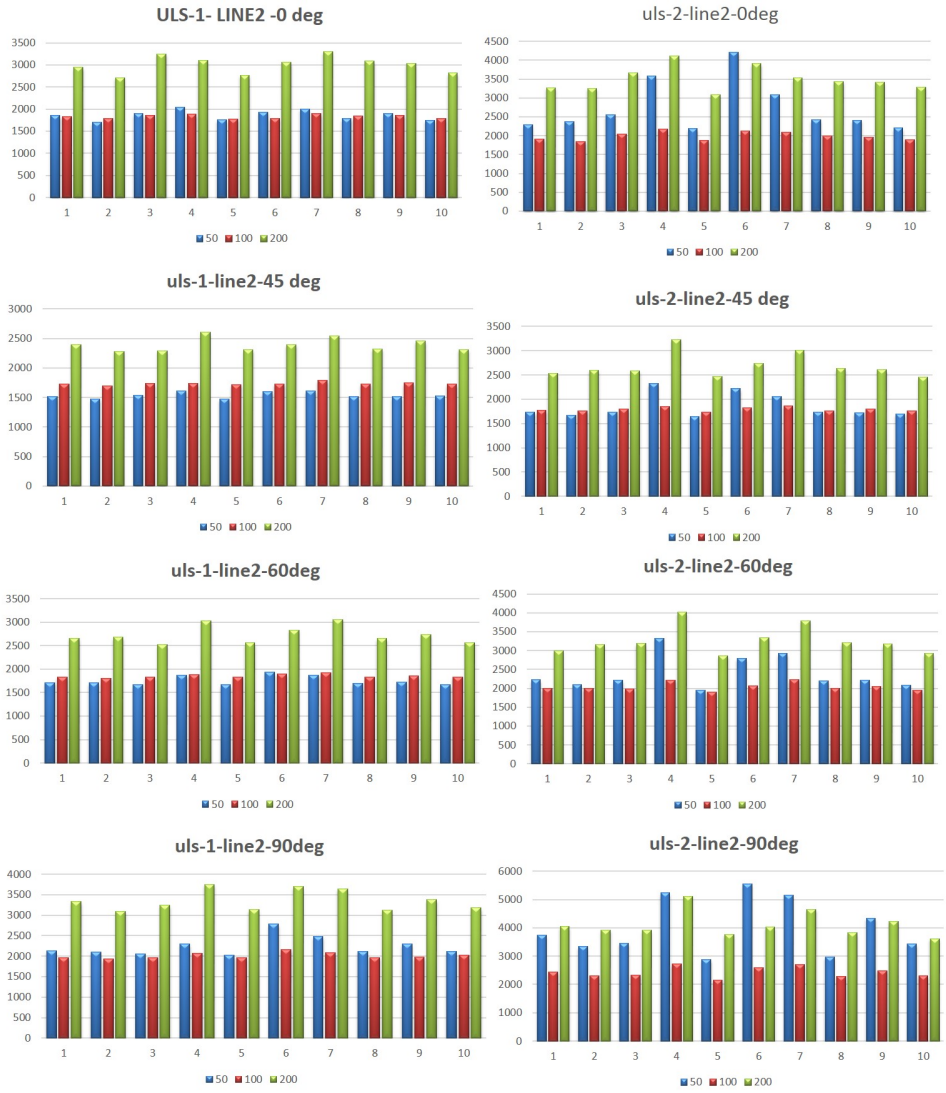

Figure. C.2 *Mooring lines 2 tension for 200 m, 100 m and 50 m in two extreme conditions with four wave directions (0 deg in first row, 45 deg in second row, 60 deg in third row and 90 deg in last row) (ULS-1 condition in left column, ULS-2 condition in right column)*

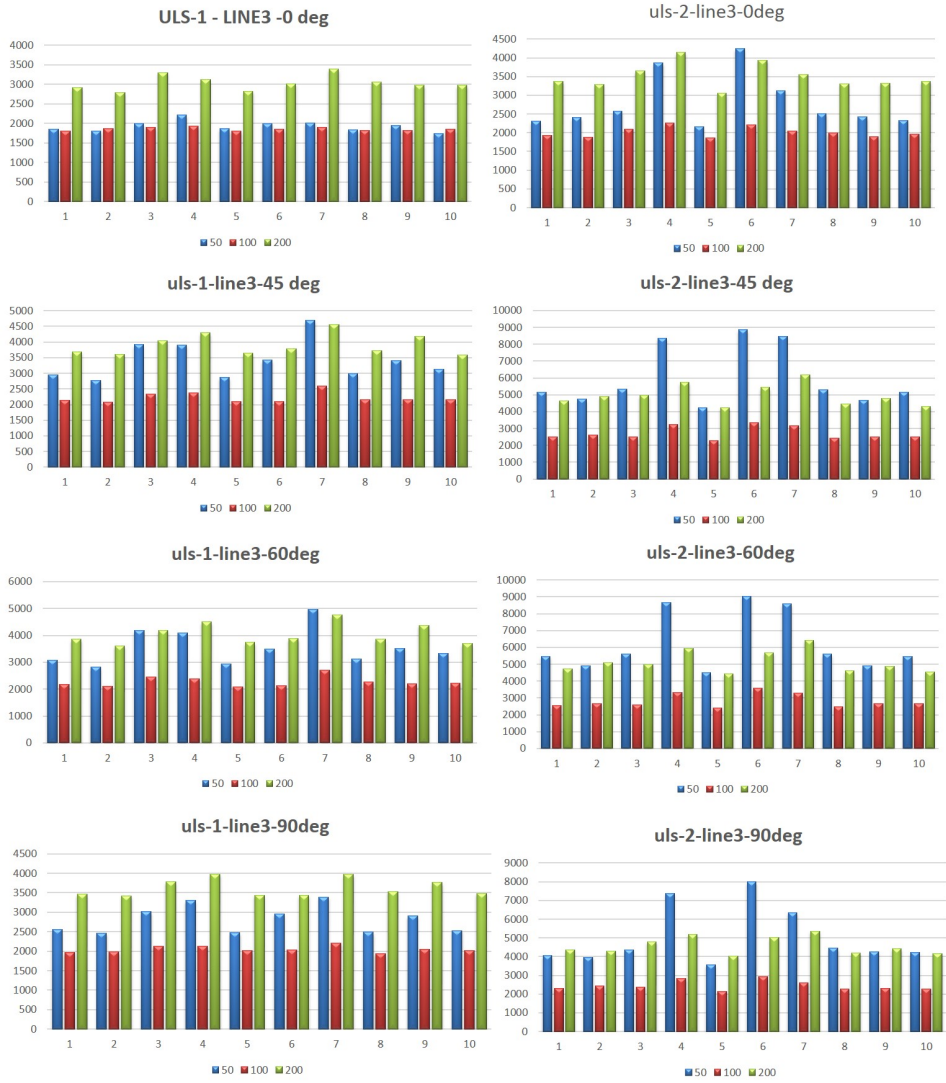

Figure. C.3 *Mooring lines 3 tension for 200 m, 100 m and 50 m in two extreme conditions with four wave directions (0 deg in first row, 45 deg in second row, 60 deg in third row and 90 deg in last row) (ULS-1 condition in left column, ULS-2 condition in right column)*

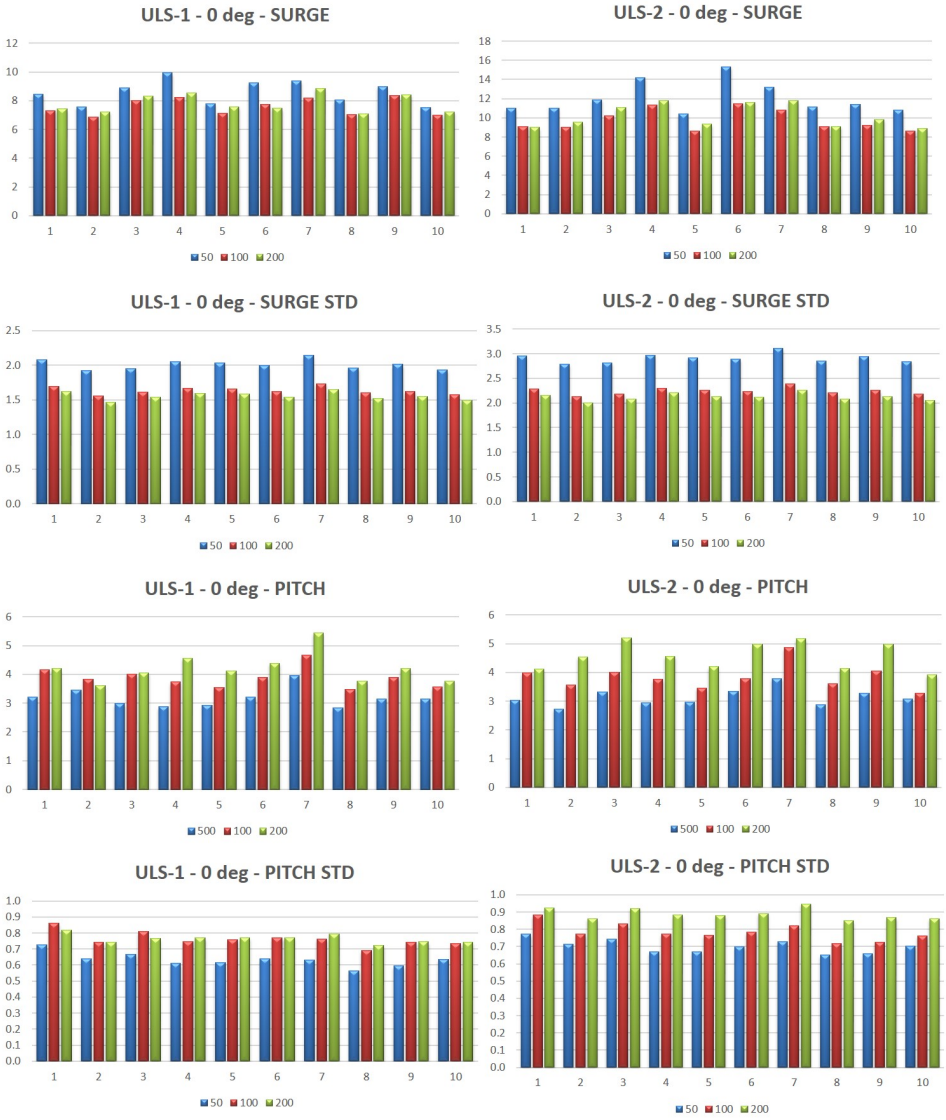

Figure. C.4 *Floater motion (surge and pitch) for 200 m, 100 m and 50 m in extreme condition with wave coming from* ***0 deg***

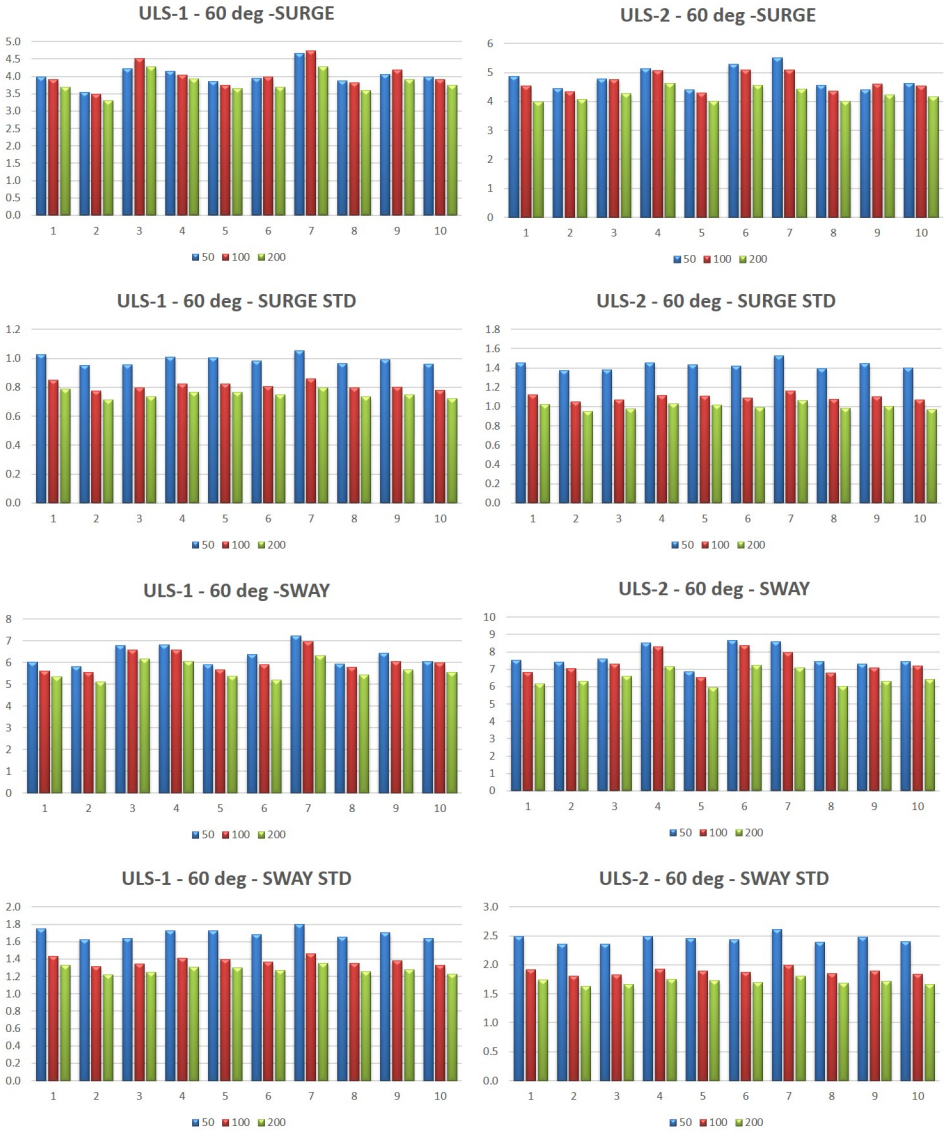

Figure. C.5 *Floater motion (surge and sway) for 200 m, 100 m and 50 m in extreme condition with wave coming from* ***60 deg***

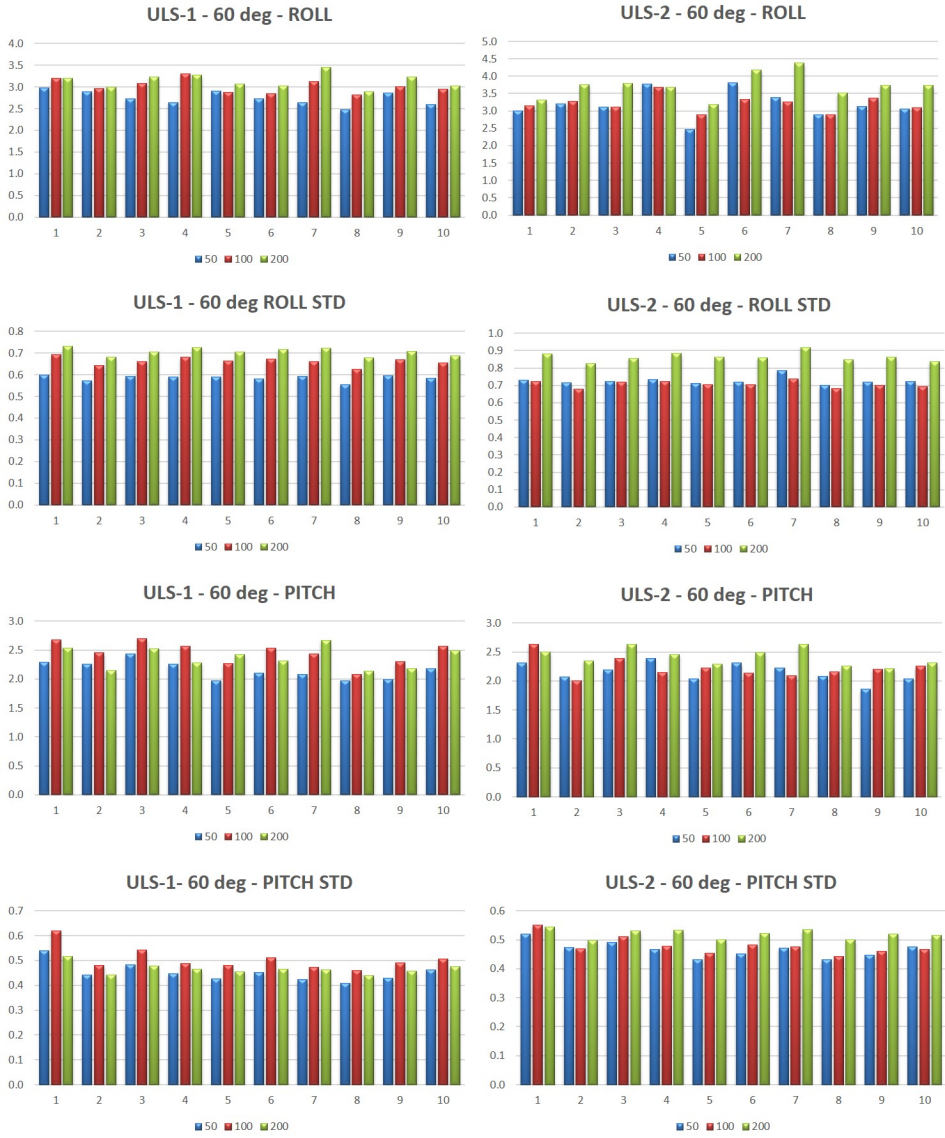

Figure. C.6 *Floater motion (roll and pitch) for 200 m, 100 m and 50 m in extreme condition with wave coming from* ***60 deg***

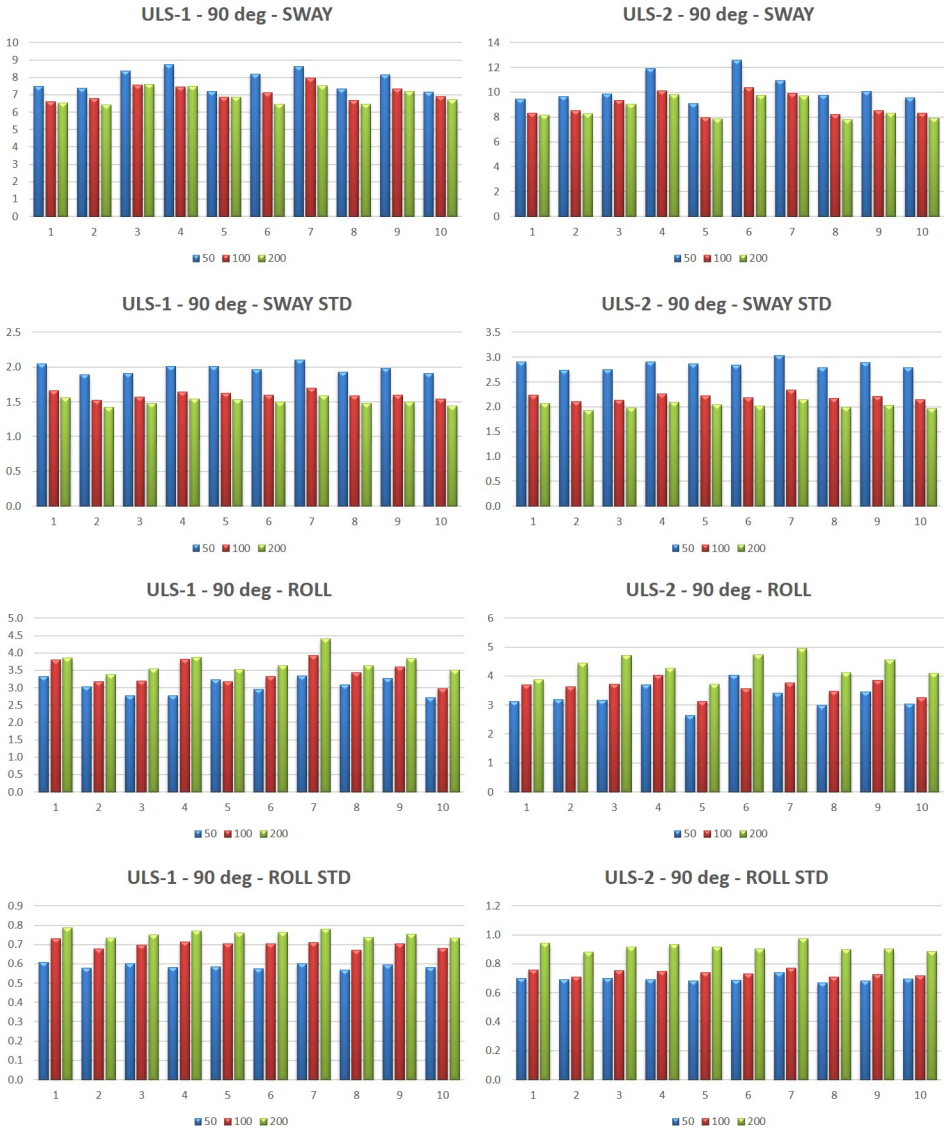

Figure. C.7 *Floater motion (sway and roll) for 200 m, 100 m and 50 m in extreme condition with wave coming from* ***90 deg***

D Response Spectra in Extreme Condition Test

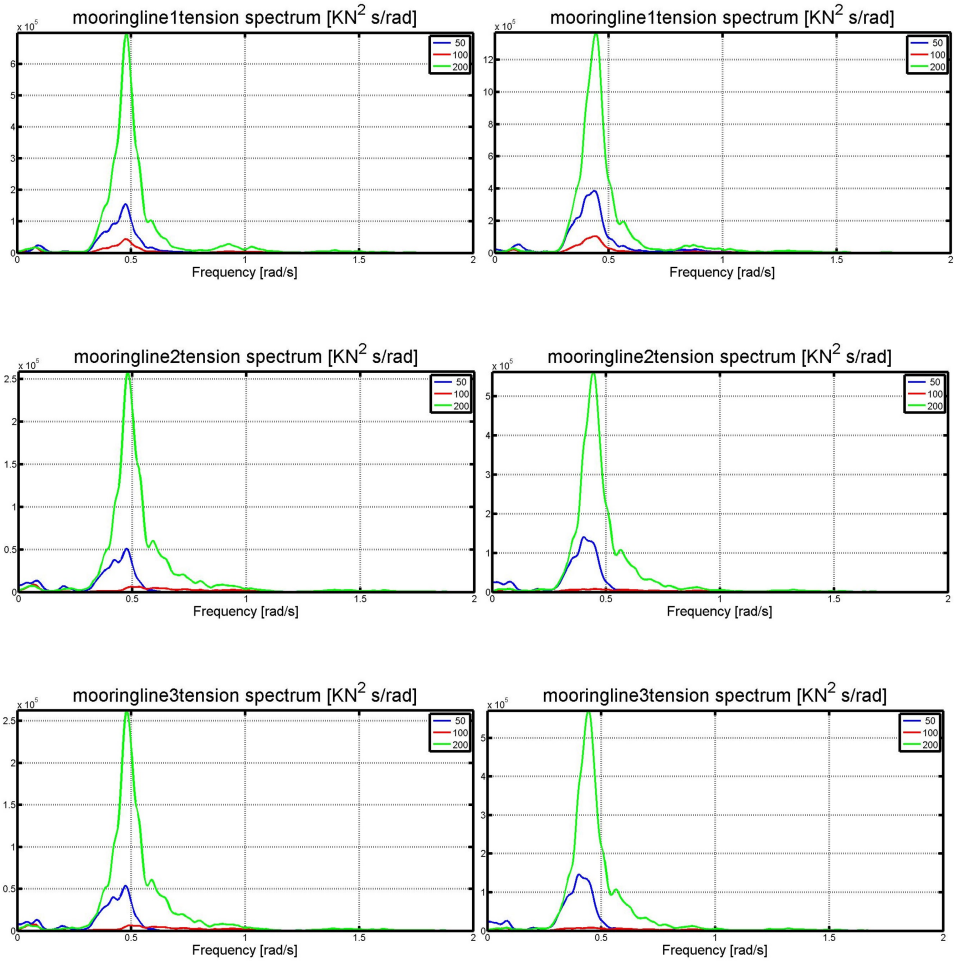

Figure. D.1 *Spectra of mooring line tension in ULS-1 and ULS-2 condition with wave direction* ***0 deg*** *(left column: ULS-1 condition, right column: ULS-2 condition)*

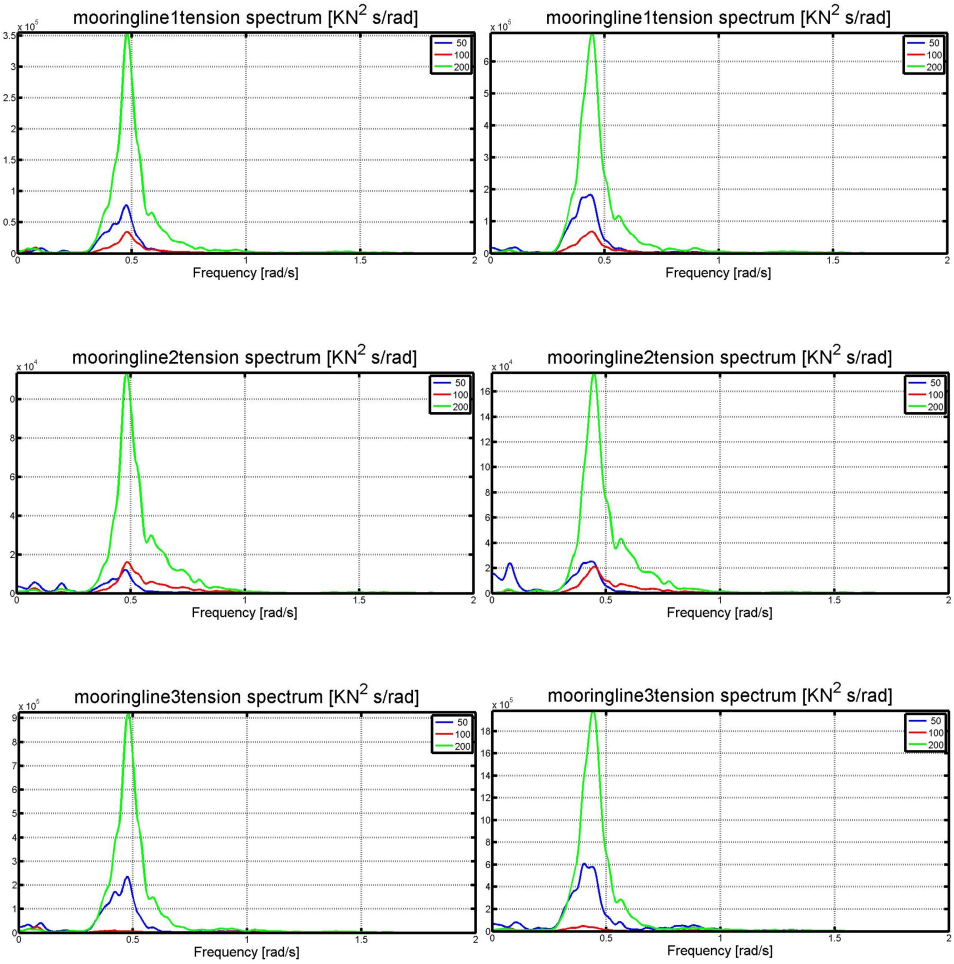

Figure. D.2 *Spectra of mooring line tension in ULS-1 and ULS-2 condition with wave direction* ***45 deg*** *(left column: ULS-1 condition, right column: ULS-2 condition)*

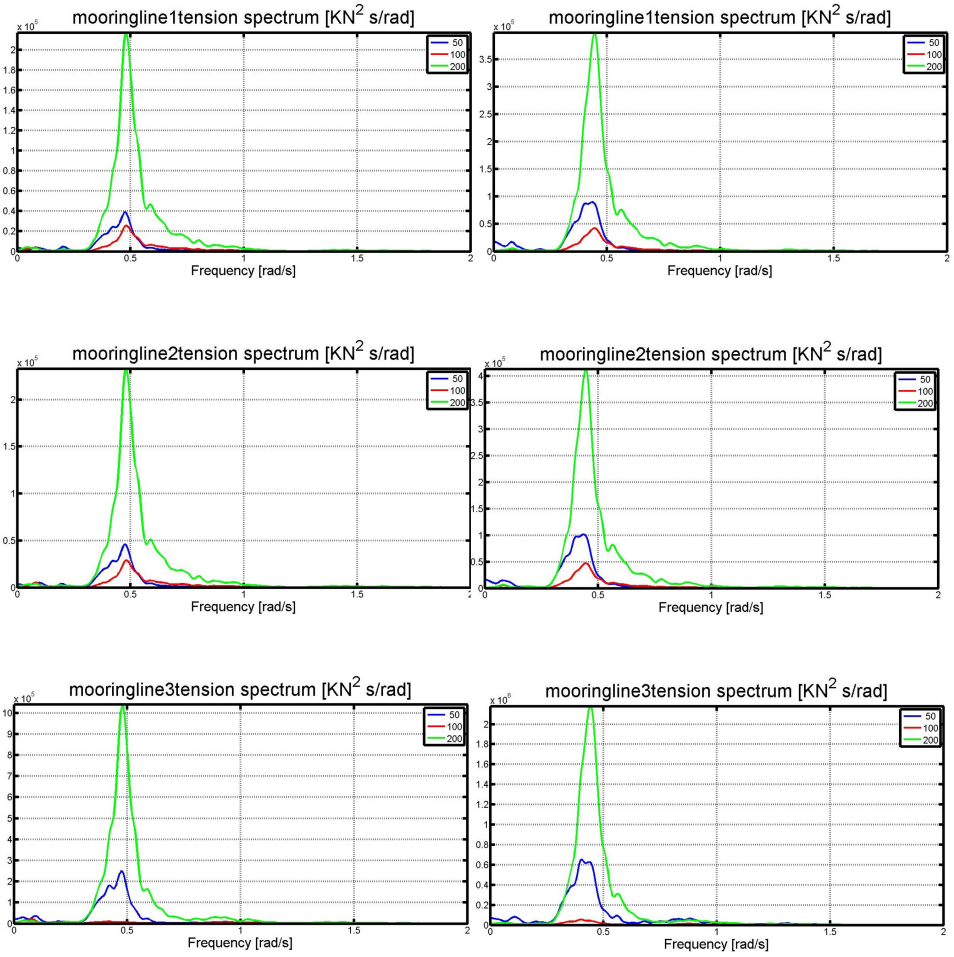

Figure. D.3 *Spectra of mooring line tension in ULS-1 and ULS-2 condition with wave direction* ***60 deg*** *(left column: ULS-1 condition, right column: ULS-2 condition)*

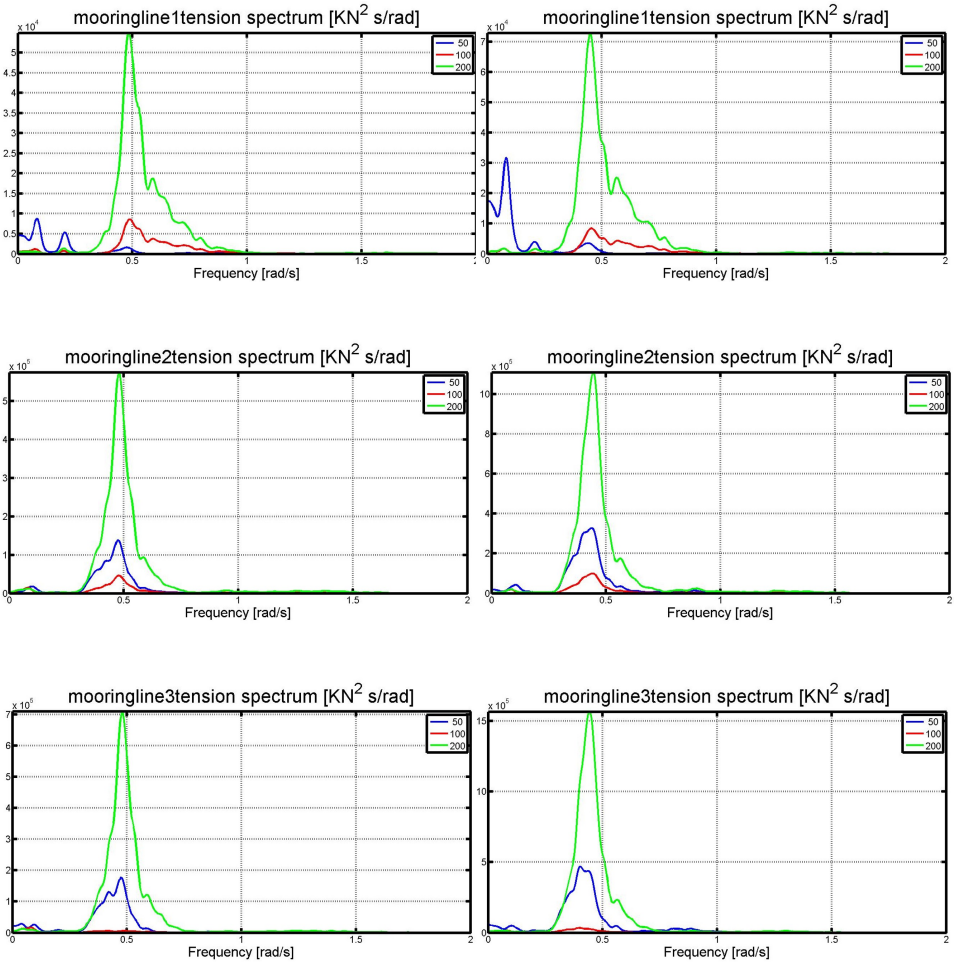

Figure. D.4 *Spectra of mooring line tension in ULS-1 and ULS-2 condition with wave direction* ***90 deg*** *(left column: ULS-1 condition, right column: ULS-2 condition)*

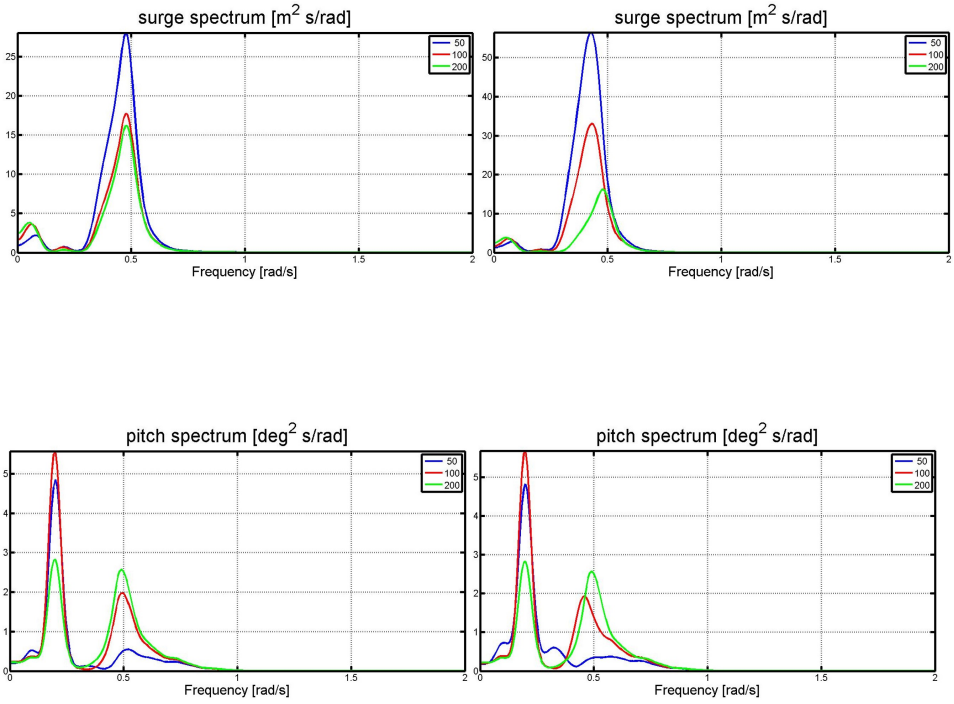

Figure. D.5 *Spectra of floater motion (surge and pitch) in ULS-1 and ULS-2 condition with wave direction* ***0 deg*** *(left column: ULS-1 condition, right column: ULS-2 condition)*

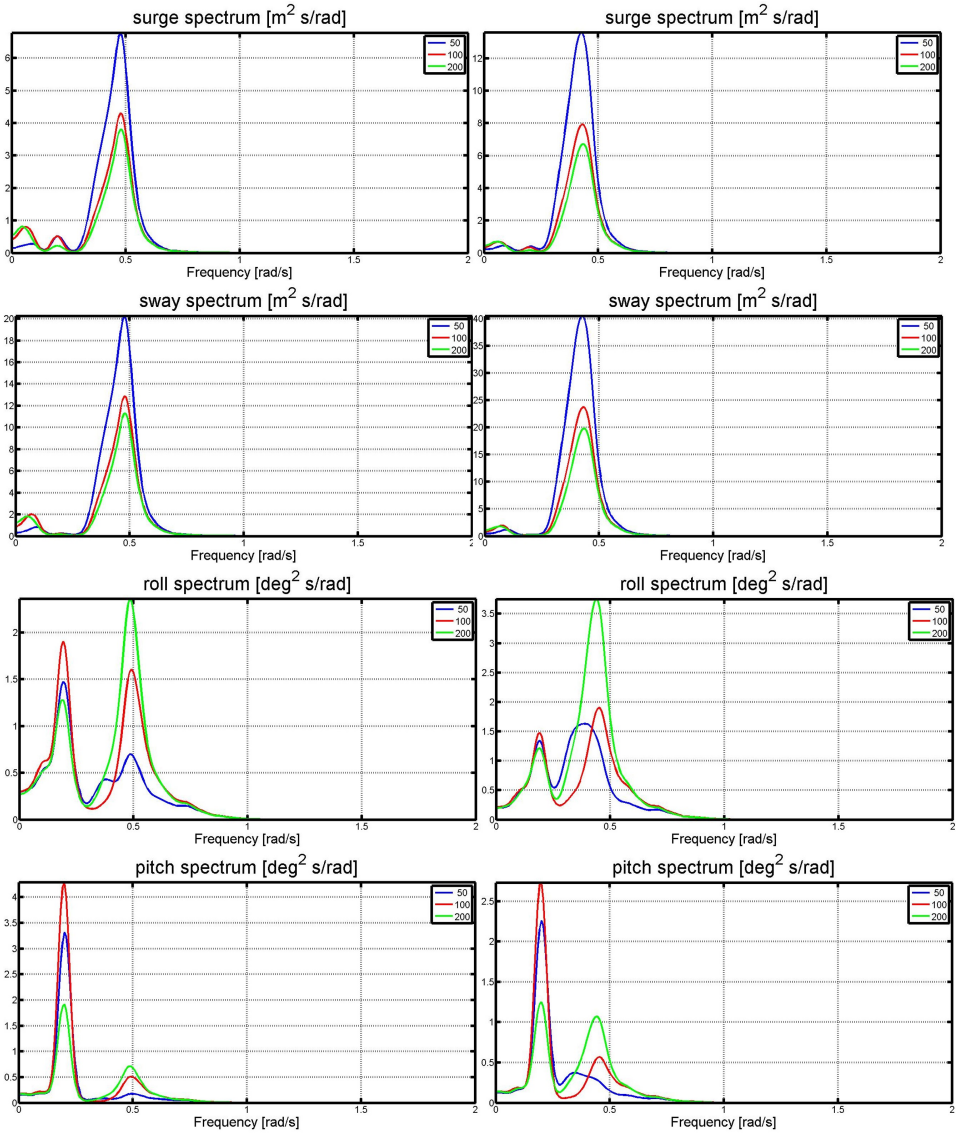

Figure. D.6 *Spectra of floater motion (surge,sway, roll and pitch) in ULS-1 and ULS-2 condition with wave direction* ***60 deg*** *(left column: ULS-1 condition, right column: ULS-2 condition)*

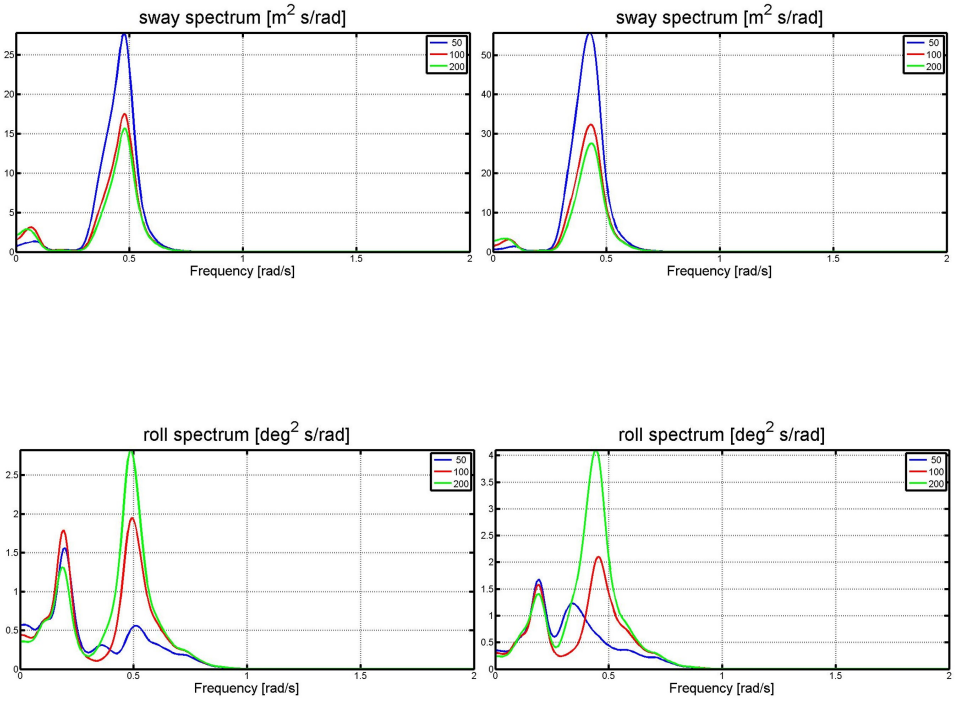

Figure. D.7 *Spectra of floater motion (sway and roll) in ULS-1 and ULS-2 condition with wave direction* ***90 deg*** *(left column: ULS-1 condition, right column: ULS-2 condition)*

E Responses in Operational Condition Test

Figure. E.1 *Responses for 200 m, 100 m and 50 m in operational conditions*

F Response Spectra in Operational Condition Test

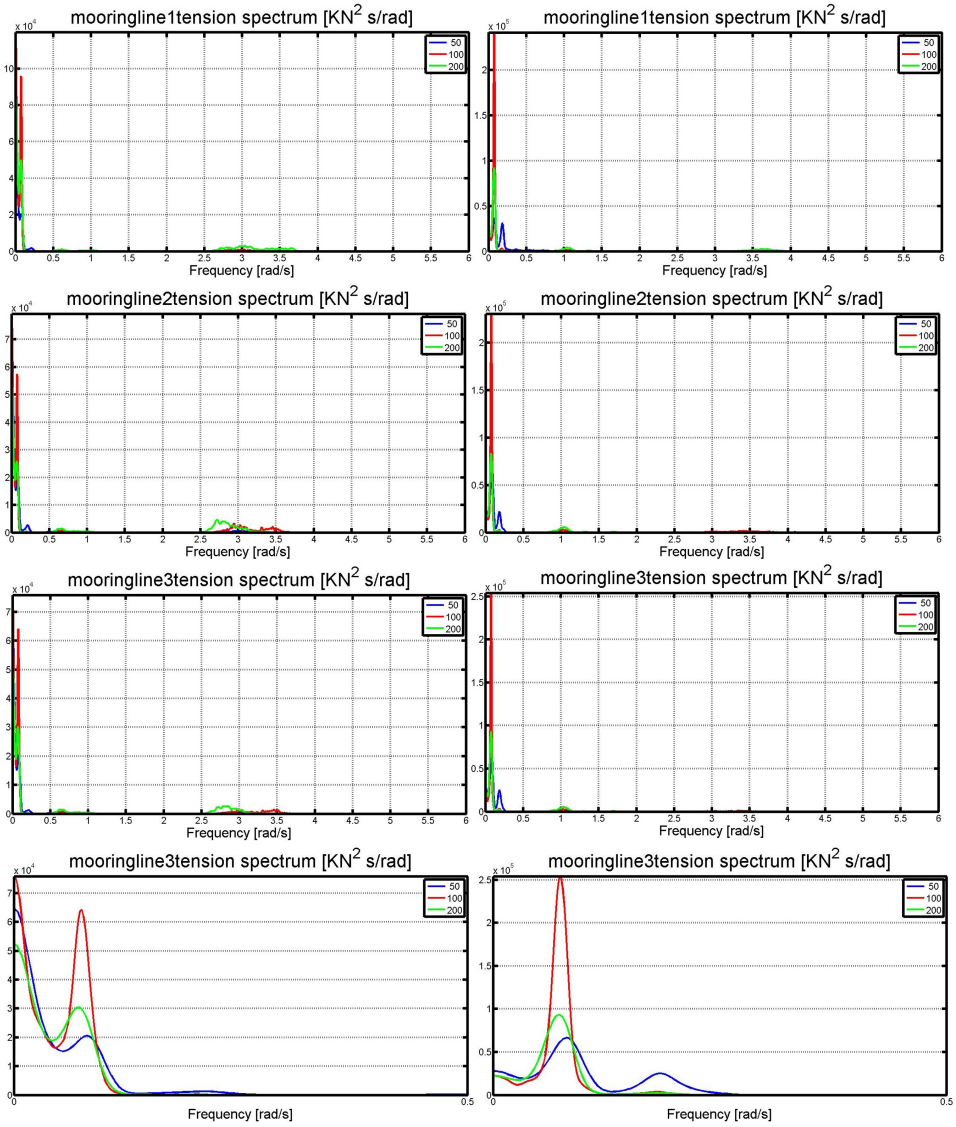

Figure. F.1 *Spectra of mooring line tension in operational condition with wave direction* ***0 deg*** *(left column: FLS-6 condition, right column: FLS-8 condition)*

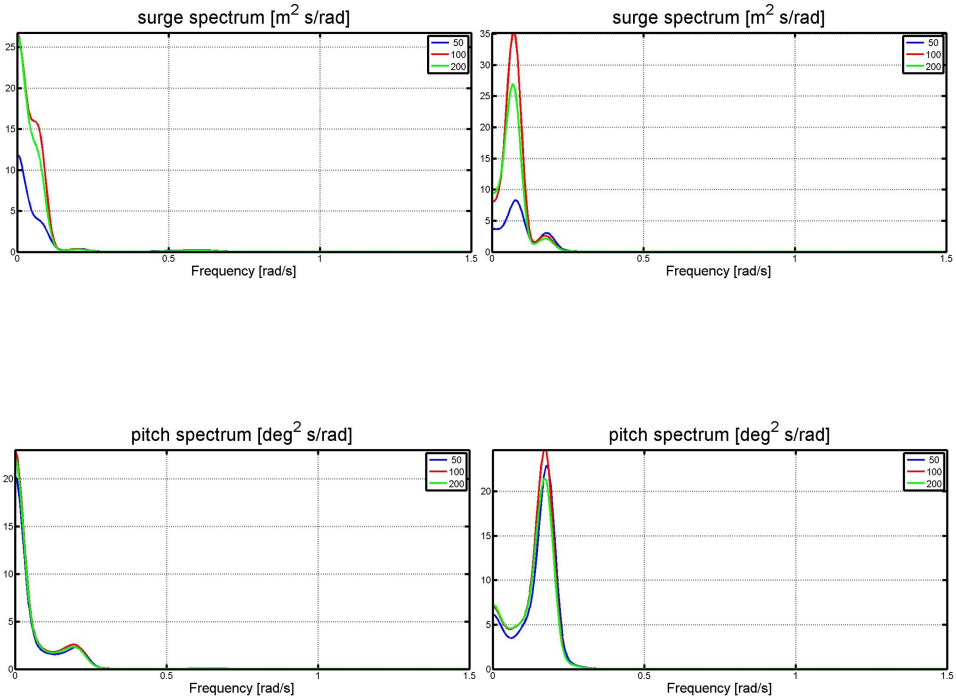

Figure. F.2 *Spectra of floater motion in operational condition with wave direction* ***0 deg*** *(left column: FLS-6 condition, right column: FLS-8 condition)*

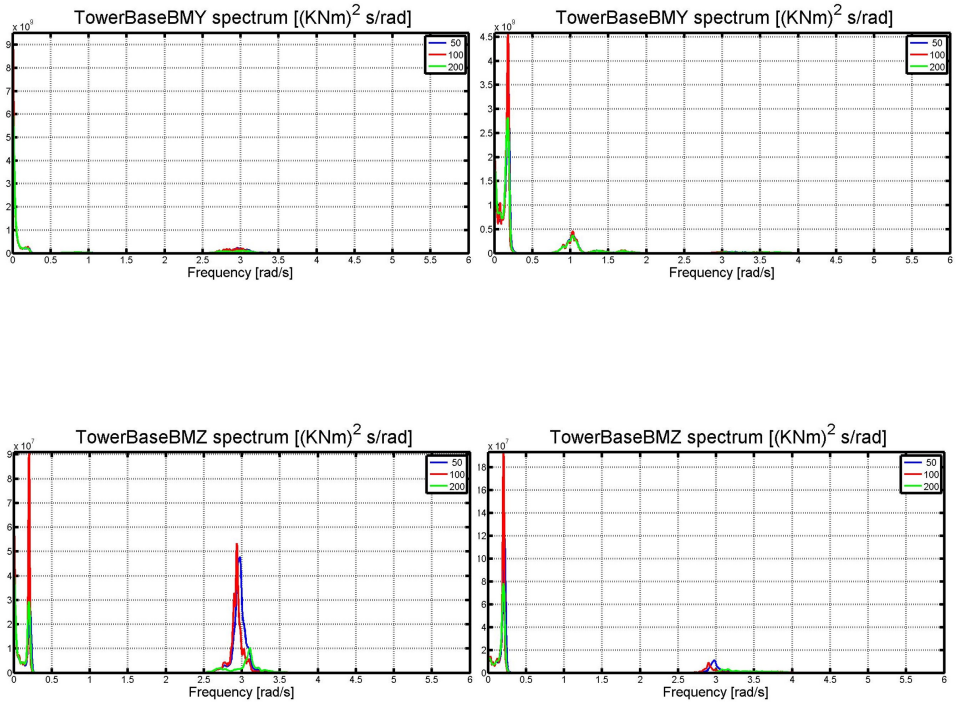

Figure. F.3 *Spectra of tower base bending moment in operational condition with wave direction* ***0 deg*** *(left column: FLS-6 condition, right column: FLS-8 condition)*